HIGH RESOLUTION POPULATION MODELING FOR URBAN AREAS

REZAUL RONI
February 2018

SUPERVISORS:
Dr. P. Jia
Dr. M. Belgiu

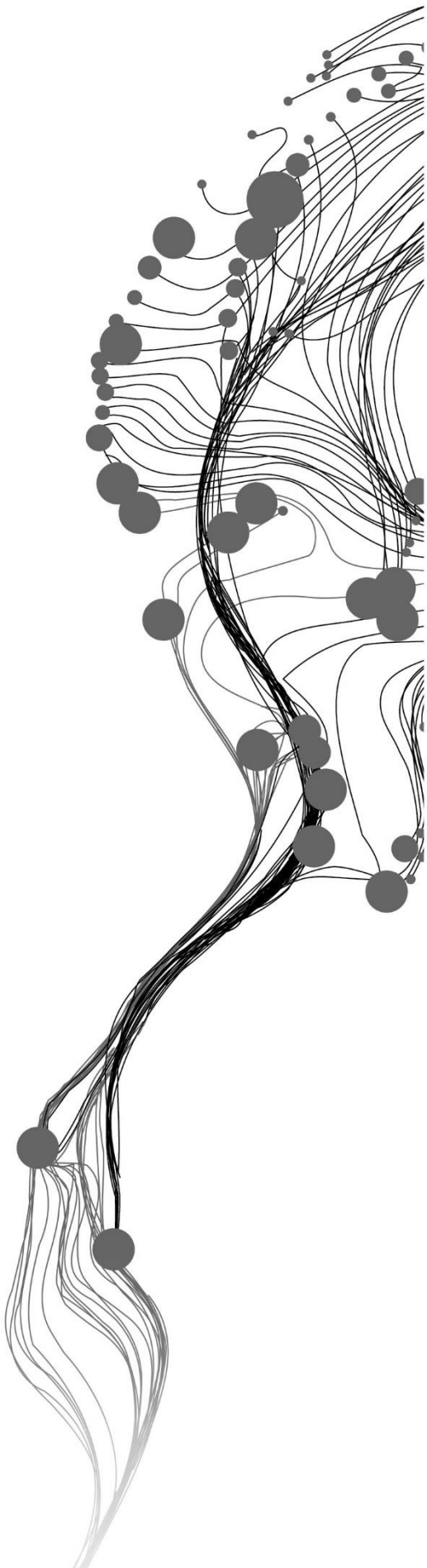

HIGH RESOLUTION POPULATION MODELING FOR URBAN AREAS

REZAUL RONI
Enschede, The Netherlands, February, 2018

Thesis submitted to the Faculty of Geo-Information Science and Earth Observation of the University of Twente in partial fulfilment of the requirements for the degree of Master of Science in Geo-information Science and Earth Observation.
Specialization: Geoinformatics

SUPERVISORS:
Dr. Peng Jia
Dr. Mariana Belgiu

THESIS ASSESSMENT BOARD:
Professor Dr. Ir. A. Stein (Chair)
Dr. Tiejun Wang, Assisstant Professor, ITC-NRS, University of Twente (External Examiner)

ABSTRACT

Traditional choropleth maps on a basis of administrative units cannot accurately represent the distribution of the population due to its high spatial heterogeneity and temporal dynamics. Even in situations where a high spatial resolution is not necessary, updating population data is time-consuming and costly, and hence not feasible to be conducted frequently for developing countries. Dasymetric mapping has become an important technique to produce high-resolution gridded population surfaces (HGPS) from which many disciplines can benefit. In this study, I chose Dhaka City of Bangladesh as a study area and applied a dasymetric model to disaggregate population counts from wards onto cells based on multiple sources of ancillary data, including census, satellite image, land use, and road network data. A multi-resolution segmentation process in the object-based image analysis method and a rule set was used to extract buildings from WorldView 2 imagery and classify them according to land use land cover (LULC) data layer. The overall accuracy of the building classification was 77.75% with a kappa coefficient of 0.76. Four different types of models were designed with Geographically weighted regression (GWR) and Ordinary least square (OLS) regression model to estimate the population using buildings and LULC data. GWR model showed significantly better result through RMSE, CV, R^2 and adjusted R^2. Thereafter, GWR model was adopted during the dasymetric process to disaggregate the population over building at 5X5 meter resolution pixel level. Again the population product was checked by re-aggregating the pixel specific population density to ward level population counts and compare the result with actual population. This time RMSE was found 194, which is less than the any other four models. The final HGPS product was stored with a spatial resolution of 5m for ease to directly integrate with some high-resolution data sources such as Satellite data or products with a resolution of 5m, or to be further aggregated for integrating with medium and relatively coarse-resolution data sources, such as Satellite data or products with a resolution of 15m and 30m. It holds the potential to improve the demographic, social, environmental and health research in Dhaka City. Furthermore, this study provides a new research framework of implementing a high-resolution population modeling process in a complex urban setting, which is expected to be applied to more complex urban areas in both developing and even developed countries (e.g., New York City). Future work includes using Very High Resolution (VHR) data to extract the building height for further improving the accuracy of HGPS in urban areas, to meet higher demand in some specific areas/situations, such as emergency/disaster response.

ACKNOWLEDGEMENTS

I had a dream to study in Geoinformatics and ITC made that dream true. Therefore, I would like to thank all those people who contribute a lot to my degree and without those people, this could never become true.

Firstly, I would like to express my very great appreciation to both of my supervisors Dr. Peng Jia and Dr. Mariana Belgiu. They gave me the opportunity to do this research and believe in my ability to complete this research. I am grateful to both of you for your cordial support and guidance, which greatly improved the manuscript. Both of the supervisors were so friendly to provide insight and expertise that greatly assisted the research. I wish I could do further research with you. I would also like to show my gratitude to the all ITC teaching staffs for sharing their pearls of wisdom with us during the whole period of degree.

European Space Agency (ESA) is undoubtedly Claimant of recognition for this research. They provide me the satellite image and without their help, this research could not be able to complete. Thanks to all the persons who were engaged during the evaluation process of my proposal.

I heard that "Nothing is possible without sacrifices". It proved again true. My parents and laws family – thanks to all of them. I am lucky to have such a wonderful family who was the constant source of my strength and inspiration to live here all alone. In addition, I want to thank especially to my late father-in-law who passed away during this period and encouraged me a lot.

Rumaisa, my daughter, you are the heart of mine and completed my life. I just spent my time here thinking of your early childhood and waited when you will be in my arm. Your memories were the magic for removing my tiredness and you deserve a great hug from me for your sacrifices. Nazia, if I give you a thank, it will be very less for you. Your continuous support gave me strength and without you, I would never be here where I am today in my life.

I would like to offer my special thanks to the Jahangirnagar University authority and all the colleagues from my departments of Geography and Environment. They extended their cordial support to me to able this opportunity. I am particularly grateful for the assistance given by my mentor Professor Dr. Shahedur Rashid and my guide Professor Dara Shamsuddin.

I wish to acknowledge the help provided by the Bangladeshi peoples here namely Md Marufur Rahman, Mostarin binte Ahmed, Goutam Roy, Tuhin, Tanvir, Hashem, Kallol-Mahua family, Jewel-Turin family, Hasib-Labony family etc. I will not forget your hospitality during my hard time and friendliness behave as a brother when I am far away from home. I have spent a wonderful time with you and made me feel home. Also, I would like to give a thank to all of my friends here in ITC, who made a family live with. It will not be finished by telling the names but some of them are very special such as Mcokeyo, Adlan, Ahmed, Aman, Noe, Deepshikha, Sravanthi, Joseph, Yaping, Salma, Gideon, Aldino, Daniel, and others.

Finally, I would like to thank the Almighty Allah, who made my journey smooth and comfortable. All credit goes to Allah the Almighty.

Rezaul Roni
Enschede, February 2018.

TABLE OF CONTENTS

LIST OF FIGURES

LIST OF TABLES

1. INTRODUCTION

1.1. Motivation and problem statements

The accurate spatial distribution of the population is enormously important to researchers in many fields, such as risk assessment, policy-making, disaster management, accessibility modelling, poverty mapping, and human health adaptive strategies (Chakraborty J., Tobin G. A., 2005; Dasvarma, 2010; Gaughan, Stevens, Linard, Jia, & Tatem, 2013; Maantay & Maroko, 2017). Consequently, mapping high-resolution population distribution became an important technique to produce high-resolution gridded population surface (HGPS) from which many disciplines can benefit. Traditionally, the census has been the main data source for such mapping, but the census is normally conducted about every 10 years in most countries, which is insufficient to fully capture fast dynamics of population changes over time. Using traditional methods to update population data frequently is time-consuming, costly, and even infeasible at a large scale (Li & Lu, 2016).

Many researchers have developed a wide range of methods for mapping spatial distribution of the population with the aid of Geographic Information Systems (GIS) technology in the past decade. However, as the population is not uniformly distributed over space within administrative and even fine-scale census units (Hay et al., 2005), GIS-based discrete, aggregated choropleth maps cannot represent the spatial distribution of the population accurately (Martin, 2011). Recently, some products incorporated various ancillary data, including land use/land-cover (LULC), night-time lights, transportation network, waterbodies, elevation, slope etc., to model high-resolution population distribution globally, such as Gridded Population of the world (GPW) (Balk & Yetman, 2004), Global Rural-Urban Mapping Project (GRUMP) (CIESIN, 2004), and LandScan Global (Dobson et al., 2000), and WorldPop (Asia, Africa, and South America). Some other studies have been undertaken for modeling population distribution based on remote sensing (RS) imagery, for example, deriving LULC from satellite imagery (Linard et al., 2010), correlation between population density and satellite image derived information such as land surface temperature, LULC classification from Landsat Imagery (Li & Weng, 2010), and using image texture indices (Chen, 2002). However, the spatial resolution of all aforementioned products ranges from 100m to 1km, which cannot meet the demands in some specific areas and situations such as emergency/disaster response and resource allocation, especially in low- and middle-income countries (LMICs) where resources are usually extremely limited. Moreover, the product quality in urban areas is even poorer than average due to high heterogeneity of urban features. Given the increasing urbanization being experienced worldwide especially in some rich developing countries, the demand for high-resolution population mapping is also increasing accordingly.

Very high-resolution (VHR) satellite imagery can provide a suitable solution to serve as ancillary data for high-resolution population mapping, by allowing us to identify LULC classes even finer-scale information such as building type. Most previous work has been focused on using medium- to coarse-resolution images (Chen, 2002), where only some populated/unpopulated classes identifiable on a large scale were used, such as water, urban/rural areas, vegetation/forest areas built-up/non-built-up areas, urban/non-urban areas, and agriculture (Eicher & Brewer, 2001; Vijayaraj et al., 2008; Tenerelli et al., 2015; Wei et al., 2017).

Dasymetric mapping is a particular cartographic process where census data are disaggregated to spatial units/grids with aid of ancillary data to refine the population distribution (Mennis, 2003). This technique provides a supportive environment to incorporate parcel/building information into the population

modeling process. In addition, the dasymetric mapping can produce high-resolution population distribution map. Figure 1-1 describes the general concept, how population density could be disaggregated according to land use classes in fine scale. Population density varies from different types of settlement patterns and choropleth method is not realistic for mapping (Wright, 1936). Population density varies from census unit to census unit and even from different land use within the census unit. In addition, it can vary for same land use type in a different ward. It becomes a very challenging job if someone tries to map at building level population density or very high-resolution population product and building level data is not available. However, opportunities of using building information instead of classified impervious surface area derived from VHR satellite imagery in dasymetric mapping have not been explored fully yet.

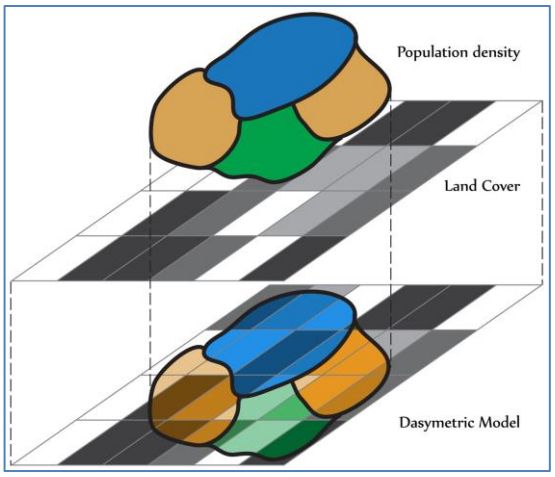

Figure 1-1: A concept of dasymetric model considering land use data (Nagle et al., 2014).

1.2. Novelty of the research

This study develops an integrated approach to Object-based Image Analysis (OBIA) for building detection and Geographically weighted regression (GWR) model in dasymetric modeling to produce high-resolution population product for Dhaka city. Various RS techniques have been applied for detecting buildings from VHR images. However, not all of them are suitable for all urban areas as every urban area has a unique characteristic as well as the different heterogeneous structure and land cover compositions such as vegetation area, water body, impervious area, road network. The challenges increase when these complex areas need to be differentiated in satellite images. One of the main focuses of this research is the detection of buildings from VHR. Many researchers attempted to develop various methods to extract buildings automatically from VHR images. However, these methods were applied to extract buildings from a small area only. OBIA method to extract buildings is used in this work. Automatic identification of buildings from VHR is the first initiative for buildings mapping in Dhaka City. In addition, various mapping methods were developed for visualizing the distribution of population density. Dasymetric mapping is one of the mostly used interpolated methods for population mapping. There were various types of dasymetric mapping techniques available so far, where land use land cover (LULC) data were used as ancillary data. In this study, a GWR model was adopted in the dasymetric mapping process to make the population density over each ward.

1.3. Research objective and research questions

The main goal of this study is to develop a population disaggregation model in Dhaka City by taking advantage of VHR satellite imagery, GIS, and statistics from national census. The specific research objectives and questions are listed below:

Objective: 1: Conduct a systematic literature review of population modeling and building extraction from VHR images.

Questions:

- What are the existing high-resolution population products (focusing primarily on country/continental levels)?
- What are the existing methods of high-resolution population modeling?
- What are the existing methods used for extracting buildings from VHR images?

Objective: 2: Extract and classify urban buildings from VHR satellite images as ancillary data for population modeling in Dhaka City.

Questions:

- Which building extraction method could be used for Dhaka City?
- How accurate is the applied method for the study area?

Objective: 3: Implement a dasymetric model to disaggregate population counts onto 5x5m raster cells.

Questions:

- Which population model could be used for population mapping of Dhaka City?
- How accurate is the dasymetric product in Dhaka?
- What factors may contribute to the inaccuracy of the resulting population distribution product?

1.4. Study area

Dhaka is the capital city of Bangladesh and has a long history of 400 years. It is located on the bank of Buriganga river and surrounded by others six rivers such as Balu and Sitalakhya on the eastern side, Turag, and Buriganga on the western side, Tongi *Khal* to the north and Dhaleshwari to the south (Zaman, 2017). There is no clear evidence of the exact time of starting of settlement at this area where present Dhaka is located (Ahmed et al., 2014). However, it is assumed that human settlement as urban growth center started here from the seventeenth century. From that period, Dhaka faced five different period, which has different contribution to its development and the periods are - Pre-Mughal Period (Before 1604), Mughal Period (1602–1764), British Period (1764-1947), Pakistani Period (1947–1971) and Bangladesh Period (Since 1971) (Chowdhury & Faruqui, 2009). Figure 1.2 shows the physical extent of the Dhaka city at different periods. It was established as Municipality in 1864 and the name was replaced to Dhaka Municipal Corporation in 1983 and finally in 1991, to Dhaka City Corporation (BBS, 2011a). Now, Dhaka City Corporation (DCC) has two parts (Dhaka North and Dhaka South) with 136.34 km^2 and consists of 92 wards. Dhaka North City Corporation (DNCC) consists of 36 wards, which covers 82.638 km^2 and Dhaka South City Corporation (DSCC) consist of 56 wards, which covers 43.7 km^2 (BBS, 2011). Figure 1.3 shows the location of the study area as compared to Dhaka Zila and surrounding areas.

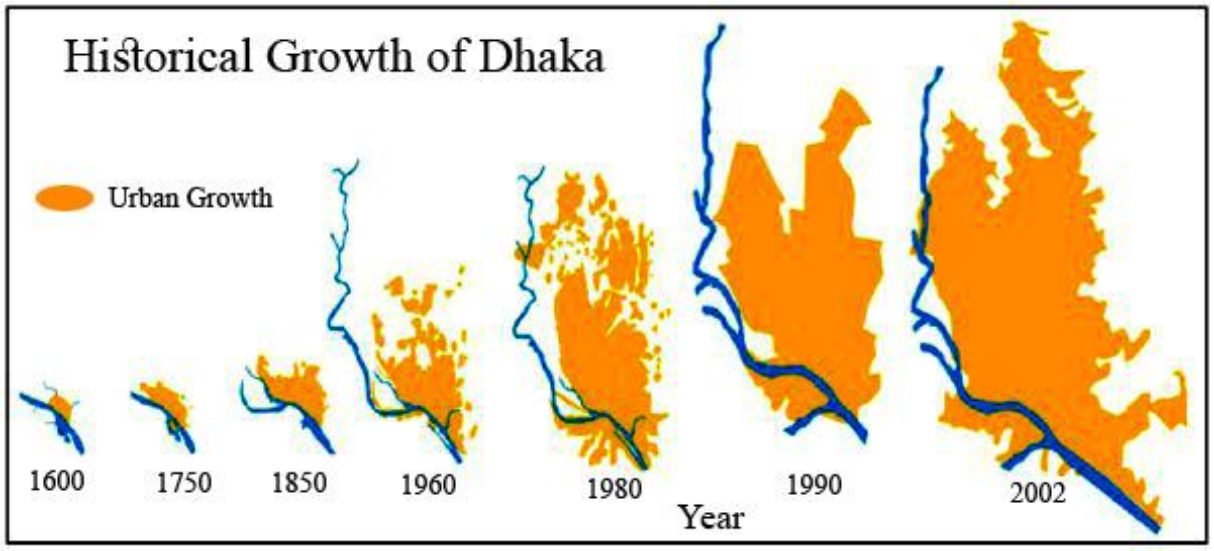

Figure 1-2: The Historical growth of Dhaka City from the 16th century. Source: Urban Planning Department, Dhaka City Corporation, 2004.

People started to live in Dhaka in the early 12th century (Ahmed, 1986). According to 2011 National Census, the total urban area of Bangladesh is 8867.42 km² with a population of 35094684, which is 23.3% of the total population and 6% of the total land of Bangladesh. Among this, Dhaka has a number of 6970105 population (male 3876586 and female 3093519), which is the 19.86% of the total urban population having a population density of 55169 people per km², whereas national population density is 976 person per km² (BBS, 2011b). A historical overview of Dhaka City's population is given in the following table 1-1. The population growth rate increases at 3.2% with the expansion of industries, commerce, and business, housing and infrastructure since 1981.

Table 1-1: Dhaka City in different Census (from 1981-2011)

Items	**2011**	**2001**	**1991**	**1981**
Area (sq. km.)	126.34	153.84	153.84	131.6
Household	1576746	1109514	634328	367513
Population (Both sex)	6970105	5327306	3612850	2475710
Male	3876586	3021970	2051760	1449314
Female	3093519	2305336	1561090	1026396

Source: (BBS, 2011a)

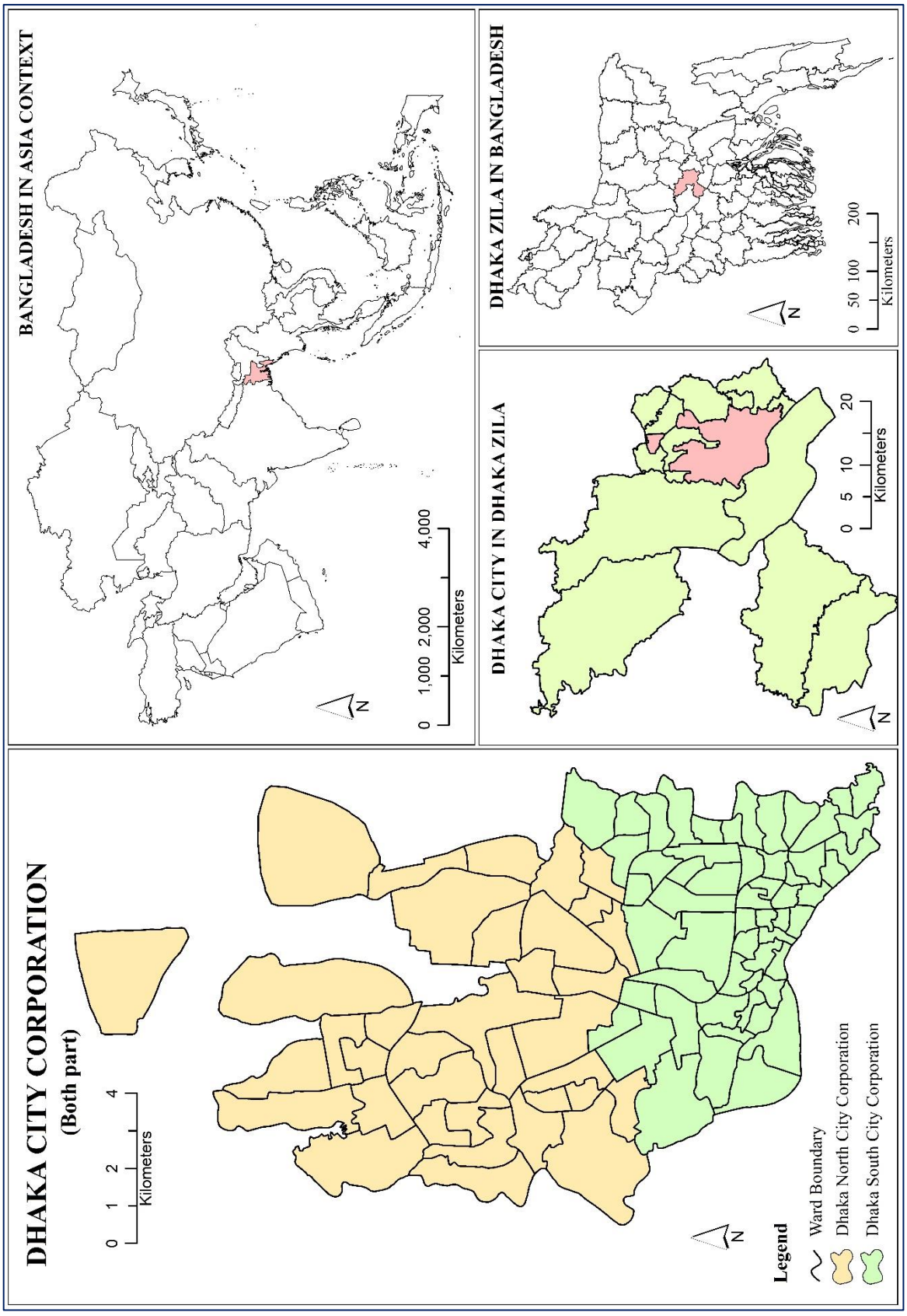

Figure 1-3: Location map of the study area in the context of Zila, Bangladesh and Asia.

2. LITERATURE REVIEW

Population distribution is an essential part of spatial demography research. Consequently, various studies have been conducted for population disaggregation modeling using various methods over the last few decades. These methods were developed based on the availability of information and eventually with the development of statistical, GIS and RS approach. Most of the population disaggregation methods were designed with areal interpolation methods. Areal interpolation means zonal transformation which involves transforming demographic information from one set to another set of spatial source zones (Lam, 1983). In the context of interpolation, census data are used as vector-based source zones and are interpolated into raster-based grids. It is focused on the population estimation, which minimizes the errors estimation of the population from the original areal aggregation (Wu et al., 2005). The quality mostly relies on how well both zones are defined, the degree of generalization and the characteristics of the partitioned surface (Lam, 1983). Depending on whether or not to use the ancillary information such as LULC, the influence of road, distance from central business districts (CBD) etc. interpolation of population disaggregation methods could be categorized into two types- population modeling without ancillary data (Section 2.1) and population modeling with ancillary data (Section 2.2).

2.1. Population modeling without ancillary data

The population disaggregation models without the consideration of ancillary data could be categorized into two types – point-based and area-based methods, based on how population data are interpolated from a coarse level of units to a fine level of units. The point-based interpolation methods convert administrative units (i.e., source zones) into geometrical centroids (i.e., summary points), which contain the population counts over source zones and result in gridded maps (Martin, 1989). There are many point-based interpolation methods developed and applied in population modeling over the past decades. Lam (1983) identified two types of point-based interpolation methods: exact and approximate. The exact method depends on the original values of the points without having any type of absolute, relative, maximum or minimum value, while the approximate method performs a surface function of $f(x, y)$. The surface function does not give the same value as the observed value. There are few techniques found in the exact methods for population disaggregation such as distance-weighting (Sampson, 1978), kriging (Meng et al., 2013), spline (Stein, 1999), finite difference (Petersen et al., 2017) etc. and in approximate methods such as least square, least squares fitting with splines (Varah, 1982), Fourier series models (Asfiji, Isfahani, Dastjerdi, & Fakhar, 2012). The results from all these techniques seriously depend on the quality of original data and especially the density and spatial distribution of the points and complexity of the surface of the ground (Wu et al., 2005). Based on former's simplicity, flexibility and reliability, exact methods were found more reliable than approximate methods (Lam, 1983). Point-based areal interpolation methods have some drawback (Lam, 1983; Wu et. al., 2005). When center point of the source zone is not symmetrically distributed then it creates error while interpolating values from the source point to target zones. In this regard, the area-based interpolation method is introduced to overcome this shortcoming.

The area-based interpolation methods mainly focus on volume preserving techniques, which is a very simple areal weighting method. The technique depends on overlaying operation, where geometric properties of source zone overlay on target zones (Fisher & Langford, 1995), which is very easy and simple to calculate the population density. There is no need for any ancillary data for this interpolation (Mitchel Langford, 2006). However, the population density is considered homogeneous throughout the study area, which is the major drawback of this volume preserving technique. Another area-based interpolation method is

pycnophylactic interpolation, which was introduced by Tobler (1979) and widely quoted. He introduced the smooth volume-preserving density function in this interpolation method, which gives a non-negative value and also has a finite value for each geometric location. After that, Rase (2001) expanded Tobler's formula to surface representation which is based on Triangular Irregular Network (TIN). He argued to have better results compared to the original grid-based methods. This method is difficult to implement because it has complex program structure.

2.2. Population modeling with ancillary data

The population density may vary across a range of socio-environmental characteristics of an area (Winsborough, 1965; Liu & Yamauchi, 2014). Thus, different interpolation methods have been developed by considering various types of ancillary data, such as land use, land cover, road network, water body, and socioeconomic data, etc. Different types of population interpolation modeling considering ancillary data were described in next following sections.

2.2.1. Dasymetric mapping

The term *Dasymetric* was coined by a Russian cartographer Tian-Shansky in 1920 (Preobrazenski, 1954 in Bielecka, 2005). After that, Jhon Wright (1936) used this method arguing that population is not a continuous phenomenon and its mapping with choropleth method is unrealistic. Dasymetric mapping is a particular cartographic process where spatial data is disaggregated to fine-resolution considering ancillary data to refine the locations of the population (Mennis, 2003). The use of dasymetric mapping increased with the rapid development of GIS and RS technologies (Mennis, 2009). It covers a wide variety of research areas including cartography, ecosystem studies, statistical analysis or criminology (Petrov, 2012). Dasymetric mapping gained its momentum in the 1990s when various ancillary data started to be used (Tapp, 2010; Holt & Lu, 2011). In addition, there are some studies on 3-D dasymetric modeling where population was modeled at census level using a number of buildings with volumes (Qiu, Sridharan, & Chun, 2010; Lwin & Murayama, 2011). About 75% of indexed journal articles on dasymetric mapping were published at the 2000s and after that another, about 1000 articles were published between 2011 and 2017 (Petrov, 2012). Figure 2.1 shows the summary of the published articles from the 1920s to 2017.

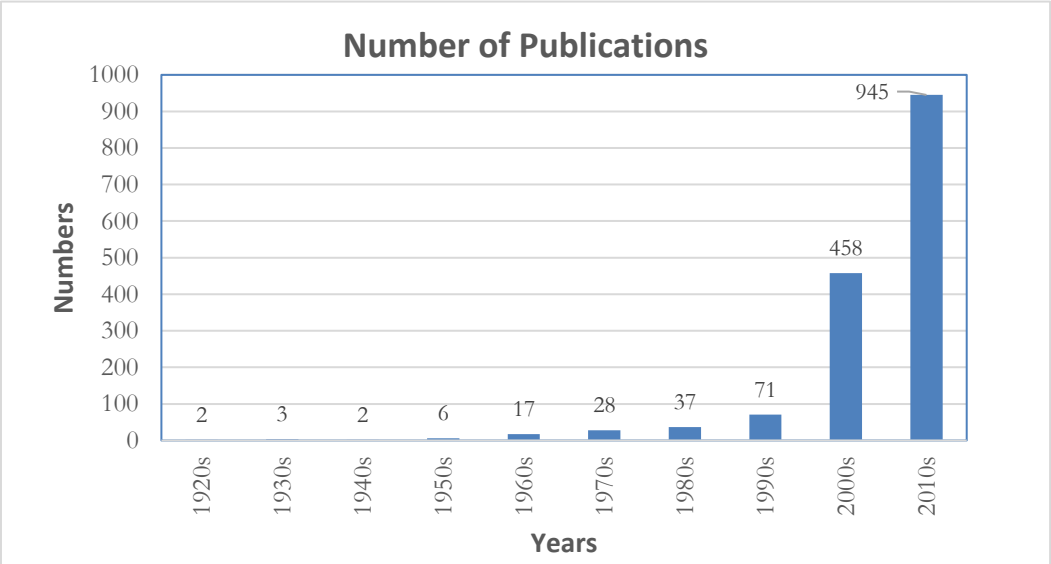

Figure 2-1: Number of published articles on dasymetric mapping over the past century (reconstructed from Petro, A. 2012, google scholar, where "dasymetric mapping" and "population" were the keywords).

Eicher & Brewer (2001) described five type of dasymetric methods such as grid binary, polygon binary, polygon three-class, grid three-class, and limiting variable methods. Apart from those methods, different types of dasymetric methods were developed at different times so far. Therefore, studying all these dasymetric methods, it could be categorized into three classes 1) classification based on the binary class of LULC, 2) classification based on multi-class of LULC and 3) classification based on data-driven weighted value.

A. Classification based on binary class of LULC

Binary method was developed as a mapping technique (Langford, Maguire, & Unwin, 1991; Langford & Unwin, 1994) basically, it solved the areal interpolation problem, where it was assumed that the population density is homogeneous within the source unit (Fisher & Langford, 1995; Cockings, Fisher, & Longford, 1997). In the binary method, the whole land cover area needs to divide into two classes (binary) like Eicher and Brewer (2001) divided into urban and agricultural/woodland, which is derived from the raster dataset and output was in grid cells. There are no other classes like forested areas or water. Based on this approach, the binary classes are marked either as inhabitable areas or as non-inhabitable areas. Using this binary technique Holt et al. (2004) and Langford et al. (1991) did some studies by categorizing the land cover area into two classes (residential and non-residential). Another binary method called polygon binary method, where also two types of land category used for population or housing density mapping against census unit area (Eicher & Brewer, 2001). However, these methods are unable to differentiate between complex and heterogeneous areas, where population distribution varies in different land uses, for example, Dhaka City of Bangladesh.

B. Classification based multi-class of LULC

Urban areas consist of complex LULC and population density is not equal to those classes. Considering a various number of LULC classes, various dasymetric methods have been developed. The three-class method is one of the most practiced methods earlier. In the three-class method, the study area needs to classified into three land use classes such as urban, agricultural/woodland and forest area and a weighting order is assigned to these land use classes. Holloway et al. (1996) assigned 70% weight to urban areas, 20% to agricultural/woodland areas and the remaining 10% to forested land. Again, Mennis (2003) used different types of land classes such as high-density residential, low density residential and non-urban areas instead of the classic land cover classes used in previous studies. However, this method neglects the area of each LULC or more than three LULC classes, which is the major drawback of this method. Despite this limitation, the method is easier to implement (Eicher & Brewer, 2001). Grid three-class method is the grid representation of the polygon three-class method. However, this method was considered as a development of the binary method.

Limiting variable (LV) is another dasymetric model where predefined weighted values are used in multi-class of LULC used. Wright (1936) first introduced the limiting threshold value method and after that McCleary (1969) described briefly in pure polygonal form. In addition, Gerth (1993) and Charpentier (1997) tested this method in their GIS applications (Eicher & Brewer, 2001). There are few steps in this method. The first step is assigning a simple areal weight value to all inhabitable polygons of the country, which was previously classified to three land use classes: urban, woodland/agricultural and forested. Next step is setting a threshold limit of maximum density for the particular land class such as water is no limit, woodland/agricultural may limit to 50 and the forested area may limit to 15 people/km^2 (Gerth, 1993). Tapp (2010) reclassified fifteen national land cover dataset to four classes (unpopulated, urban, agricultural/woodland and forest) to use this method and limit 15 people/km^2 to the forest area, 50 people/km^2 to agricultural/woodland and remaining people to the urban area. Wei et al. (2017) used city-

scale dasymetric modeling for Pearl River Delta area of southern China area where they incorporated historical census data. They used Landsat imagery (from 2000, 2005, 2010, and 2015) with a 'limiting variable' for three land use classes of urban areas, rural areas, and vegetation areas to generate a gridded population density.

C. Classification based on data-driven weighted values

There are more dasymetric methods, which may be classified as data-driven weighted dasymetric methods. The street weighted (SW) method is one of them, where a weight was given to each street segment according to its length (Reibel & Bufalino, 2005). The address weighted (AW) method, where address points were used as ancillary data (Zandbergen, 2011). The AW method is simplified than SW method, assuming that all address points are evenly distributed along the country. The parcel distribution (PD) method is a combination of the limiting variable and the binary mask method (Tapp, 2010). PD could generate enhanced resolution and better accuracy in rural. Jia et al. (2014) argued that High-resolution Gridded Population Surface (HGPS) based population distribution provides more reasonable estimation than census units and land cover. In addition, monotype property block can give more straightforward indicator than land cover types. Though he used seven property types previously (Jia et al., 2014), later four land type (open space, low intensity, medium intensity and high intensity) were used for dasymetric mapping on Alachua County, Florida (Jia & Gaughan, 2016).

2.2.2. Population modeling relation with other phenomenons

All the population researchers agreed that urban population distribution is influenced by various morphological phenomenon such as distance from the central business district (CBD), distance to roads and industrial area, the location of important infrastructures etc. Considering all morphological factors, they started using statistical modeling from the 1950s. Additionally, data derived from remote sensing (e.g., aerial photograph) were used in statistical modeling in the mid-1950s especially as an alternative to population census (Wu, Qiu, & Wang, 2005). Various studies have been conducted with statistical modeling for population mapping depending on what types of ancillary data are being used and how they are related to population density distribution. Lo (1986) and Liu (2003) tried to categorize all these approaches into five based on the relationship between population and (i) urban areas, (ii) land use, (iii) dwelling units, (iv) image pixel characteristics and (v) physical or socio-economic characteristics. Based on this category the recent researches are incorporated here.

2.2.2.1. Population relation with urban areas

So far the first study on this method was done by Nordbeck (1965), which is developed from the biological law of allometric growth (Huxley, 1932). He found a relationship between built-up area and population in a proportional way (Nordbeck, 1965 in Wu, Qiu, & Wang, 2005). Tobler (1969) used satellite imagery first to study the population distribution considering urban areas. His work revealed a high correlation coefficient of 0.87 between population and cities assuming that city shapes vary with time. After the availability of Landsat satellite imagery and image processing techniques, the study of the relationship between population and urban areas increased enormously. Prosperie and Eyton (2000) used for example urban light volume for mapping population and found a very high relation between population and light volumes ($R^2 = 0.974$). In addition, Lo (2002) found a correlation coefficient of 0.91 between the light volume of Chinese cities and non-agricultural population.

2.2.2.2. Population relation with land use

Human population density or distribution is very much related to the landscape, for example, land use and transport facilities (Liu & Herold, 2006). Kraus et al. (1974) estimated population density based on four different residential land use type (single family residence, multi-family residence, trailer park residence and all commercial or industrial) using aerial photographs and found combined error rate of only 4.51% which was the most accurate population density product at that time. Langford et al. (1991) established a multivariate regression model, which uses land use data to estimate the population density. Weber (1994) classified six types of land use from SPOT HRV XS image for urban population estimation of Strasbourg, France and found kappa coefficient of 0.915. Lo (2003) found a correlation coefficient of 0.878 between population and six different types of land use like - high density, low-density, cultivated/exposed land, cropland or grassland, forest and water derived from Landsat TM. A regression model integrated with decision trees using QuickBird image was used to study population for Pakistan. In that study, 22 variables were used to classify only two type of land classes (built-up/ non-built-up) for population mapping. (Azar, Engstrom, Graesser, & Comenetz, 2013).

2.2.2.3. Population relation with dwelling units

Population estimating with dwelling units is another largely practiced method. The multiplication of dwelling units and the number of person living gives the total population. By using categorical dwelling units and a different persons-per-dwelling unit ration, the population estimation for the total area could be easily calculated (Wu et al., 2005). A correlation method was applied between residential dwelling density classification derived from Landsat MSS and population density (Chen, 2002) and accuracy was found 85%. Karume et al. (2017) used GeoEye satellite images for identifying the dwelling units for population counting for the capital city of South-Kivu Province with 200m by 200m grid cells. A summary of population estimation studies using dwelling units is given below.

Table 2-1: Some major studies of population estimation using dwelling units

Authors	Year	Source
Green, N. E.	1956	Aerial Photographs
Porter	1956	Ground observation
Hsu	1971	U.S Census Tract
Dueker and Horton	1971	Aerial Photographs
Lo and Chan	1980	Field Survey
Lo	1989	Residential building from Raster
Webster, CJ.	1996	Residential dwelling units from VHR
Alahmadi et al.	2013	Landsat ETM+, ward-level census population and dwelling units

Source: Compiled by authors from (Wu et al., 2005)

2.2.2.4. Population relation with remote sensing pixel characteristics

Remote sensing data are one of the most useful resources for the population study as spectral reflectance of pixels has a strong correlation with population density (Wu et al., 2005). Hsu (1973) was the first person who introduced the idea of using pixels with multiple regression models (Lo, 1986). After him, numerous studies have been explored based on remote sensing satellite data for population distribution mapping since the 1970s (Li & Lu, 2016). A summary table is given below:

Table 2-2: Some major studies on population mapping using remote sensing pixels.

Authors & Year	Methods	Satellite Image
Iisaka & Hegedus (1982)	Calculation of interdependence of population with the spectral radiance	Landsat MSS
Lo (1995)	Regression between spectral radiance and population densities	SPOT
Webster (1996)	Regression model with spectral and textural measure	Landsat TM
Chen (2002)	Correlation between population and dwelling units	Landsat MSS
J. T. Harvey (2002)	Correlation between population and pixels	Landsat TM
Jack T Harvey (2002)	Expectation-maximization (EM) algorithm for iteratively calculating population on spectral indicators of pixels	Landsat TM
Vijayaraj et al. (2008); Liu et al. (2006)	Grey level Concurrence method (GLCM) for urban area extraction and population estimation	IKONOS & Quickbird
Lu & Li (2006); Wu & Murray (2007)	Residential impervious surface fraction estimation	Landsat ETM & MSS
Wang & Wu (2010); Joseph et al. (2012)	Geographically Weighted Regression (GWR) population and land use classes	Landsat ETM+
Alahmadi, Atkinson, & Martin (2013)	Regression analysis between density of dwelling units and built area	Landsat ETM+
Liu et al., (2006); Yang et al. (2012)	Markov Random Field (MRF)	google earth images
Linard, Gilbert & Tatem (2011)	Correlation between Global land cover data and population	AVHRR, MODIS, GLC2000, and GlovCover
Ural, Hussain, & Shan (2011)	Disaggregation of population based on extracted residential buildings	Aerial Images
Li & Lu (2016)	Impervious surface area (ISA) distribution	Landsat TM
Karume et al. (2017)	Dasymetric modelling	GeoEye
Tobergte & Curtis (2013); Xie et al. (2015)	Morphological building detection algorithm with Linear regression modeling	LiDAR point cloud

2.2.2.5. Population relation with other physical and socio-economic characteristics

There are other methods where various physical and socio-economic data are used to calculate, estimate or mapping the distribution of the population. The final product of those methods is either grid or census units and scale dependent. Tobler et al. (1997) reported on *World population in a grid of spherical quadrilaterals* (GPWv1) by calculating world population of 19000 subnational geographic units based on total population data of 1994. Following that, GPWv2 in 2000 also was produced based on the total population of 127000 subnational geographic units. GPWv3 in 2005 come out with an increased number of subnational geographic units of 400000 and finally, GPWv4 comes with more than 12500000 with various social data such as sex, age, urban/rural along with total population. All the above population product was produced

considering other physical phenomenon such as water area, hilly area, agricultural area, forest area etc. The final version of GPW has an accuracy nearly close to census units.

2.3. Population mapping at different aggregated levels

Previous population estimation studies focused on either country (Lu et al., 2006), regional (Sutton, Taylor, & Elvidge, 2010) or city scale (Joseph, Wang & Wang, 2012). Many developed countries can produce city scale population product as they have easy access to various data such as roads/streets, urban land use/land cover, very high-resolution imagery, detailed census data up to block or smallest census unit level (Li & Weng, 2010). This high-resolution population product plays a vital role in studying land use changes and change in environmental conditions (Li & Lu, 2016). The availability of high-resolution satellite images and various geospatial databases gave us the possibility to study global human population at high resolution gridded scale (Lioyd et al., 2017). Several gridded population mapping products have been produced in various scale such as Gridded Population of the world (GPW) in 30 arc second (1km) (Balk & Yetman, 2004), Global Rural-urban Mapping Project (GRUMP) in 30 arc second (1km) (CIESIN, 2011), LandScan Global in 5X5 minutes (Dobson et al., 2000), and LandScan USA in 3 arc second (~90 meter) (Bhaduri et al., 2007), WorldPop in 100-m X 100-m (Lloyd et al., 2017). These products were generated using different approaches. For example, GPW used an areal-weighted interpolation method to disaggregate population from census units to raster grid cells. The precision and accuracy of the final product produced through this method depend on the size of the input areal unit (Doxsey-Whitfield et al., 2015). To solve this problem, an alternative approach was introduced in GRUMP method. This approach relies on various land use/land cover datasets extracted from satellite images. Furthermore, other studies dedicated to population mapping started using various statistical methods with a large number of covariates derived from satellite images such as WorldPop population distribution dataset. Callegari et al. (2013) developed a combination of the theoretical, empirical and technical implementation of an agent-based modeling (ABM), where they used a high-performance computing (HPC) approach to study human population dynamics on a small spatial and temporal scale. Yao et al. (2017) introduced a framework for urban population distribution at building levels. Author firstly calculated points-of-interest (POIs) and real-time Tencent user densities (RTUD) with random forest algorithm and downscaled to grid level. Then, developed a building-population gravity model for population mapping at the building scale. WorldPop Project produced a 3 and 30 arc-second resolution gridded data for the world where various ancillary data were used like- transport networks, land cover, nightlights, precipitation, travel time to major cities, and waterways (Lloyd et al., 2017). The spatial resolution of the population product derived from all these efforts ranges from 100 meters to 1km. There is not enough research on population density at high spatial resolution scale like 5 meter/10 meter in developing countries.

2.4. Building extraction methods from VHR images

Buildings are main man-made urban features for a city. There is a robust correlation found between urban feature derived from the satellite image and high-resolution population distribution. (Zha et al., 2003). VHR satellite images can detect urban complexities and potentially reflected as a reliable source of urban features mapping (Ural et al., 2011). Various methods have been conducted to detect buildings using different methods from VHR images. For example, Salah et al. (2009) used Self-Organizing Map (SOM) on VHR images to generate attributes of buildings with a series of image processing techniques. A combination of OBIA and threshold-based approach was applied on VHR and LiDAR data to detect buildings, where the threshold values were set by Normalized Difference Vegetation Index (NDVI) and Normalized Digital Surface Model (nDSM), referring to the presence of vegetation and the height of buildings, respectively (Hermosilla et al., 2011). A combination of clustering and edge detection techniques were used to extract buildings from high-resolution panchromatic QuickBird images, where buildings were separated by selecting

histogram threshold in the cluster and they were refined by edge detection techniques (Wei, Zhao, & Song, 2004). Ok (2013), Li et al. (2017) and Ma et al. (2017) conducted a detailed study on previous research on building detection. Thereafter, the authors listed several methods for buildings detection including morphological features (MFs) (Pesaresi & Benediktsson, 2001), fuzzy pixel-based classifier (Shackelford & Davis, 2003), graph-based approach (Kim & Muller, 1999; Huyck et al., 2005; Katartzis & Sahli, 2008), Scale invariant feature transform (SIFT) and graph tools (Sirmacek & Unsalan, 2009), spectral textural (Miura, Midorikawa, & Soh, 2012), support vector machine (SVM) (Fauvel & Benediktsson, 2008; Koc-San & Turker, 2014), Morphological building index (MBI) (Huang & Zhang, 2012), conditional random forest (CRF) (Li et al., 2015). Despite this diversity of methodologies proposed for building extraction, none has so far proved to be effective in all conditions and for all types of data (Salah et al. 2009). Extracting buildings from VHR images with high accuracy remains a challenging task (Freire & Santos, 2012). Moreover, various remote sensing characteristics such as spectral range, number of bands, sensor types and spatial resolution play a very important role in detecting buildings. Furthermore, the image classification techniques vary depending on areas and complexities as every urban environment has its own unique spectral characteristics (Herold, Gardner, & Roberts, 2003).

2.5. Object-based image analysis for building extraction and population mapping

Population density as a social science phenomenon cannot be derived from satellite images directly. Nevertheless, satellite imagery can describe the urban morphology such as built-up or non-built up areas through pixels (Mennis, 2003). However, studying population in RS pixels is a challenging approach where identifying the corresponding units of observation and appropriate linkage between them plays an important role (Entwisle et al., 1998). People live in buildings and remote sensing technique can extract those buildings in pixels as objects. Furthermore, those pixels can be categorized overlying by plot (smallest land unit in Bangladesh considered as plot) boundary or census unit, which can easily help to study population. Figure 2-2 shows how pixels could be related to the population study. However, most of the time identifying each building inside the plot is very difficult for the highly complexed city in developing country.

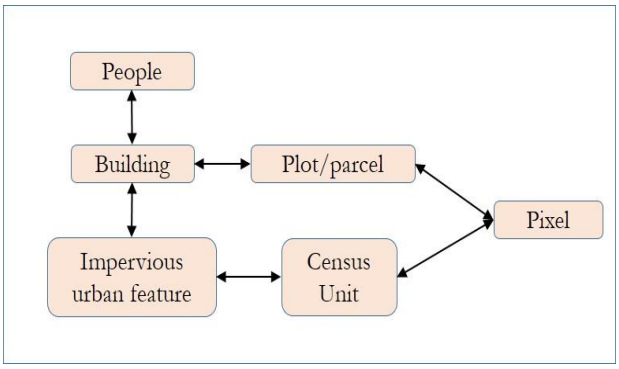

Figure 2-2: Links between various units of observation and population. Here, each element is connected to the related observational unit, which is shown by the bi-directional arrow. The figure gives an idea of the intermediate observational unit, which needs to be considered for population study through pixels (modified from Entwisle et al., 1998).

The urban and suburban area is continuously changing due to the construction of new infrastructures. Therefore GIS database needs to be updated accordingly. Traditionally updating task is done through photo interpretation or physical feature survey, which is a very expensive and time-consuming task (Hermosilla et al., 2011). OBIA method could be one of the effective solutions to detect the buildings from VHR satellite images and could minimize those constraints. Several images classification studies have demonstrated that OBIA method is an alternative to pixel-based classification methods (Blaschke & Strobl, 2001). The OBIA

called as a sub-discipline of GIScience by Hay and Castilla (2006), produce visually perceptible image objects from satellite images, which were typically represented by clusters of similar neighboring pixels that share a common referent or meaning (Chen et al., 2018). It assesses the spatial and spectral characteristics of a pixel during the classification process. OBIA can replicate visual interpretation of satellite images in both automated and semi-automated ways, which increases productivity and reduce labor and time consumption. The OBIA technique starts with a segmentation process where an image is divided into regions based objects with specific user-defined parameters (Hamedianfar et al., 2014). In this study, bottom-up image segmentation process was adopted (figure 2-3).

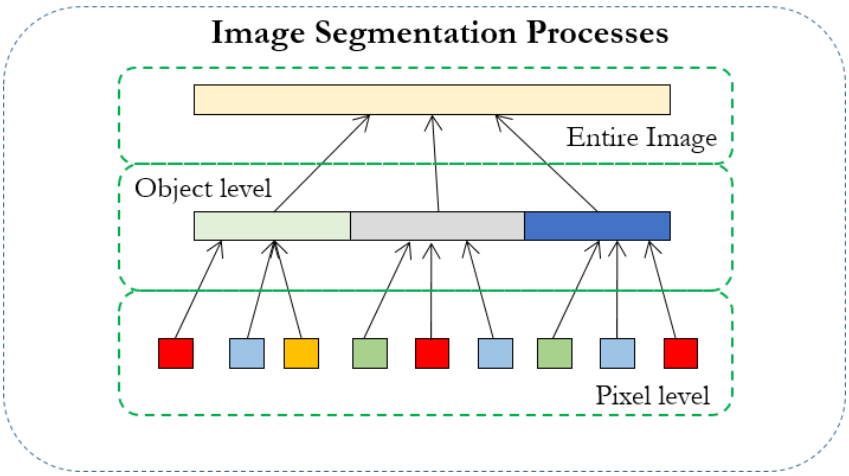

Figure 2-3: A generalized bottom-up segmentation processes (Lein, 2012).

Munoz et al (2003) describe advantages and disadvantages of different segmentation methods and state that there is no single perfect segmentation procedure to detect objects. Multi-resolution segmentation is the main basic process in the software eCognition to fragment VHR images at multiple scales. The scale of the segmentation controls the heterogeneity of image objects. Determining the optimal scale parameters is challenging task to represent exact objects (Baatz & Schäpe, 2000; Johnson et al., 2015). A lower value will give too many small segments, referred to as over-segmentation, and a higher value will give larger segmented areas, referred to as under-segmentation. In this study, the multi-resolution segmentation algorithm (Baatz & Schäpe, 2000) in eCognition developer software (version 9) was performed. Mismatches between the target object and over- or under-segmented area lead to irrelevant features (Troya-Galvis et al., 2015). As a result, both over and under-segmentation could reduce the classification accuracy. Therefore, the optimum scale for segmentation depends not only on the shape and size of targeted objects (Tian & Chen, 2007) but also on the complexity of the scene. Ziaei et al. (2014) found in his study that, the rule-based system can give better accuracy than support vector machine (SVM) or nearest neighbor (NN). OBIA with random forest (RF) or OBIA with Artificial Neural Network (ANN) also can have better results than rule-based system but they need lots of input variables and training samples. Rule-based classification is one of the common image classification methods, which works on user-defined rules (Ziaei et al., 2014). However, the rules development is the most challenging task to identify the target features as the characteristics of urban features vary from each other's (Zhang & Zhu, 2011). Sometimes brightness or other characteristics such as spatial, spectral, textural features of images objects with NDVI may form a rule set together. Furthermore, rule set building depends on human knowledge on the specific study area and specific characteristics and attributes of target features of that area (Hamedianfar & Shafri, 2015, Ziaei et al., 2014).

With the increasing availability of VHR (less than or 1m) such as IKONOS (launched in 1999), QuickBird (2001), OrbView (2003) or WorldView (2007) sensors, OBIA started to be used by remote sensing

community for a wide variety of applications (Blaschke, 2010). VHR images help to identify very small detectable objects which are larger than the spatial resolution of the image within heterogeneous urban areas. Sometimes it creates confusion on similar man-made objects in different places due to lack of contextual information of neighborhood pixels (Zhao, Du, Wang, & Emery, 2017). To deal with this problem, one should incorporate the context information of neighborhood pixels through OBIA (Förster, 2008). OBIA is being increasingly used in population study for extracting various ancillary data from VHR images, such as land use/land cover, built up area, buildings etc. For example, Lung et al. (2013) carried out a population disaggregation study based on buildings extracted from QuickBird images using OBIA in western rural Kenya. Extracted buildings were used as input data for population modeling. The model included the coefficient of buildings for five factors such as the proximity to roads, rivers/streams, markets, schools and slope gradient as ancillary data. A study in Riyadh, Saudi Arabia, was conducted using OBIA to derive residential land use class only and estimating population distribution (Alahmadi, Atkinson, & Martin, 2015). Another dasymetric mapping study used OBIA to classify the Pearl River Delta (PRD) mega-region in southern China into urban, rural and vegetation classes based on Landsat images (Wei et al., 2017).

3. DATA AND METHODS

3.1. Data

3.1.1. Census data

The population counts over *wards* in Dhaka City is equivalent to census blocks in other countries such as the United States, were collected from Bangladesh Bureau of Statistics (BBS). The tabular population data with other variables were also available. The following table 3-1 gives an overview of the area of Dhaka City.

Table 3-1: Summary of the ward-level areas.

Items name	value	Items name	value
Number of Ward	92	Min Area (sq. km)	0.14
Total Area (Sq. km.)	126.34	Max Area (sq. km)	15.05
Dhaka North (Sq. km.)	92.55	Dhaka South (Sq. km.)	43.38

The 2011 census data for Dhaka city were collected from BBS in a tabular format. There are 92 wards in Dhaka City Corporation divided into two part of the city. One is Dhaka North City Corporation (DNCC) and another is Dhaka South City Corporation (DSCC). According to BBS, Dhaka has the total of 6,970,105 population in 2011 (BBS, 2011a). The statistics of the population distribution of Dhaka city is given below in table 3-2.

Table 3-2: Summary statistics of the population of the Dhaka city.

Items name	value	Items name	value
Min pop^{n}	18170	1st Qu	46361
Max pop^{n}	196479	3rd Qu	96156
Mean pop^{n}	75762	Total pop^{n}	6970105
Median	65637	Male	3876586
Standard deviation	41474.61	Female	3093519

3.1.2. Very high-resolution satellite image (VHR)

We select WorldView-2 (WV2) image to extract the buildings from complex urban areas. WV2 has one panchromatic (450-800 nm) band with a resolution of 0.50 meter and eight multi-spectral bands (blue, coastal blue, green, yellow, red, red edge, NIR, NIR2) with a spatial resolution of 2 meters for enhanced multispectral analysis (Figure 3-1). Together they are designed to improve classification of land and aquatic features beyond any other space-based remote sensing platform (WorldView-2, 2017). The spectral characteristics of the image of WV2 of the study are given in table 3-3. European Space Agency (ESA) provided the WV2 image used in this research.

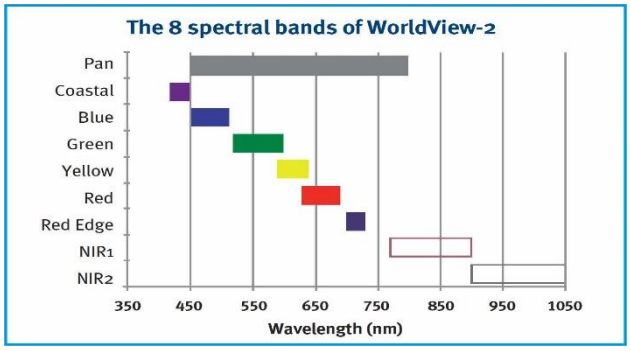

Source:https://content.satimagingcorp.com/static/galleryimages/worldview-2-satellite-spectral-bands.jpg
Figure 3-1: Various wavelength of the multispectral image of WorldView2 with 8 bands.

Table 3-3: Characteristics of the WorldView2 Image used in this research.

Acquisition date	: 2017-05-15	Resolution	
Image Clouds	: 7.0%	Panchromatic	: 0.50 meter
Image Nadir	: 15.6°	Multispectral	: 2.0 m
Bands	: 8	Image Extent:	
Max GSD	: 0.49m	Top	: 23.88444°
Sun Elevation	: 72.5°	Bottom	: 23.68083°
Max Target Azimuth	: 277.4°	Left	: 90.32556°
		Right	: 90.45389°

3.1.3. Land use data

The land use data were collected from Rajdhani Unnayan Kartipakkha (RAJUK), which is a Governmental organization, responsible for Capital of Bangladesh. The study area is consists of 126.34 km^2 and categorized with 15 land use classes (Appendix: 1). However, among these fifteen land use classes, people do not live in each land use class. Therefore, we considered all land use classes into two classes based on inhabitability-inhabitable and non-inhabitable. There are eight different classes found in the inhabitable class and all others classes were converted to one class called "others". 76.83% of total land is inhabitable and rest of the area (23.18%) is non-inhabitable. A summary of compiled land use with the area is given in table 3-4.

Table 3-4: Summary of land use of Dhaka city (both part), area in acres.

Types	Dhaka North City Corporation (area in acres)	% of Grand Total	Dhaka South City Corporation (area in acres)	% of Grand Total	Grand Total (area in acres)
Administrative	411.00	1.22	563.20	1.67	974.20
Commercial	648.20	1.92	532.60	1.58	1180.80
Educational	403.90	1.20	526.90	1.56	930.80
Manufacturing	533.50	1.58	63.30	0.19	596.80
Mixed Use	415.60	1.23	1281.10	3.79	1696.70
Residential	12744.60	37.74	5996.30	17.76	18740.90
Restricted Area	1430.10	4.23	203.40	0.60	1633.50
Service Activity	69.90	0.21	65.40	0.19	135.30
Others (non-inhabitable)	5218.70	15.45	2662.50	7.88	7881.20
Grand Total	**21875.50**	**64.78**	**11894.70**	**35.22**	**33770.20**

Source: Calculated from Vector file from RAJUK

3.1.4. Road data

The road network data in vector format (polygon) was also collected from RAJUK. The total length of Dhaka city for both parts is 1740 km where Dhaka North part has 1130 km and Dhaka South part has 610 km road length. The minimum width of the road is 2.5 meter and the maximum is 45 meter. This road layer was used into intersection process with extracted building later so that it removed the misclassified objects of the road to buildings.

3.1.5. Projection parameters

The Transverse Mercator (TM) projection (customized for Bangladesh) was used for all vector layers. All the analysis were done using this projection parameter. The maps were produced following this projection and the parameters are given below:

Table 3-5: Projection parameters used in analysis and mappings.

Projection	: Transverse Mercator	False_Easting	: 500000
Geographic Coordinate System	: WGS_1984	False_Northing	: -2000000
Datum	: WGS 1984	Central_Meridian	: 0.0
		Scale_Factor	: 0.9996
		Latitude_Of_Origin	: 0.00
		Linear Unit	: Meter

3.2. Methods

3.2.1. Image pre-processing

The image was obtained from an ortho-rectified and radio-metrically corrected by the DigitalGlobe, which included one single panchromatic band with a spatial resolution of 0.5m and eight multi-spectral bands with a resolution of 2m, which were further pan-sharpened. A high pass filter (HPF) method was used for pan sharpening multi-spectral bands as it could help to detect both building and shadow (Li et al., 2015). The resulting pan-sharpened image not only maintained the original spectral resolution from multispectral bands but obtained the same spatial resolution of the panchromatic band (i.e. 0.5m). Figure 3-2 shows the sample of panchromatic, multispectral band and the result of the pan-sharpened image. Spectral enhancement technique was not implemented here during image pre-processing.

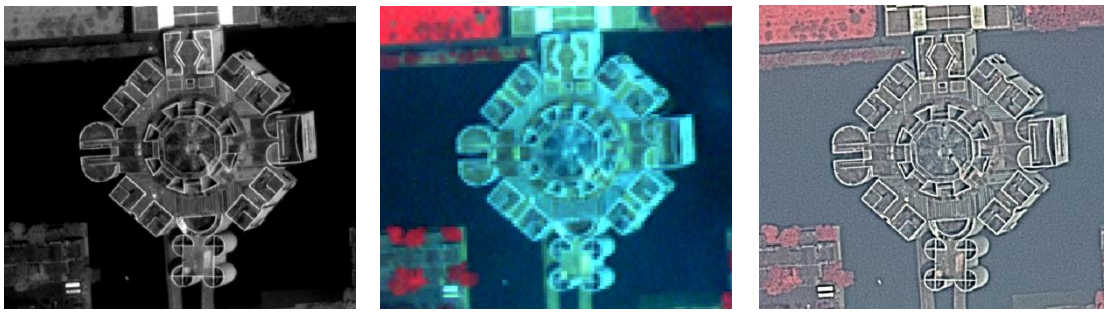

Figure 3-2: Result of pan-sharpened by HPF method. A panchromatic band with a resolution of 0.5m (left), multispectral bands with a resolution of 2m (middle), and the resulting pan-sharpened image with a resolution of 0.5m (right) through HPF method.

3.2.2. Object-based Image Analysis (OBIA) for buildings extraction

OBIA can incorporate not only spectral, but also textural and spatial information during the classification process, and therefore, it can contribute to distinguishing similar objects from the others (e.g. buildings, roads, etc.). Considering these advantages, in this study, a multi-resolution segmentation process and a rule sets were used in OBIA method to extract the buildings for Dhaka city. A detailed buildings extraction process is described in figure 3-3.

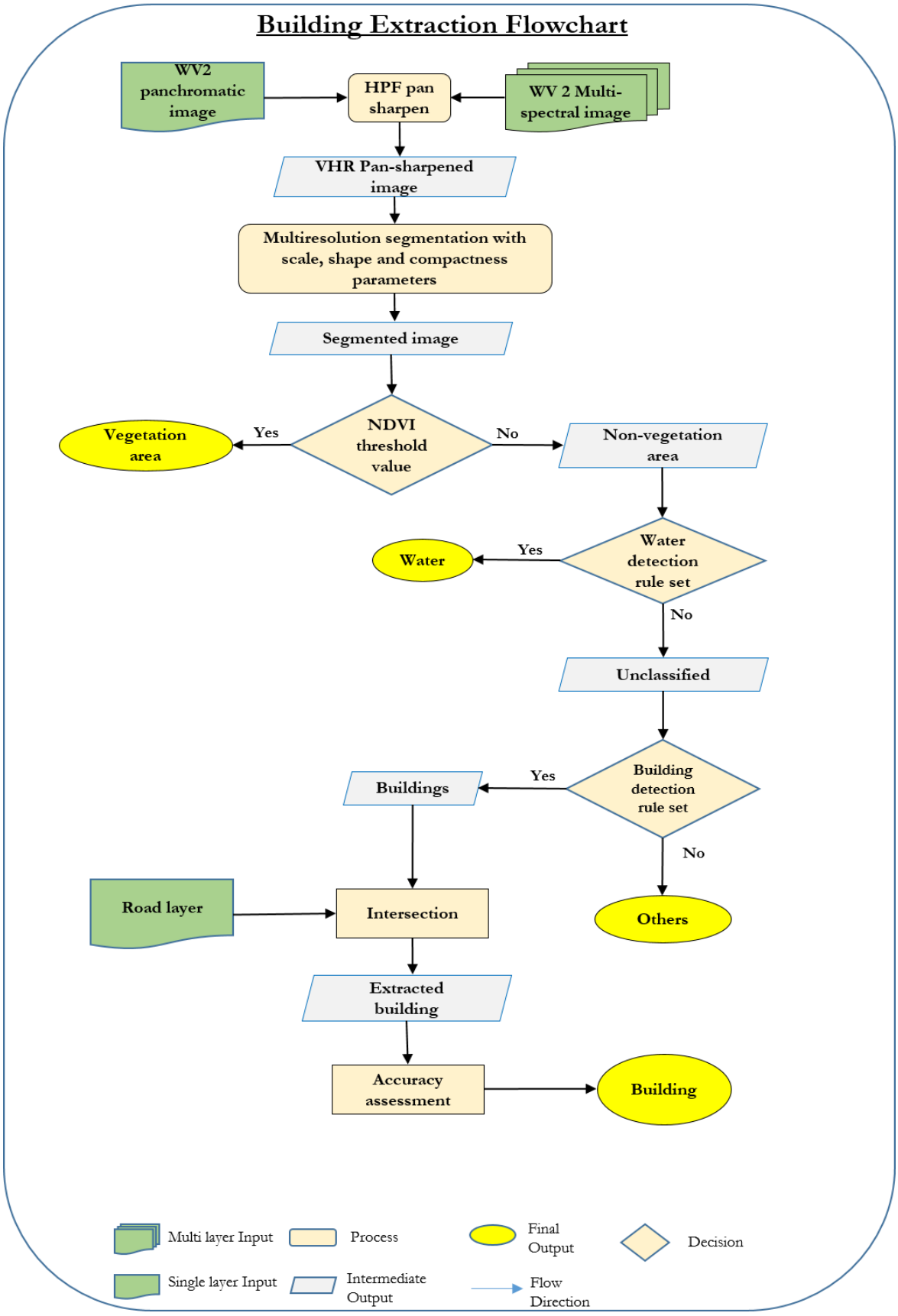

Figure 3-3: A detail methodological flow chart for building extraction process from WorldView 2.

3.2.2.1. Image segmentation process

The multi-resolution segmentation process starts with an iterative process of local optimization based on homogeneity of the created segments. The measure of homogeneity depends on two components - spectral and spatial component. The spectral homogeneity called as "*shape*", is defined by the spectral reflectance of the pixels within the segment. A lower value indicates the higher influence of color on the segmentation process. Since the color of building roof can play a very important role in detecting the building from the image, the value for *shape* was set to 0.2. Spatial homogeneity is based on two attributes – *scale* and *compactness*. Different *scale* parameters were tried including 10, 20, 30, 40, and 50 for segmentation, and finally, 30 was fixed by the visual interpretation of the segmentation results. Figure 3-4 shows the effects of different scale parameters on the same image of the study area.

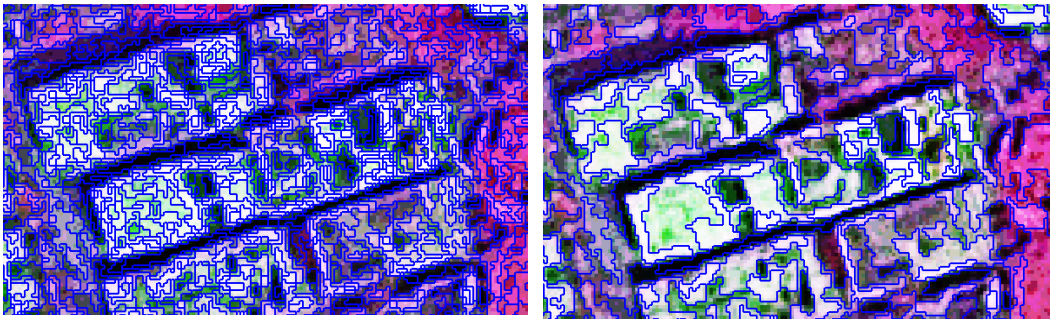

Figure 3-4: Segmented images (buildings) with various scale (left image 10, right image 30), shape and compactness parameters are 0.2 and 0.8 for both images respectively.

In addition, the *compactness* is defined by a value which indicates the closeness of objects to each other. A higher value of compactness means objects are more compact. The characteristics of buildings of the study area are more blocked and hence the value was set to 0.8.

3.2.2.2. Rule-based classification and rule-set development

In this study, buildings are the main target to extract. Buildings are very complex in size and have different textural character due to different spectral reflectance. Therefore, a hierarchical classification process was followed to classify the image into vegetation and non-vegetation area, then again non-vegetation area into the water, buildings and others classes (the remaining unclassified area). In this study, various indices/rules such as NDVI, Normalized Difference Water Index (NDWI) (Gao, 1996), Green band ration (RatioG), image brightness value (level of spectral radiance e.g., 2^{16} bit = 65536 level), mean spectral reflectance value from green (MeanB3) band within the segmented area and value of relation to building (closeness to previously classified building) were used during the development of rules set (Table 3-6 and Table 3-7). Finally, by defining these rules and constraints, the desired features classes were classified.

Table 3-6: The indices used for defining the rule set of OBIA.

Name	Formula	Descriptions
Normalized Difference Vegetation Index (NDVI)	$\frac{NIR1 - Red}{NIR1 + Red}$	To distinguish the vegetation from other classes
Normalized Difference Water Index (NDWI)	$\frac{Green - NIR1}{Green + NIR1}$	To identify the water bodies from other classes
RatioG	$\frac{Green}{Blue + Green + Red + NIR1}$	To identify the building's roof

Table 3-7: The image characteristics, which were used to classify different target object.

Parent class	Finer class	Rules and Constraints
WV2 image	Vegetation	0.23< NDVI
	Non-Vegetation	NDVI ≤ 0.23
Non-Vegetation	Water	0.1 ≤ NDVI < 0.15 AND 0.3 < NDWI < 0.4 AND 325 < brightness < 350 AND Number of pixel > 500
	Buildings	• 0.18 < RatioG < 0.32 AND 470 < MeanB3 <510 AND Brightness > 440 • 0.32 < RatioG < 0.36 AND 470 < MeanB3 <510 AND Brightness >390 AND Relation to Buildings = 1 • 0.42 < RatioG < 0.55 AND 470 < MeanB3 <510 AND 150 < Brightness < 390 AND Relation to Buildings > 0.5 • 0.32 < RatioG <0.68 AND 470 < MeanB3< 510 AND 150 < brightness < 460 AND Relation to Buildings > 0.8 • 0.1 < RatioG < 0.25 AND 510 < MeanB3 < 530 AND Relation to Buildings > 0.2 AND Brightness > 650
	Others	Unclassified

3.2.3. Accuracy assessment of building extraction

The accuracy assessment of extracted buildings was performed by comparing classification results with reference data, which were collected from the visual interpretation of the study image using a random sampling method. Congalton (1991) suggested to have 75-100 samples for each class if the image covers a large area or the classified image has a large number of LULC categories, such as more than 12 classes. Hashemian et al. (2004) found that accuracy results were stable for the large study area if the sample size was approximately 70 for each class. However, this study area covers a very large area with 136 sq.km and the image was classified into four classes (i.e., buildings, water, vegetation, and others), so the reference sample size was fixed at 400 in total and 100 for each class. The accuracy of the building extraction by OBIA was evaluated in terms of error matrices from overall, producer's and user's accuracies (Congalton, 1991), and kappa coefficient (Cohen, 1960).

3.2.4. Building types

The extracted buildings were used in the intersection process with existing generalized land use areas, which included nine categorical building classes with eight of them inhabitable (Appendix 2). Figure 3-5 showed an example of the output of intersecting extracted buildings and land use classes. In the next step, all categorical building types were intersected with wards so that we could calculate the area of each inhabitable buildings within the ward.

Figure 3-5: A generalized idea of intersecting extracted buildings area with land use classes for identifying categorical building area.

3.2.5. Population modeling

3.2.5.1. Choice of model

Now we have three types of polygonal data – building type, land use, and ward boundary with actual population. Population density over a ward is not accurate as it considers the whole area within the ward including road, open space, park, water body etc. To increase the accuracy problem we considered to use regression model. Therefore, we choose both Ordinary Least Square (OLS) regression and Geographically weighted regression (GWR) model to deal with land use and building type data. Therefore, four different regression models have been constructed to estimate the population over land use and/or building types, including 1) using OLS based on land use data (variable density of each land use class across wards), 2) using OLS based on building data (variable density of each building type across wards), 3) using GWR based on land use data (variable density of each land use class across wards), and 4) using GWR based on building data (variable density of each building type across wards). After accuracy assessment and comparison, the model with the best accuracy was adopted for the following dasymetric mapping to disaggregate the population to the cell.

We used population counts as dependent variable for all four models. The area of each building type data was used as independent variable while constructing both models - using OLS based on building data and using GWR based on building data. Again land data were used as independent variables while constructing both models - using OLS based on land data and using GWR based on land data. All the models give an estimated population based on the linear relationship between the dependent and independent variables. The following equations were used for both OLS models (using OLS based on building data and using OLS based on land data).

$$p_i = \alpha_0 + \alpha_1 * A_{adm} + \alpha_2 * A_{Com} + \alpha_3 * A_{Edu} + \alpha_4 * A_{Manuf} + \alpha_5 * A_{Mix} + \alpha_6 * A_{Res} + \alpha_7 * A_{Restr} + \alpha_8 * A_{Serv} + \varepsilon \quad \text{..... (3.1)}$$

Here, p_i denotes estimated population over ward, α_0 denotes as intercept value and ε denotes as residual error. And others $\alpha_{1.....8}$ are the coefficients of the regression equation, which is constant for each land type or building type and represents the rate of change of dependent variable (population) with the change of corresponding independent variable such as administrative, commercial, educational, manufacturing, mixed, residential, restricted and service related land use data or building type data respectively. The product of coefficient and specific land use/building type area data will give the population for that particular land use or building type within the ward.

The GWR model considers locally varying parameters through regression model where spatial relationships are hypothesized. While producing the estimated population based on land data or building data using GWR, it produces centroid points for each ward and calculates spatial weight based on the observations. The weights are calculated using a distance-decay function for assigning weights according to their distance of each ward so that near locations have more control than further positions. The following equations were used for both GWR models (using GWR based on building data and using GWR based on land data).

$$p_i = \beta_0 + \sum_{j=1}^{n} (\beta_j * A_{ij}) + \varepsilon_i \quad \text{..... (3.2)}$$

Here, p_i = Estimated population over ward *i*,
β_j = Coefficient for the building type *j* or land use type *j,*
A_{ij} = Area of the building type *j* or land use type *j* over ward *i,*
B_0 = Intercept
ε = Residuals
The range of *i* = 1, 2, 3,….92 and *j* = 1, 2, 3,…8.

3.2.5.2. Accuracy assessment of the models

In order to access the statistical accuracy of estimated population product among the four models, we need to compare the estimated population with the actual population of the wards. The Root Means Square Error (RMSE) is one of the most widely used indicators for the accuracy of the estimation. The difference between estimated and actual is called ward specific estimated error. Thereafter, this ward specific error was squared to eliminate the negative values and calculated the mean squared error for the whole Dhaka City. Finally, the square root function was used on this mean squared error to get the RMSE (Equation 3.3). This is how we calculated the RMSE for all four models - 1) building-based OLS model, 2) building based GWR model, 3) land use based OLS model and 4) land use based GWR model.

$$\text{RMSE} = \sqrt{\frac{\sum_{i=1}^{n}(P_i - \hat{p}_i)^2}{n}} \qquad \text{……..…. (3.3)}$$

Here,

P_i = Population for ward *i*,
$\hat{p}_i$ = Estimated population for ward *i*,
n = Number of wards.

The RMSE value may vary depending on the areal unit of the observational unit (Tapp, 2010b). To compare the variability among the different population models, we used another method, the coefficient of variance (CV). The CV is computed by dividing RMSE with the average areal unit. In this research, the CV is calculated dividing RMSE by the ward-specific average population within that specific ward. This CV was calculated for each model by using following equation (Equation 3.4).

$$\text{CV} = \frac{RMSE}{\overline{p_i}} \qquad \text{……..…. (3.4)}$$

Here,

$\overline{p_i}$ = Average population for each ward,

As the population is expected to vary across wards and building area is expected to be the more refined location of the population than land use area, so ranking of accuracy from high to low is calculated for each RMSE, CV, R^2 and adjusted R^2. These ranks gave us which one is more important for future population estimation studies.

3.2.5.3. Population disaggregation

In order to disaggregate the population to a high-resolution grid cell, a dasymetric model was proposed. A detail flowchart of dasymetric modeling is given in figure 3-6. Initially, the building type data were converted to a 5-meter resolution raster cells to transfer the population data from irregular spatial area to regular grid

raster cells. It is assumed that population is equally distributed within each building type in a ward. This resolution of the raster cell will be the final output of the dasymetric model. The selection of 5-meter resolution was based on the spatial characteristics of buildings of Dhaka City and to consider the small buildings of the study area. Any cell larger than 5-meter resolution may lose the smallest building information during the data transformation from vector to raster format.

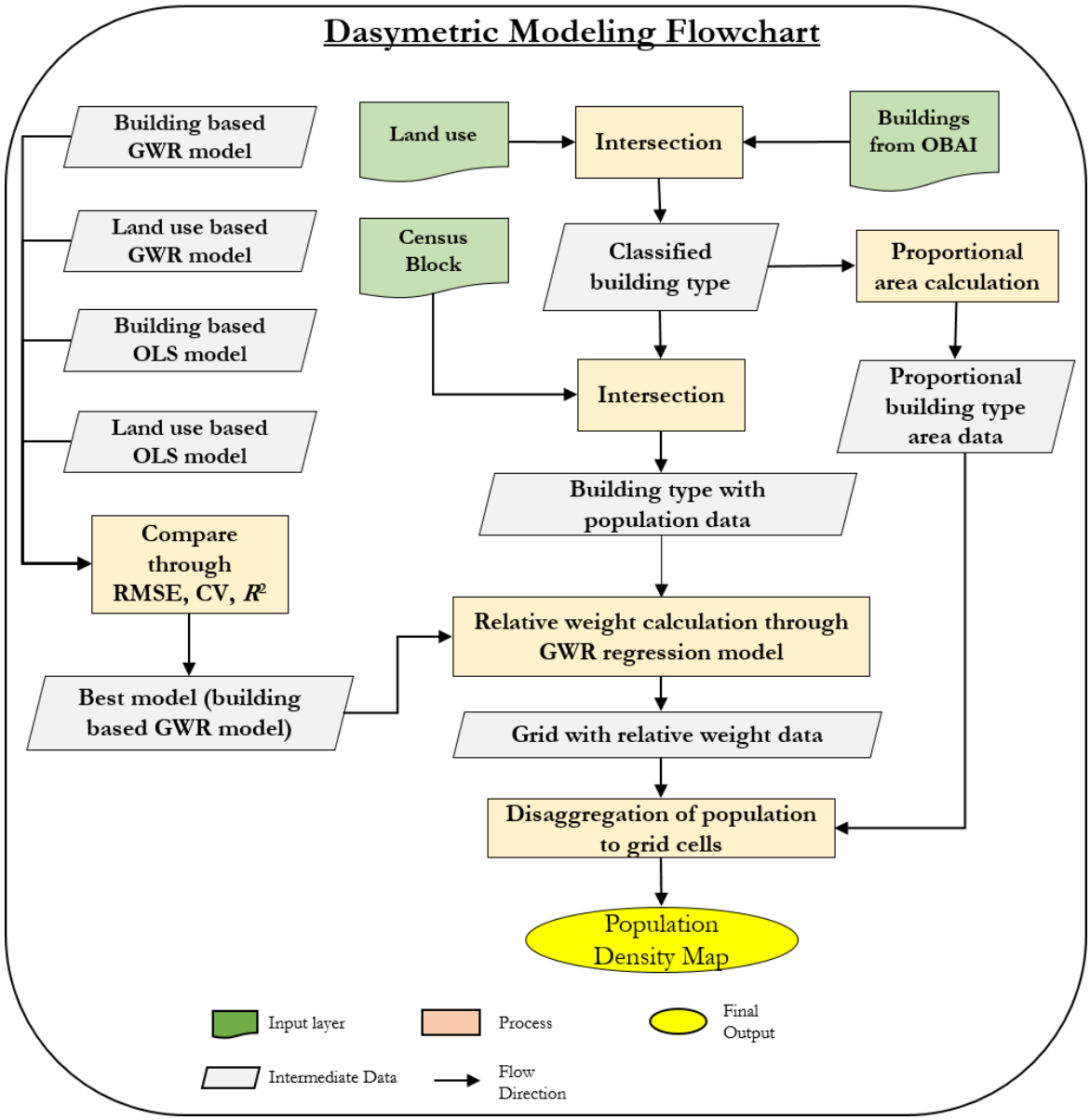

Figure 3-6: Flowchart for dasymetric modeling for the study area.

The population of each ward was distributed to a cell in each building type based on two factors: (1) the relative weight of population among the building types within the ward; and (2) the expected population of each building type within the ward. Firstly, In order to determine the relative weight the building based GWR model was used (Equation 3.2). The ward specific total population was used as dependent variable and building type areas were used as independent variables. The model returned with the estimated total population (p_i), constant intercept (β_0), coefficient (β_i) for each building type *j* and the residuals (ϵ_i) within the ward (*i*). The coefficient value multiply by corresponding specific building type area ($\beta_j * A_j$) gives the

estimated population (P_{ij}) for each building type (j) over ward (i). The estimated population of building type j in ward i divided by estimated total population for that ward gives the proportional population for that building type which was termed as Relative weight (R_w) of population and calculated by following equation.

$$R_{w_{ij}} = \frac{P_{ij}}{T_{P_i}} * 100 \quad \text{..... (3.5)}$$

Here, P_{ij} = Estimated population for each building type j in ward i,
T_{Pi} = Estimated total population for ward i,
R_{wij}= Relative weight of population for each buildings type j in ward i.

The higher relative weight value means more population for that particular building type than the other within the ward. This calculation is necessary considering that, the difference in population among the same building types varies from ward to ward. Thereafter, a raster layer was created with the relative weight value into 5-meter grid cells.

Secondly, in order to calculate the expected population for each building type over each ward, two things are needed. One is a proportional area of each building type within the ward and the relative weight. The proportional area of each building type is calculated by dividing individual building type area with the total building area of each ward. The following equation was used to calculate the expected population for each building type. Therefore, the expected population was rasterized into 5-meter grid cell for further use.

$$E_{P_i} = \sum_{j=1}^{n} R_{w_{ij}} * P_{A_{ij}} \quad \text{..... (3.6)}$$

Here, E_{P_i} = Expected population of ward i,

$R_{w_{ij}}$ = Relative weight of population for each building type j in ward i, and
$P_{A_{ij}}$ = Proportional area of each building type j in ward i.

Finally, to disaggregate the population to each cell, the following equation was used. Here, the product of ward-specific population (P_i) and relative weight (R_{wij}) will give the absolute population for each building type within the ward. Therefore, the value was divided by the product of total area and expected the population of that ward. the result was multiply by 25 as the cell size would be 5X5 meter grid cell. The result will give the estimated population density per cell. The equation is given below:

$$p_{ij} = \frac{(R_{w_{ij}} * P_i) * 25}{E_{P_i} * A_{T_i}} \quad \text{..... (3.7)}$$

Where,

p_{ij} =Estimated population density per cell over the building type j in ward i,
R_{wij} = Relative weight of population for each buildings type j in ward i.
P_i = Total population in ward i,
E_{Pi} = Expected population of ward i,
A_{Ti} = Total building area of ward i.

However, this population density per cell is not the actual rather it gives an idea of population density distribution among each building type within the ward. The aggregation of the population density of each cell within the building type and ward will give the total population counts of that ward. ArcGIS (version 10.5) was used to calculate the whole dasymetric mapping of the study area.

3.2.5.4. Accuracy assessment of population disaggregation

The accuracy assessment of the dasymetric model was done by calculating the RMSE and mean CV of population counts. The final product of the dasymetric model gives the population density per 25 square meter grid cell as the resolution was fixed at that level. Therefore, multiplying the population density with cell counts for each building type within the ward and summed the value will give the total estimated population for each ward. Calculating RMSE (equation 3.3) from the estimated population from the dasymetric model and actual population and comparing the RMSE value with previous four models will give an idea of the accuracy of the population disaggregation.

4. RESULT AND DISCUSSION

4.1. Accuracy assessment of the building detection

The standard value of accuracy is 85 % and nowadays this value is used widely in thematic mapping through image classification (Congalton & Green, 2009; Foody, 2008). The classification result is shown in table 4-1, where the overall classification accuracy is 77.75%. The average producer's accuracy for the classification was 81.31% and average user's accuracy was 77.75%. Vegetation has highest accuracy value in both producer's and user's accuracy with 100% and 96 % respectively. This means OBIA has a high potential to extract the vegetation area from VHR image with NDVI indices and segmentation with a certain scale. The next highest accuracy was water with 92.98% though the user's accuracy shows very poor of 53%. As mentioned earlier, there was some confusion between water and other urban features such as buildings and roads, which reflected on this matrix. Out of 100 samples 47 number of samples (11 samples in buildings and 36 samples in others) we misclassified as others category. The reason behind that is the materials of building roofs. Every building has a water tank on top of the roof, which sometimes overflows and fills with water. In addition, the buildings, which besides another tall building may affect with shadow. The shadow and water reflect very low same as water and caused confusion between water and buildings.

Table 4-1: Classification results for the OBIA of Dhaka City.

		Reference data					
Classification data	**Class Name**	**Buildings**	**Others**	**Vegetation**	**Water**	**Total**	**User Accuracy (%)**
	Buildings	**85**	15			100	85
	Others	19	**77**		4	100	77
	Vegetation		4	**96**		100	96
	Water	11	36		**53**	100	53
	Total	**115**	**132**	**96**	**57**	**400**	
	Producer Accuracy (%)	73.91	58.33	100.00	92.98	**Overall Accuracy 77.75 % Kappa Coefficient 0.76**	

The producer's accuracy achieved for buildings was 73.91% and user's accuracy was 85%. The value of the producer's accuracy metric is relatively low due to some reasons. Firstly, the spectral reflectances of building's roofs were misclassified with roads and sometimes with water bodies because the building's roofs are made of concrete and the brightness were very low. The various parameters which were used for buildings detection such as brightness, mean band 3 value, green band ratio did not perform well enough as the reflectance characteristics of the buildings were very close to other urban features such as parking areas, bare ground, roads etc.

Secondly, Dhaka city has a practice of roof gardening which increased the challenge of building's roof identification as they were categorized as vegetation area. Figure 4-1 shows examples of roof gardening from the city.

Figure 4-1: Some nature of roof gardening on top of the building's roof in Dhaka City. Source: left image (Karim, 2017), right image (Jahan, 2016).

Furthermore, the accuracy of building detection depends on the parameters of multi-resolution segmentation during the building detection process as well. These parameters such as scale, shape, compactness were set in trial and error method through visual interpretation of the result and applied over the entire study area at once. Sometimes the buildings were over-segmented or under-segmented during the segmentation process (figure 4-2). The rule worked very well on buildings of some part of study area but it got worse on another part by either over-segmenting or under-segmenting the objects. This error is called segmentation error. This error decreases the accuracy of building detection.

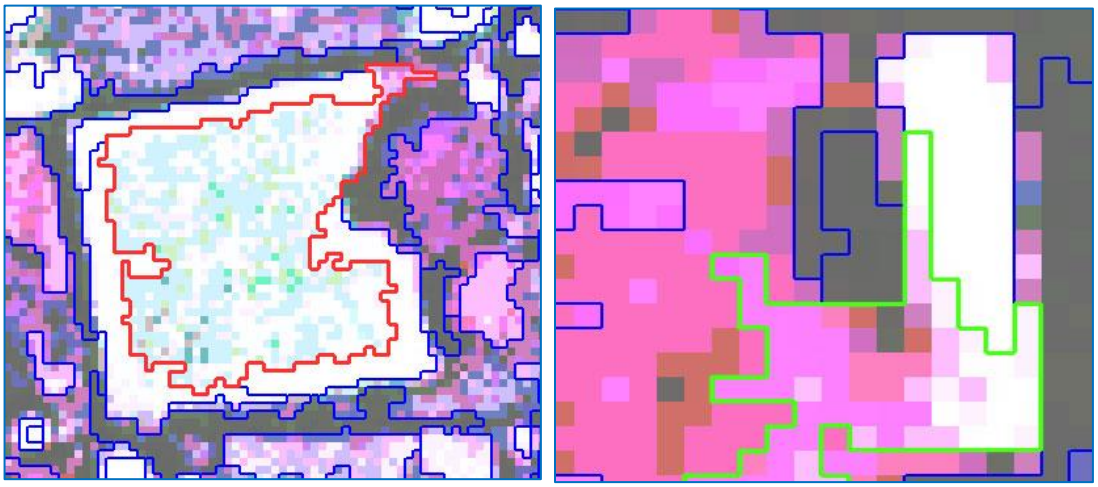

Figure 4-2: Visualization of over-segmented and under-segmented error of building detection. Left image: red line corresponding to over-segmentation result, whereas the whole white color represents the building. Right image: green line corresponding to under segmentation result, whereas some portion of the building (white color) was merged with other urban features (purple color).

Finally, the geometrical shape of the building was not as perfect as the real object. The rule set was design based on spectral and spatial characteristics such as a number of pixels and neighborhood pixels of the objects from the image. The rule set performed on entire study area at once and may have an error for detecting building in a perfect shape. These geometrical shape of the buildings caused the error for calculation of building area.

The main target for this OBIA was building's roof identification, whereas the remaining classes were categorized as "others" class. The producer's accuracy for this class was very poor with 58.33%, which indicates the complexity of study area. Some of them were misclassified as roads, buildings, and water because of similarity in their spectral reflections. As a consequence, it was a challenging task to separate

them from buildings. Therefore, the ancillary data road layer was used to separate them from buildings and marked as others category.

The overall accuracy with 77.75% and kappa coefficient with 0.76 indicate the satisfactory result for a complex city like Dhaka city. Sometimes various communities produce maps with low accuracy to fulfill the specific demand or fit for purpose. This low accuracy may be accepted in remote sensing considering the complexity of the study area (Foody, 2008).

4.2. Building use categorization

The buildings were exported from eCognition software, as vector layer used in the further process. As we know, the uses of buildings cannot be categorized from the satellite image as the image is the visual perception of physical properties of an object from the ground only. Therefore, the extracted buildings areas were intersected with land use classes for identifying the uses of the building classes. The total building area of Dhaka North City Corporation (DNCC) was found 30.84 km², where inhabitable buildings area was 16.26 km² and the building area of Dhaka South City Corporation (DSCC) was found 17.63 km², where habitable buildings area was 10.51 km². The total building area of Dhaka City was found 48.47 km², where total inhabitable buildings area was 26.78 km². Table 4-2 shows the detail of extracted buildings statistics and appendix 2 shows the ward specific building area and inhabitable buildings area statistics, which is found from VHR image through OBIA.

Table 4-2: Percentage of inhabitable and non-inhabitable building area in context to the total land area (in acres) of Dhaka City.

Inhabitability	Building type	Dhaka North City Corporation	Dhaka South City Corporation	Total	Percentage of Grand Total
Inhabitable	Administrative	14.23	73.32	87.55	0.26
	Commercial	162.36	119.84	282.20	0.84
	Educational	69.04	79.92	148.96	0.44
	Manufacturing	96.22	31.03	127.26	0.38
	Mixed	133.18	485.25	618.43	1.83
	Residential	3455.32	1778.57	5233.88	15.51
	Restricted	77.23	21.60	98.83	0.29
	Service related	11.46	7.94	19.41	0.06
Non-inhabitable	Others	17846.82	9292.57	27139.39	80.40
Grand Total		**21865.85**	**11890.05**	**33755.90**	**100.00**

The accuracy of categorizing the buildings depends on the LULC data, which was collected previously. The LULC data was generalized and it is obvious that the generalized LULC missed the small classes within the large area. Subsequently, it affects the building type classification.

4.3. Accuracy assessment of population modeling

The accuracy of population modeling for four different types of models were carried out through RMSE and CV. The table 4-3 shows the comparison of the models among 1) building based GWR model, 2) building based OLS regression model, 3) land use based GWR model and 4) land use based OLS regression model. The figure 4-3 shows the population density distributions created from four different models to visualize the differences among them. The RMSE of model 1 shows the better value than model 2. On the

other hand, the RMSE of model 3 is better than model 4. That means RMSE of GWR model for both buildings based and land use based are better than OLS regression models. However, among all four models the building based GWR model shows the best result. Details RMSE over each ward was shown in appendix 5. Figure 4-3 shows the comparison density map produced from different models.

Table 4-3: Comparison of accuracy of four different models based on RMSE, CV, R^2 and adjusted R^2.

Model No	Model Name	RMSE	Mean CV	R^2	Adjusted R^2	Rank
1	Building based GWR model	19106	0.183	0.78	0.72	1
2	Building Based OLS regression model	25676	0.253	0.63	0.59	3
3	Land use based GWR model	20160	0.186	0.76	0.69	2
4	Land use based OLS regression model	26259	0.266	0.59	0.55	4

In this case, we need to compare the variability of population among these models through CV. CV value not only differs from model to model but also differ according to the position as well. From the comparison based on CV, building-based GWR regression model shows the best result than any of the other models. Even though, the R^2 and adjusted R^2 shows the best result for the building based GWR regression model. After ranking from high to the low value of R^2 and adjusted R^2 and low to the high value of RMSE and mean CV, building-based GWR regression model shows the suitable model for population distribution mapping.

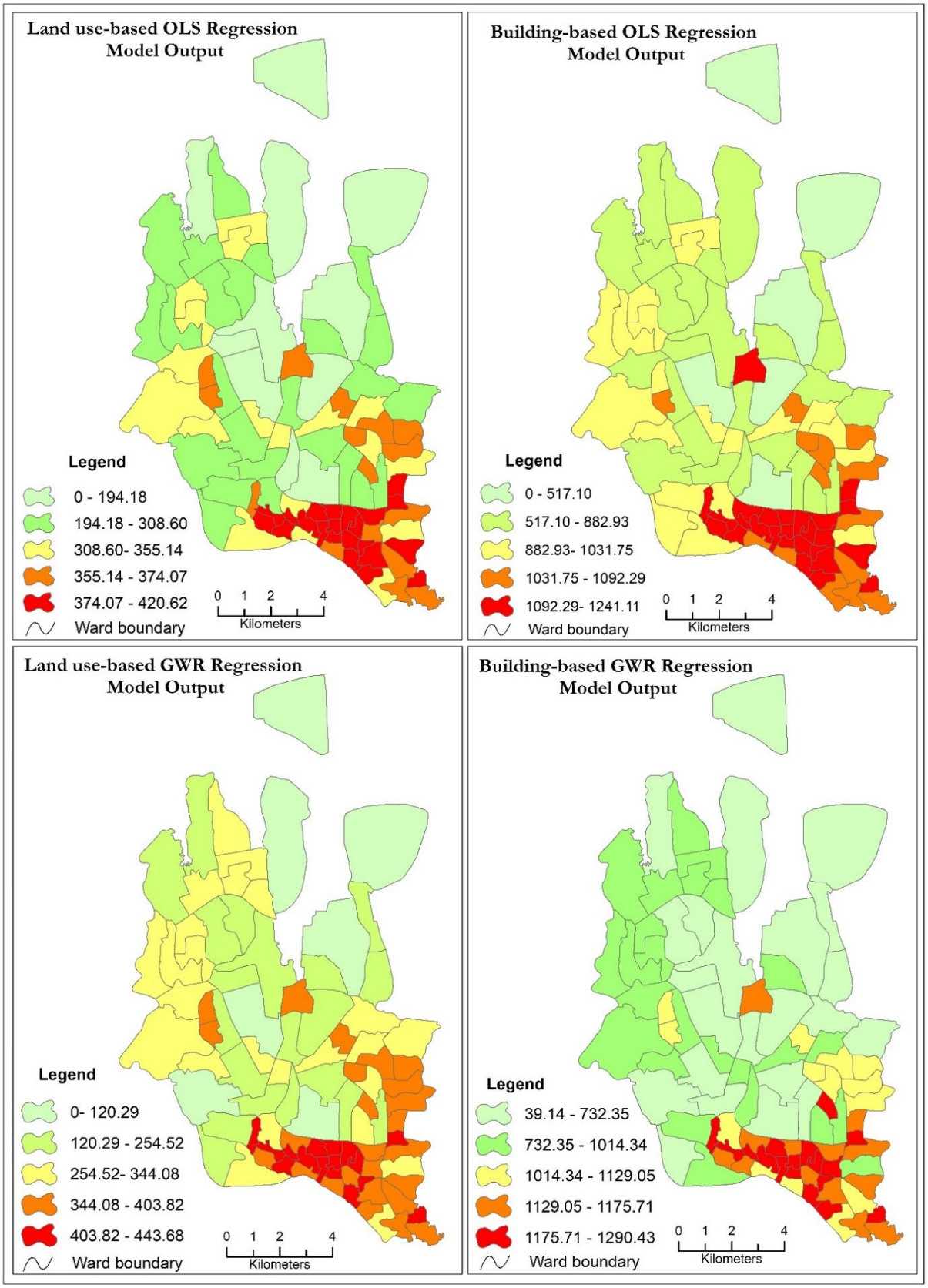

Figure 4-3: Population density distribution map of different model's outputs. The class intervals were calculated following geometrical calculation and the density was calculated in areal unit of Acres.

4.4. Relative weight calculation

The important part of the dasymetric mapping was the uses of proportional population of individual building type within the ward as we don't have population data against any lower level of administrative units. Building based GWR model gives the proportional population for each building type within the ward. Figure 4-4 shows the summary statistics of the relative weight of population for all building types. It was found that one ward from Dhaka North and six wards from Dhaka South City have full of 100% in residential building type. That means all the population of that ward live in residential building type and in that ward there is no other building type was found. In addition, most of the highest relative weight of population shows for residential building type. Rest of the category shows a similar distribution of relative weight except the manufacturing building type. It shows the lowest relative weight. Appendix 3 shows the detail individual ward specific relative weight of population for each buildings types of the study area. Some of the cells show null value, which means the particular building type, is not available in that ward. Errors in land use category may create imperfections in calculating relative weight of population as the land use was generalized.

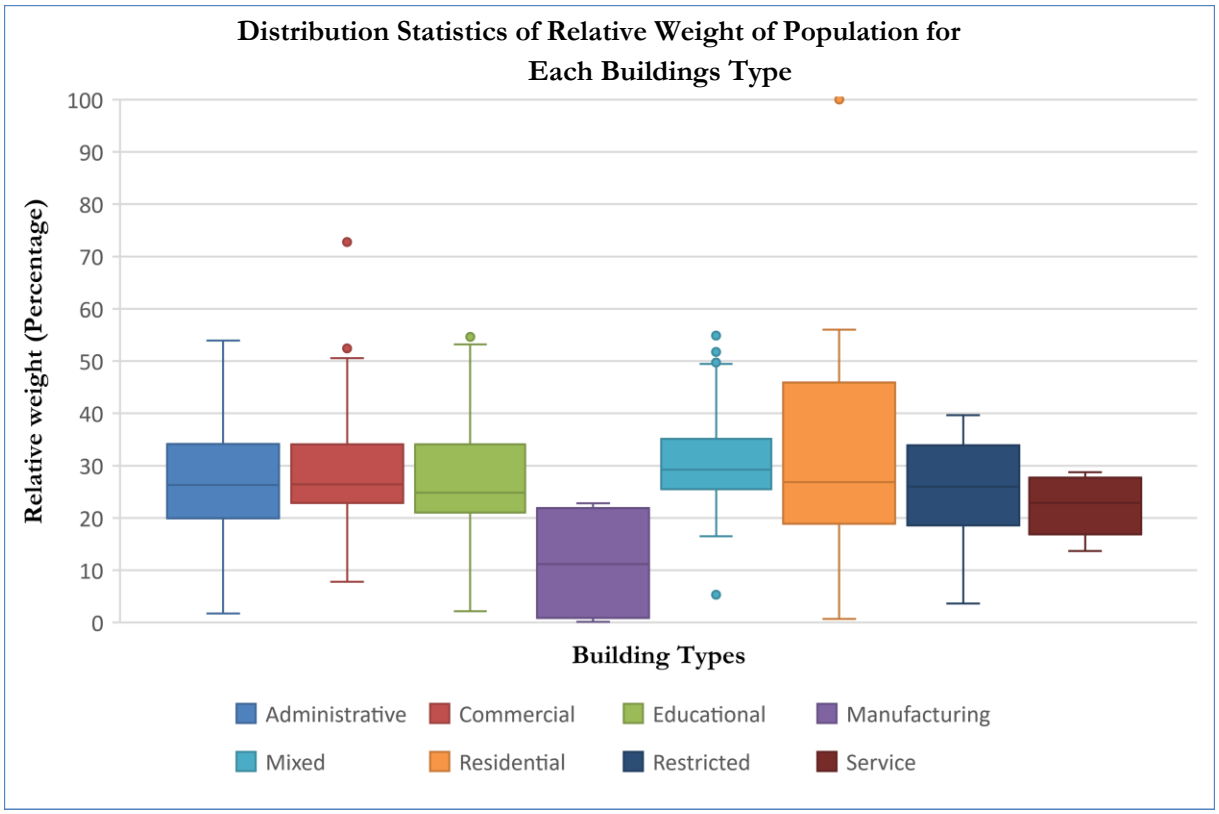

Figure 4-4: Statistical description of the relative weight of each building type.

4.5. Population disaggregation

Figure 4-5 shows the output of the dasymetric mapping of the study area. The building's area in raster grid is significantly detailed as they were produced in 5 X 5-meter spatial resolution and population were disaggregated upon those grids. Figure 4-6 shows the output of the choropleth map of Dhaka city, which was produced the total population divided by total ward area. The result of both maps shows the significant difference in population distribution and value as well. The dasymetric mapping works such a way that, the population is disaggregated within the census unit according to inhabitable building types and produce grid cells of the study area. In addition, the vector layer shows the homogeneous population distribution, whereas the raster grid cell has more concentrated population distribution (Mennis, 2003). However, in this study

area to create more accurate population distribution map, eight building type area were used in dasymetric mapping.
Appendix 4 shows the population density of Dhaka city through the dasymetric model. The dasymetric output gives a different population density distribution of the study area. As an example, Dhaka South City ward number 36 (DSCC36) has an area of 221786.43 sq. meter. The traditional choropleth map shows the population density of 2.95 people per 25 sq. meter cell considering the whole area of the census unit. However, the census unit has an area of 74123.95 sq. meters (33.42% of that census unit) buildings area extracted from VHR image with five types of building type (administrative, commercial, educational, mixed and residential)(Figure 4-7). The dasymetric mapping shows five different population density considering different types of building types such as administrative with 8.99, commercial with 9.33, educational with 9.08, mixed with 8.85 and residential with 9.24 person per 25 sq. meter area (Figure 4-8). Moreover, 66.80% land area of that census unit is used as other land use category where people do not live. Here we see that the commercial building type is highly populated than the others. The average population density for the ward is 9.10 per cell. This distribution gives a different scenario and better understanding than choropleth mapping.

Population density is highly correlated with the residential land use or building type (Li & Lu, 2016). However, in an urban context, every urban area has its own nature of land use classes with population distribution. Sometimes there is no clear boundary of a residential area or all are in mixed land classes, as the city grows in an unplanned way (e.g. Dhaka city). Consequently, population density may vary from residential areas to any other areas such as we found in this study in mixed or commercial building types.

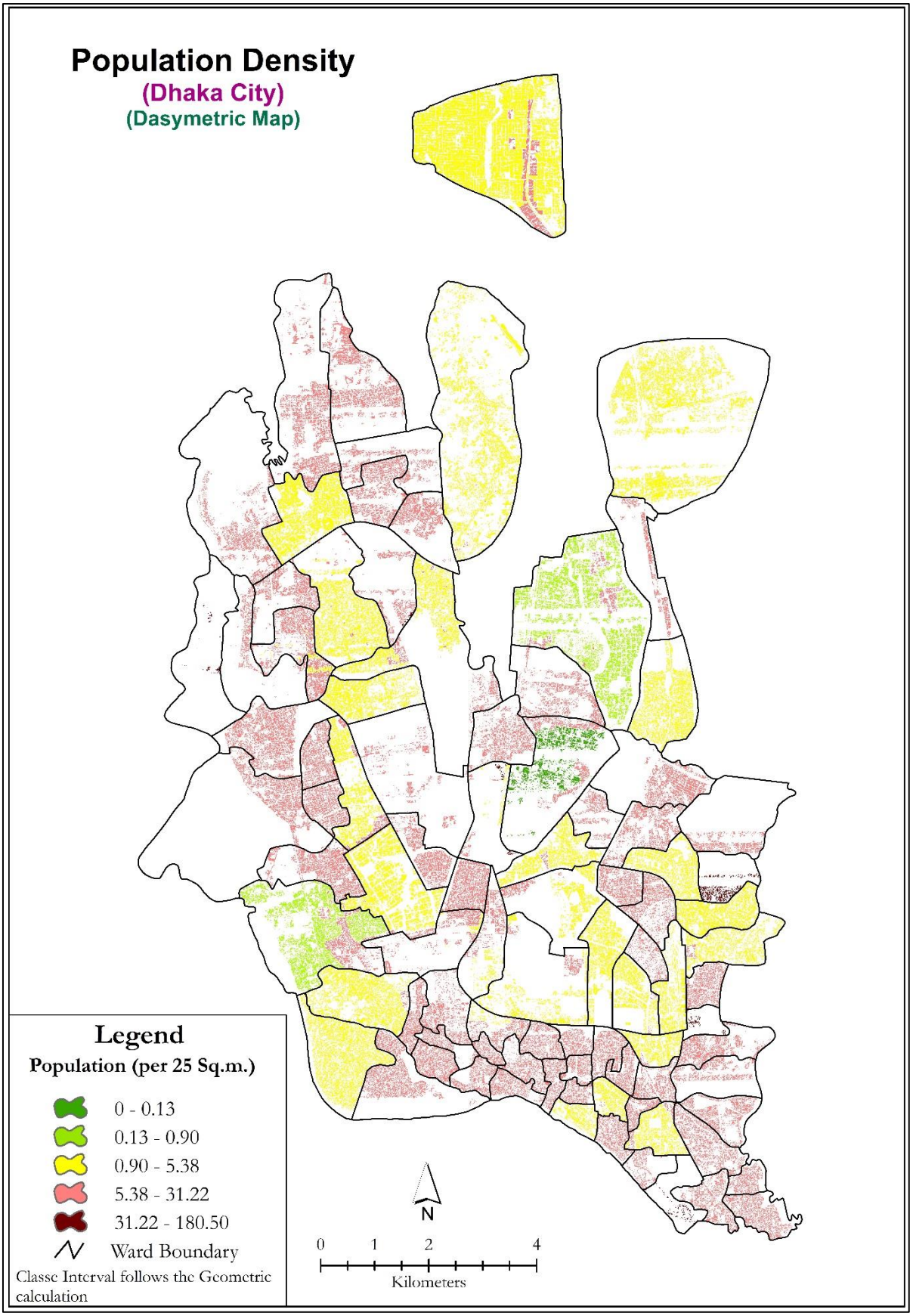

Figure 4-5: Final output of Dasymetric Mapping for Dhaka City.

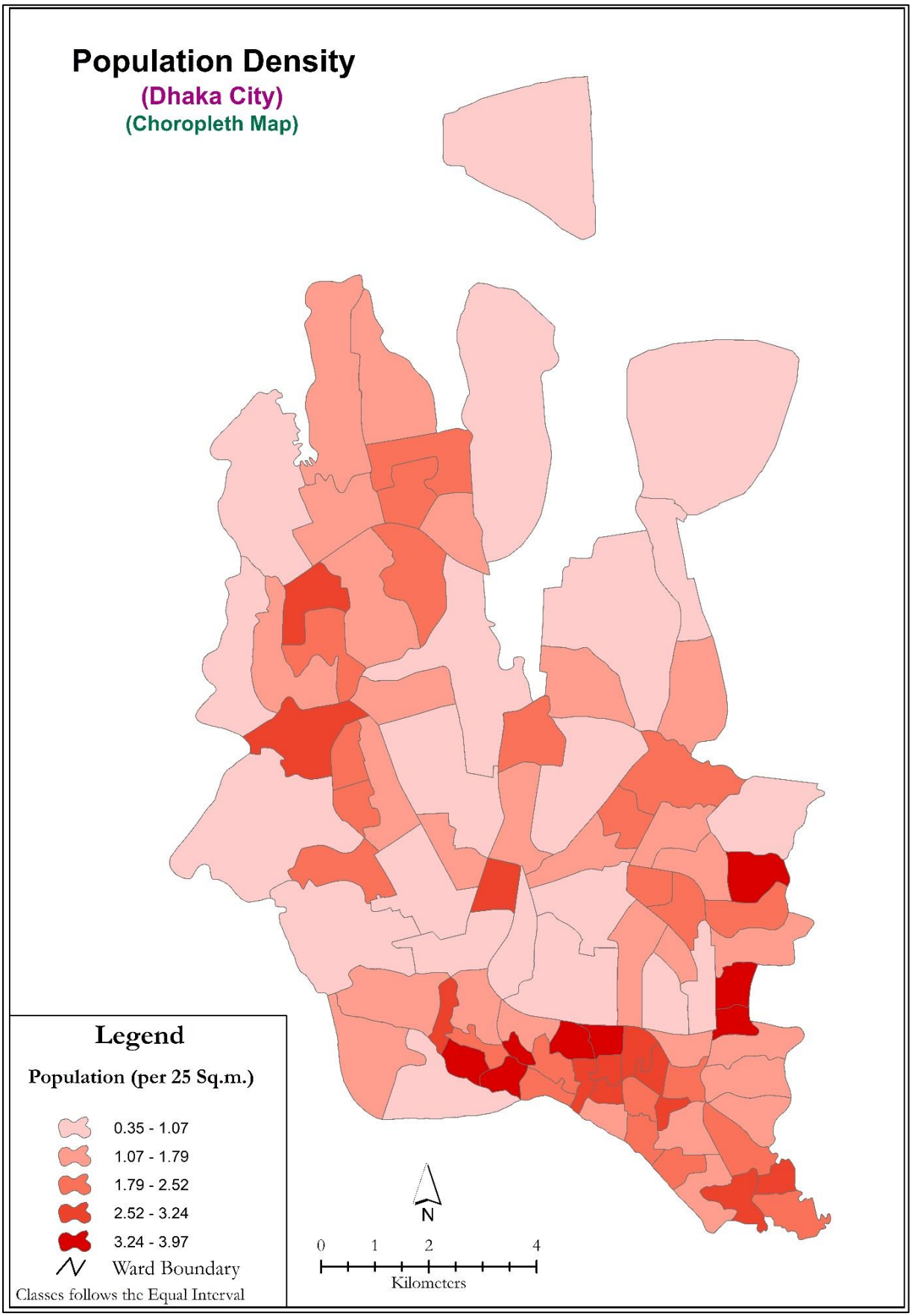

Figure 4-6: Traditional Choropleth map of the Dhaka City.

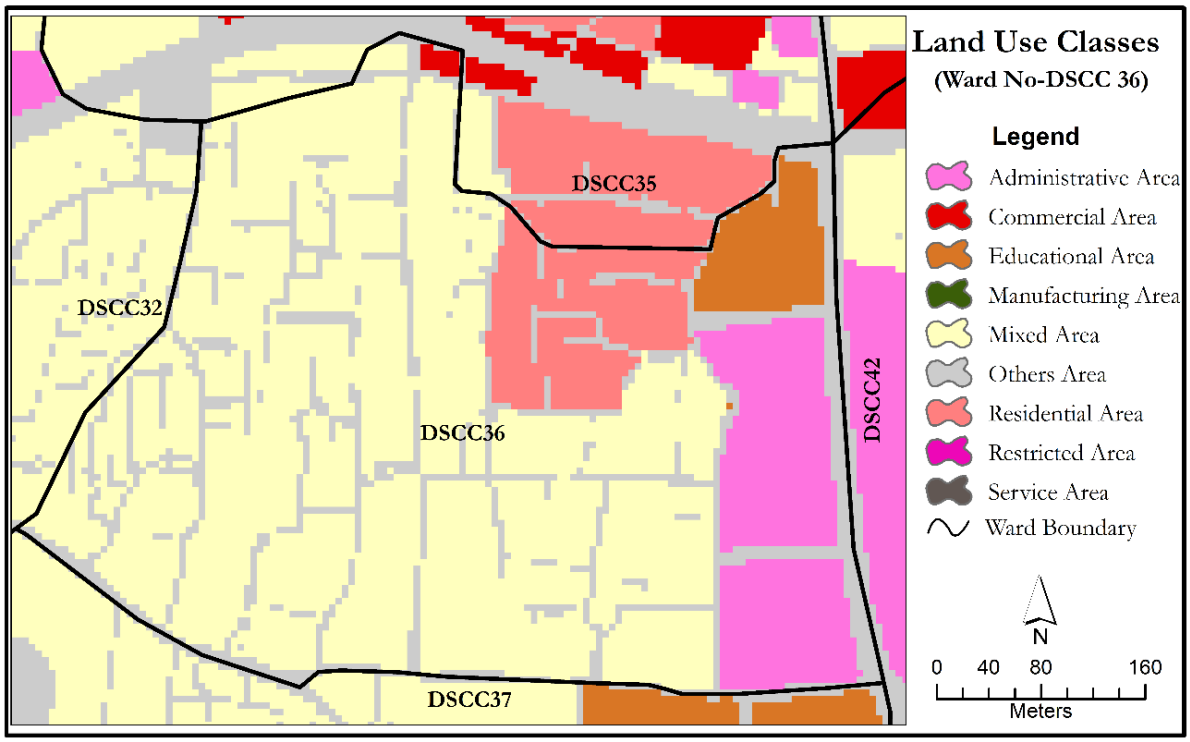

Figure 4-7: Raster-based land use map of sample ward Dhaka South 36 (DSCC36).

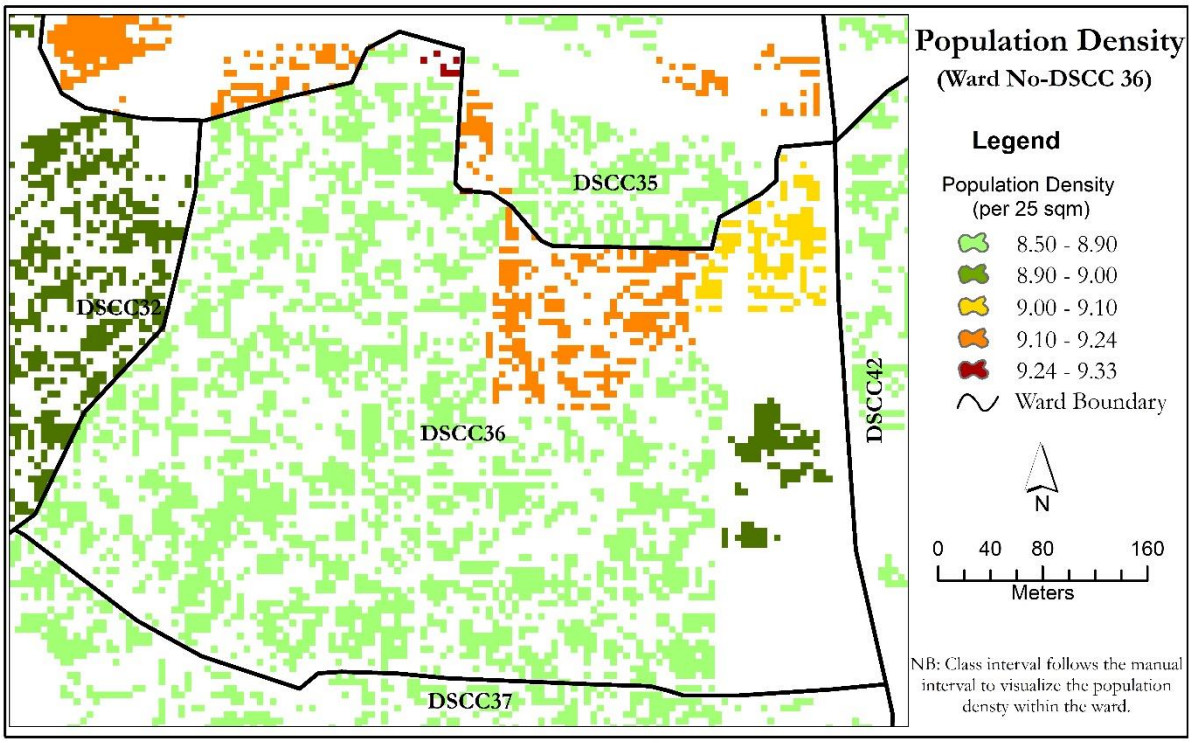

Figure 4-8: Dasymetric mapping of sample ward Dhaka South 36 (DSCC36).

.

4.6. Population density statistics

The population density result was calculated against 25 square meter raster cells, as the raster cell was produced in a 5 X 5-meter resolution grid. The total number of raster cells for each building type multiplication with 25 square meters represent the total population count in that particular building type, which was derived from the relative weight of the dasymetric model. The highest population density 177.94 per cell was found in mixed-use building type in DNCC9 and the lowest 0.1 per cell in manufacturing building type in DNCC24. The distribution of the population density for each building type shows a variation in range. A detail descriptive statistic of the population density distribution is given in table 4-4. Appendix 4 shows the detail population density for each building type within the ward.

Table 4-4: Descriptive statistics of the population density of the study area.

Land use Classes	Max	Min	Mean	Standard deviation
Administrative	19.17	2.87	8.12	3.60
Commercial	175.15	2.94	18.08	22.25
Educational	167.23	1.86	13.87	20.09
Manufacturing	10.73	0.10	5.01	1.20
Mixed	177.94	3.45	15.39	22.49
Residential	60.10	0.40	8.68	7.87
Restricted Area	44.05	5.18	12.15	5.97
Service related	**120.31**	**4.14**	**18.26**	**12.75**

4.6.1. Population density by building type

For administrative building type, the average population density for Dhaka is 8.12. Compare to both Dhaka part, the average population density in administrative land use category for North part is 9.98, which is more than the South part 7.91 person per cell. In reality, the North part of the Dhaka City increased rapidly as Central Business District (CBD) and all the administrative buildings are established there. The population density for commercial building type of North part is 34.71 and South part is 10.13 only, where the average for whole Dhaka city is 18.08. The reason behind that all the big commercial high rise buildings and shopping centers were established in this part. In addition, the area of North part for commercial building type is larger than South part. In educational building type, the north part (15.80) has more population density than the South part (11.65), where the average density for whole Dhaka is 13.87. The reasons behind that are most of all educational institutes are established in North part, which was started to established since 2000 and larger in institutes number compare to South part. The average population density in mixed land use shows for North part is 21.98 and the South part is 12.60, where the average for Dhaka city is 15.39 per cell. Dhaka City has a complex land use classes with a combination of two or more building use in a single structure such as commercial with residential, commercial with educational even though commercial with residential and educational. As a result, due to lack of enough living space and high house rent, a lot of people live in a tiny single room or apartments. Figure 4-9 shows the structures, which have mixed land use classes in one structure.

Figure 4-9: Sample buildings for mixed land use class (pictures were collected from Google Earth Street View).

The average population density in residential land use for Dhaka North part is 8.47 person per 25 square meters and for Dhaka, South part is 8.82, where the average for whole Dhaka is 8.68. This means that the population density for residential building for both parts is almost same. The maximum density in this category is 60.10 per cell, which indicates very highly populated area and that residential area was developed in an unplanned way. The population density for manufacturing building in Dhaka North part is less (2.15) than the Dhaka South part (10.73). In reality, it could be also found that all the small and medium manufacturing industries such as tannery, shoes, fruit-based processed food industries, small iron product industries etc. are established in Dhaka South part. The restricted and the service related building type have an average population density of 12.15 and 18.26 person per cell respectively for Dhaka city. But, the Dhaka North has more population density than the Dhaka South. Also, it is true that Dhaka North part has a more restricted area by Bangladesh military than the other part. Figure 4-10 describes the scenario of the average population density among the different building types.

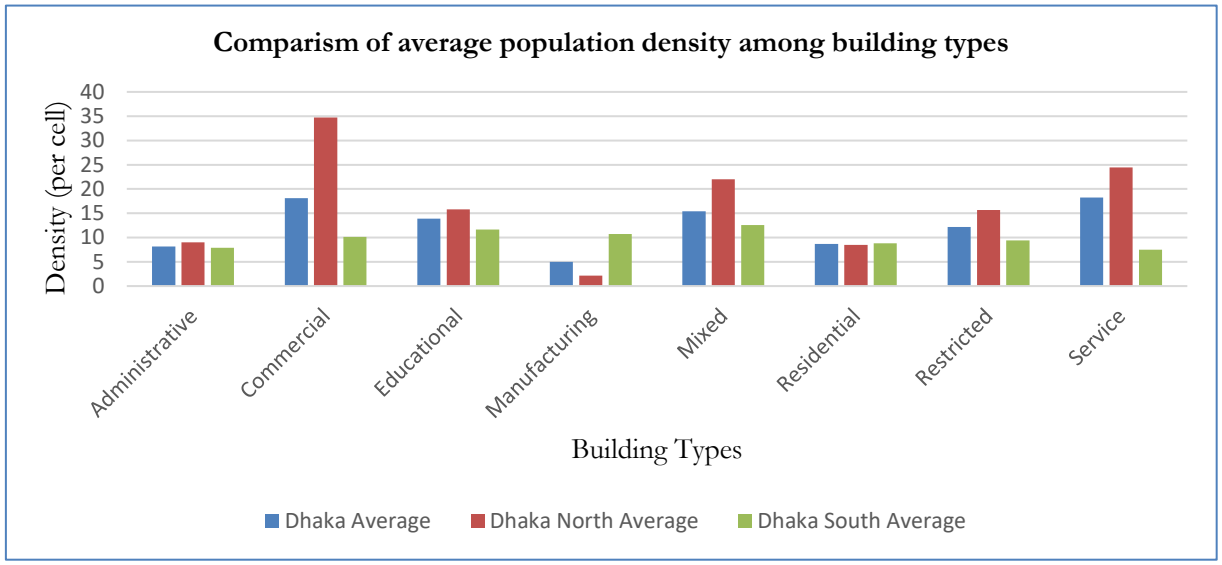

Figure 4-10: Comparison of average population density among building type areas and two part of Dhaka City.

4.6.2. Population density by census units

The maximum average population density found in Dhaka North 09 (DNCC9) ward and the value is 160.16 person per cell, where the maximum population density in mixed type is 177.94 within the ward. Also, this mixed type is the highest population density among all category of Dhaka City. The 0.1 % buildings area of the total building area of the ward is mixed. Whereas the other 99% of the census unit is the non-inhabitable area. The minimum average population density found in DNCC7 no ward with 3.03 person, where the four type of buildings were found – administrative with 2.87, commercial with 3.04, educational with 2.60 and mixed with 3.63 people per cell. There is no residential land type found and residential building type as well. But the people live in such buildings which are categorized by mixed building type.

Dhaka City consists of 92 wards with two parts. Not all the wards are in the same area or not every ward has same types of building. Therefore, the average population density for all wards is not similar. Considering building area for each ward and average population density together the average population density map was produced (Figure 4-11). The class interval for mapping was calculated in the geometrical interval. 32 wards have the average population density of 3.03-6.83 person range, which is the 34% of the total number of wards. Another largest number of wards (27 wards) belong to a density range of 7.49-11.29 person per cell. Following that, rest of the wards were classified into three-density range of 6.83-7.49, 11.29-33.25 and 33.25-160.16, where the number of wards was 9, 20 and 4 respectively.

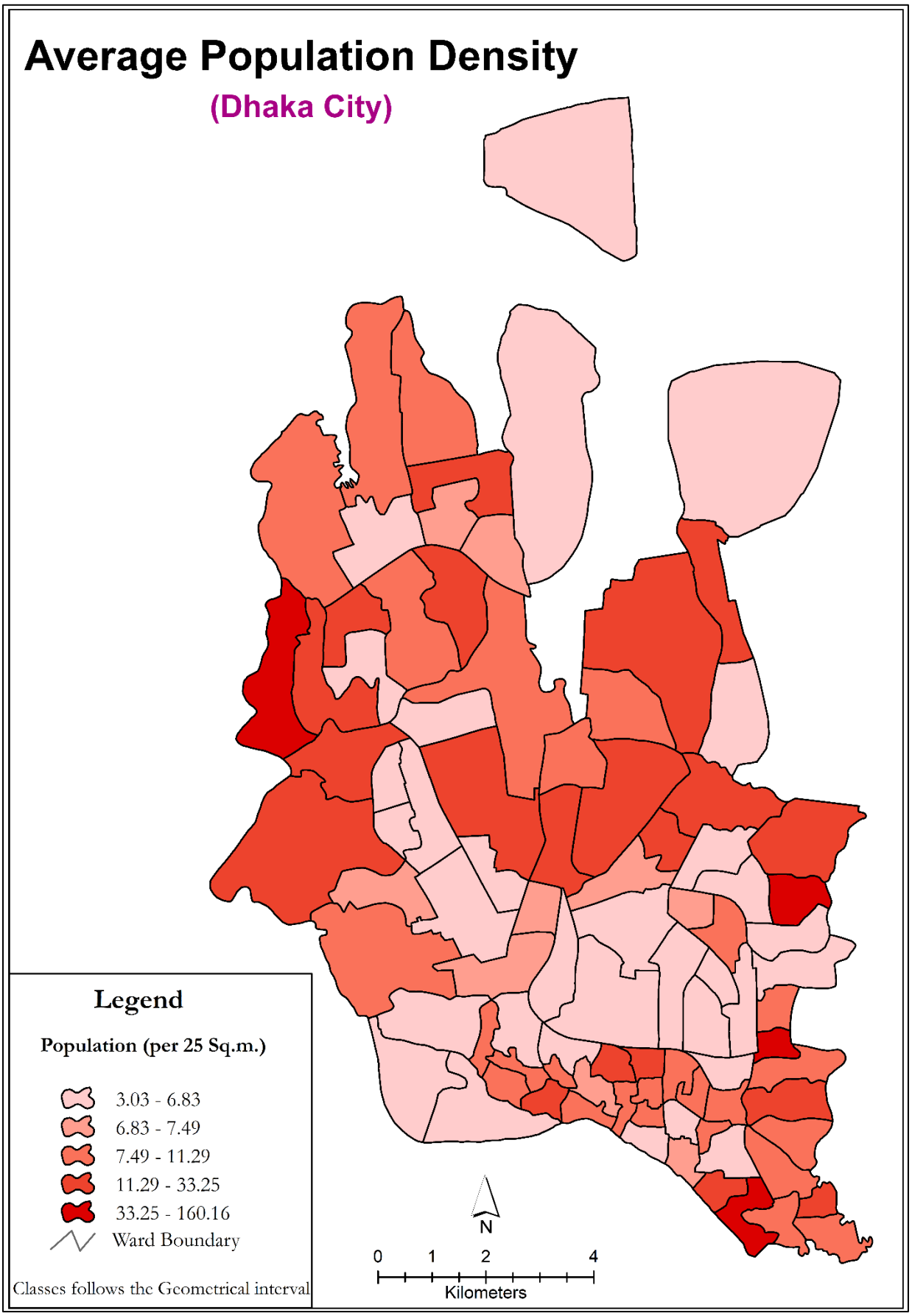

Figure 4-11: Average population density for Dhaka in per 25 square meters considering all categorical buildings area.

4.7. Accuracy of the dasymetric model

The RMSE of the output population counts from the dasymetric model with the actual population was found 194 which is less than standard accepted RMSE value (RMSE <0.3) (Appendix 5). In addition, the CV of population counts of dasymetric model is 0.001, which is the much more improved result. The RMSE and CV of population counts, both give a better result for a dasymetric model than any other population models.

The accuracy of the dasymetric model shows very high performance compared to other models. However, there are few factors to consider which might contribute the inaccuracy of the resulting population distribution product. Firstly, the height of the building were not considered in this model. As a result, the population density shows very high in some cases. For example, the population density of 12.50 per cell represents 12.50 people live in one 25 square meter cell, which may not be true in reality. The actual building height may be six storied; in that case, the population density will be six-time smaller than the calculated density of 12.50. Therefore, the population density for that certain cell will be 12.50÷6 = 2.08 people per cell. Secondly, the geometrical shape of the extracted buildings was not in perfect shape (real shape of the building) in some cases. That effected on the total building area calculation and consequently which affected the population density calculation. The generalized land use may cause the inaccuracy of building use type identification. The misclassified building type may cause the inaccuracy in building type area distribution within the ward, which may affect the population distribution within the ward. Furthermore, the geographically weighted regression model was used to calculate the proportional population among the building types within the ward. The model itself has uncertainty, which may affect the density calculation.

The most important factor was the temporal inaccuracy of the data. The population census was conducted in 2011 and data was published in 2015 by the governmental organization (BBS). Furthermore, the land use land cover data was produced by another governmental organization (SoB) in 2008. Moreover, VHR images of the study area were collected from WordView2, which was captured in May 2017. There is temporal mismatch between all the data. The population counts increased during the time period but not considered in this research. The city is now developing in a vertical way and very few developments are occurring in a horizontal way in the peripheral side, which is far away from the study area. This image was used in this study to detect buildings and assuming that there is a little structural change over the period from the population census conducted and the changes were in acceptable in this research. However, the overall temporal inconsistency may cause the inaccuracy in population distribution mapping.

Finally, the conversion of irregular vector shapefile to a regular pixel may cause the uncertainty of disaggregation of the population. Cell center option was selected as cell assignment (which define how the pixel will be assigned if more than one polygon falls within a pixel) during the pixel conversion. Sometimes the 25 square meter pixel did not fit the actual building shape, which affected the area calculation of the building. The figure 4-12 shows how pixel conversion affects the area calculation from actual building shape.

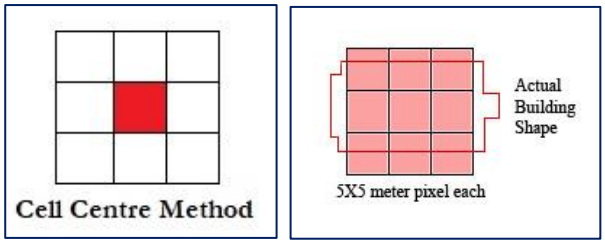

Figure 4-12: Error in pixel conversion process. The left image shows the cell center conversion process and the right image shows the error occurred during the conversion.

5. CONCLUSION

5.1. Conclusion

Studying population distribution in an appropriate and accurate way is becoming a very important research area for last few decades. Geographic information system, remote sensing, and geo-statistics are being used to support those population studies. Consequently, various techniques/methods are developed based on resource availability such as time, labor, data, and money and on fit to purpose as well. In this research, a method was tried to develop considering the above constraints, where population data published in 10 years interval and updating ancillary data is either time consuming or lack of data matter in Dhaka City. Presuming that in this research a few assumption was set - population density varies from ward to ward. It also varies in different land use type within the ward and even for the same land use type in the different ward. The traditional population density, which is calculated from population count divided by the areal unit cannot give a clear population distribution idea, where building level population data is not available.

A few worldwide population distribution products such as GPW, GRUMP, LandScan, WorldPop give a spatial resolution of 1 km to 100 meters. Besides these products, there are various population distribution products, where different types of ancillary data such as land use land cover, dwelling units, spectral characteristics of remote sensing pixels and various physical and socio-economic variables are used. However, not all of them produce very high-resolution population products. Dasymetric mapping is one of the methods, which can produce very high-resolution population distribution product considering various ancillary data. In this research, a modified dasymetric mapping method was used to produce 5X5 meter resolution population product with the help of VHR image.

VHR satellite image is very helpful to detect the urban features such as buildings, roads, and other impervious areas. Previously, medium to the low-resolution image was used only to extract urban land cover or impervious areas. However, the various small object such as buildings, trees, roadside small objects etc. are being started to extract when the VHR images are available. Various VHR images such as WorlView2/3, Ikonos, QuickBird etc. have a different number of bands with different wavelengths focusing on different objects on the ground. In addition, all the objects in the urban area do not have same spectral reflectance and same spatial extent. Moreover, they vary from different urban areas and various methods were developed to extract different complex objects of urban areas. OBIA method is one of them and was selected to extract the complex buildings from the WorldView2 image of the study area. A multi-resolution segmentation process was performed and a set of rules were used to classify the image into four urban land cover classes such as vegetation, water, buildings and other areas as the main target was the building detection. Though the urban scene was very complex and various confusion was found between buildings with roads, another road layer (vector) was used as ancillary data to reduce the misclassification. Though the buildings were not geometrically regular shaped, the accuracy was found 77.75% with the kappa coefficient of 0.76 for the study area.

The building use was classified by using another ancillary data – generalized land use of the study area, which may cause the misclassification of buildings. These building type areas and LULC areas were used into four different model for population density mapping. These models were – building based OLS regression model, building-based GWR model, Land use based OLS regression model and land use based GWR model. The result from each model produced different population products and comparing them to RMSE, mean

CV, R^2 and adjusted R^2 . The building based GWR model showed the better result than other three models as it considered the geographical location of the buildings along with areas. The output result from building-based GWR model was used in dasymetric modeling to calculate the relative weight value. This dasymetric model is a modified version of limiting variable dasymetric model type, where the relative weight was predefined. In this model, the relative weights were dynamic and calculated considering the building location and areas as well. These value helped to calculate the proportional population count and dasymetric model helped to disaggregate that population count to the predefined cell, which is 25 square meter. Finally, the whole population output product has a spatial resolution of 5 meters. The accuracy of this dasymetric product was found much better compared to other models and with a value of RMSE 194 and mean CV 0.001. In that sense, this model is accurate enough to produce high-resolution population product.

Therefore, there are few factors need to be considered here regarding the accuracy of the whole process and population product through dasymetric modeling. The final accuracy depends on the accuracy of each stage in the model and it is a cumulative effect of inaccuracy in the model. The inaccuracy of extracting building from VHR, the inaccuracy in generalized LULC, the uncertainty in the building based GWR model, the inaccuracy in the transformation of vector data to raster pixels for the dasymetric model, the temporal inconsistency of data and finally not considering the height of the building influenced the total accuracy of population disaggregation. However, considering all these aspects, the dasymetric modeling for producing high-resolution gridded population surface product shows the improved model for a future population study.

5.2. Future research

The described research method gives an acceptable high-resolution population surface product for Dhaka City. The method is a combination of OBIA and dasymetric model. In this study, various rules set were used for extracting buildings and a building based GWR model was used in dasymetric model. A multi-resolution segmentation process was used in entire image at a time, which some time did not perform very well in the different area as the spectral reflectance and spatial extent of the objects are not same in the study area. In addition, the buildings geometrical shape were not extracted properly as the buildings are adjacent to each other and sometimes the whole block is very congested by buildings. There is a scope to develop more fine-tuned rule set to extract the complex buildings through OBIA using VHR image.

A building based GWR model was performed based on building use area inside the dasymetric model. There is a scope to incorporate the height of the building, which will help to calculate the actual floor space and population distribution according to that floor space. In addition, instead of using only categorical buildings area, there is scope to use various influencing factors such as distance from the road, distance from CBD, the location of educational institutes, various urban facilities etc. inside the model. The combination of above data in the dasymetric model will give a better high-resolution population distribution product for complex study area like Dhaka City.

LIST OF REFERENCES

Ahmed, S. J., Nahiduzzaman, K. M., & Bramley, G. (2014). From a town to a megacity: 400 years of growth. In A. Dewan & R. Corner (Eds.), *Dhaka Megacity: Geospatial Perspectives on Urbanisation, Environment and Health* (p. 423). Dordrecht Heidelberg: Springer New York.

Ahmed, S. U. (1986). *Dacca: a study in urban history and development*. The University of Michigan, USA: Curzon Press.

Alahmadi, M., Atkinson, P., & Martin, D. (2013). Estimating the spatial distribution of the population of Riyadh, Saudi Arabia using remotely sensed built land cover and height data. *Computers, Environment and Urban Systems*, *41*, 167–176. https://doi.org/10.1016/j.compenvurbsys.2013.06.002

Alahmadi, M., Atkinson, P., & Martin, D. (2015). Fine spatial resolution residential land-use data for small-area population mapping: a case study in Riyadh, Saudi Arabia. *International Journal of Remote*, *36*(17), 4315–4331. https://doi.org/10.1080/01431161.2015.1079666

Asfiji, N. S., Isfahani, R. D., Dastjerdi, R. B., & Fakhar, M. (2012). Frequency population growth rate. *International Journal of Academic Research in Business and Social Sciences*, *2*(10), 524–529.

Azar, D., Engstrom, R., Graesser, J., & Comenetz, J. (2013). Generation of fine-scale population layers using multi-resolution satellite imagery and geospatial data. *Remote Sensing of Environment*, *130*, 219–232. https://doi.org/10.1016/j.rse.2012.11.022

Baatz, M., & Schäpe, A. (2000). Multiresolution segmentation: An optimization approach for high quality multi-scale image segmentation. In J. Strobl, T. Blaschke, & G. Griesebner (Eds.), *Angewandte Geographische Informations- Verarbeitung XII*. 12–23. Karlsruhe, Germany: Wichmann Verlag.

Balk, D., & Yetman, G. (2004). The global distribution of population: evaluating the gains in resolution refinement. *Center for International Earth Science Information Network (CIESIN), Columbia University*. Retrieved from http://sedac.ciesin.columbia.edu/downloads/docs/gpw-v3/gpw3_documentation_final.pdf

Bangladesh Bureau of Statistis, (BBS). (2011a). *Population & Housing Census-2011, National volume 3: Urban Area Report*. Bangladesh Bureau of Statistics, Ministry of Planning, Dhaka.

Bangladesh Bureau of Statistis, (BBS). (2011b). *Population and housing census 2011:National Report, Volume-1, Analytical Report*. Bangladesh Bureau of Statistics, Ministry of Planning, Dhaka.

Bhaduri, B., Bright, E., Coleman, P., & Urban, M. L. (2007). LandScan USA: A high-resolution geospatial and temporal modeling approach for population distribution and dynamics. *GeoJournal*, *69*(1–2), 103–117. https://doi.org/10.1007/s10708-007-9105-9

Bielecka, E. (2005). A dasymetric population density map of poland. *Proceedings of the 22nd International Cartographic Conference*, (48 22), 9–15.

Blaschke, T. (2010). Object based image analysis for remote sensing. *ISPRS Journal of Photogrammetry and Remote Sensing*, *65*(1), 2–16. https://doi.org/10.1016/j.isprsjprs.2009.06.004

Blaschke, T., & Strobl, J. (2001). What' s wrong with pixels ? Some recent developments interfacing remote sensing and GIS. *GeoBIT/GIS*, *6*(1), 12–17.

Callegari, S., Weissmann, J. D., Tkachenko, N., Petersen, W. P., Lake, G., Le´on, M. P. D. E., & Zollikofer., C. P. E. (2013). An agent-based model of human dispersals at a global scale. *Advances in Complex Systems*, *16*(4 & 5), 21. https://doi.org/10.1142/S0219525913500239

Chakraborty J., Tobin G. A., M. B. E. (2005). Population evacuation: assessing spatial variability in geophysical risk and social vulnerability to natural hazards. *Natural Hazards Review*, *6*(1). https://doi.org/http://dx.doi.org/10.1061/(ASCE)1527-6988(2005)6:1(23)

Charpentier, M. (1997). The dasymetric method with comments on its use in GIS. In *1997 UCGIS Annual Assembly & Summer Retreat*. Bar Harbor, Maine: The University Consortium for Geographic Information Science, June 15-20.

Chen, G., Weng, Q., Hay, G. J., & He, Y. (2018). Geographic object-based image analysis (GEOBIA): Eemerging trends and future opportunities. *GIScience & Remote Sensing*, *55*(1), 1–24. https://doi.org/10.1080/15481603.2018.1426092

Chen, K. (2002). An approach to linking remotely sensed data and areal census data. *International Journal of Remote Sensing*, *23*(1), 37–48. https://doi.org/10.1080/01431160010014297

Chowdhury, A., & Faruqui, S. (2009). Physical growth of Dhaka city. In S. U. Ahmed (Ed.), *Dhaka: past present future* (2nd ed., pp. 56–76). Dhaka: The Asiatic Society of Bangladesh.

CIESIN (Center for International Earth Science Information Network). (2011, January 1). Global Rural-

Urban Mapping Project, Version 1 (GRUMPv1): Urban Extents Grid. Columbia University. https://doi.org/10.7927/H4GH9FVG
Cockings, S., Fisher, P. F., & Longford, M. (1997). Parameterization and visualization of the errors in areal interpolation. *Geographical Analysis*, *29*(4), 314–328. https://doi.org/10.1111/j.1538-4632.1997.tb00967.x
Cohen, J. (1960). A coefficient of agreement for nominal scales. *Educational and Psychological Measurement*, *20*(1), 37–46. https://doi.org/10.1177/001316446002000104
Congalton, R. G. (1991). A review of assessing the accuracy of classifications of remotely sensed data. *Remote Sensing of Environment*, *37*(1), 35–46. https://doi.org/10.1016/0034-4257(91)90048-B
Congalton, R., & Green, K. (2009). Thematic accuracy. In R. Congalton & K. Green (Eds.), *Assessing the accuracy of remotely sensed data: principles and practices* (2nd ed., p. 56). Boca Raton: CRC Press, Taylor & Francis Group.
Dasvarma, G. L. (2010). The importance of population studies and the state of technical demographic training in Asia. *Asian Population Studies ISSN:*, *6*(1), 1–2. https://doi.org/10.1080/17441731003603330
Dobson, J. E., Bright, E. A., Coleman, P. R., Durfee, R. C., & Worley, B. A. (2000). LandScan: A global population database for estimating populations at risk. *Photogrammetric Engineering and Remote Sensing*, *66*(7), 849–857. https://doi.org/10.1016/j.scitotenv.2008.02.010
Doxsey-Whitfield, E., MacManus, K., Adamo, S. B., Pistolesi, L., Squires, J., Borkovska, O., & Baptista, S. R. (2015). Taking advantage of the improved availability of census data: a first look at the gridded population of the world, version 4. *Papers in Applied Geography*, *1*(3), 226–236. https://doi.org/http://dx.doi.org/10.1080/23754931.2015.1014272
Eicher, C. L., & Brewer, C. A. (2001). Dasymetric mapping and areal interpolation: implementation and evaluation. *Cartography and Geographic Information Science*, *28*(2), 125–138. https://doi.org/10.1559/152304001782173727
Entwisle, B., Walsh, S. J., Rindfuss, R. R., & Chamratrithirong, A. (1998). Land use/land cover and population dynamics, Nang Rong, Thailand. In D. Liverman, E. F. Moran, R. R. Rindfuss, & P. C. Stern (Eds.), *People and Pixels: linking remote sensing and social science* (pp. 121–144). Washington, D.C.: National Academy Press.
Fauvel, M., & Benediktsson, J. (2008). Spectral and spatial classification of hyperspectral data using svms and morphological profile. *IEEE Transactions on Geoscience and Remote Sensing*, *46*(11), 3804–3814. https://doi.org/10.1109/TGRS.2008.922034
Fisher, P. F., & Langford, M. (1995). Modeling the errors in areal interpolation between zonal systems by monte-carlo simulation. *Environment and Planning A*, *27*, 211–224. https://doi.org/10.1068/a270211
Foody, G. (2008). Harshness in image classification accuracy assessment. *International Journal of Remote Sensing*, *29*(11), 3137–3158. https://doi.org/10.1080/01431160701442120
Förster, M. (2008). *Integration of Geo-Information in Classification Processes of Satellite Imagery for NATURA 2000 Monitoring*. PhD thesis. School VI – Planning Building Environment. Technische Universität Berlin. Retrieved from https://depositonce.tu-berlin.de/handle/11303/2337
Freire, S., & Santos, T. (2012). Extraction of buildings in heterogeneous urban areas: Testing the value of increased spectral information of WorldView-2 imagery. *Computational Modelling of Objects Represented in Images III: Fundamentals, Methods and Applications*, *2*, 175. Retrieved from https://books.google.at/books?hl=de&lr=lang_de%7Clang_en%7Clang_fr%7Clang_it%7Clang_es&id=Z5ph3owFbMEC&oi=fnd&pg=PA175&dq=worldview-2+vegetation&ots=Zqfc4w9fKn&sig=RD_RgFcw7cZWazea596Ur6C-NMg
Gao, B. C. (1996). NDWI - A normalized difference water index for remote sensing of vegetation liquid water from space. *Remote Sensing of Environment*, *58*(3), 257–266. https://doi.org/10.1016/S0034-4257(96)00067-3
Gaughan, A. E., Stevens, F. R., Linard, C., Jia, P., & Tatem, A. J. (2013). High resolution population distribution maps for southeast asia in 2010 and 2015. *PLoS ONE*, *8*(2), e55882. https://doi.org/10.1371/journal.pone.0055882
Gerth, J. (1993). *Towards improved spatial analysis with areal units: The use of GIS to facilitate the creation of dasymetric maps*. Master Thesis. Ohio State University.
Green, N. E. (1956). Aerial photographic analysis of residential neighborhoods : an evaluation of data accuracy. *Social Forces*, *35*(2), 142–147.
Halliman H. Winsborough. (1965). The social consequences of high population density. *Law and Contemporary Problems*, *30*(1), 120–126. https://doi.org/10.2307/1190689

Hamedianfar, A., & Shafri, H. Z. M. (2015). Detailed intra-urban mapping through transferable OBIA rule sets using WorldView-2 very-high-resolution satellite images. *International Journal of Remote Sensing*, *36*(13), 3380–3396. https://doi.org/10.1080/01431161.2015.1060645

Hamedianfar, A., Shafri, H. Z. M., Mansor, S., & Ahmad, N. (2014). Improving detailed rule-based feature extraction of urban areas from WorldView-2 image and lidar data. *International Journal of Remote Sensing*, *35*(5), 1876–1899. https://doi.org/10.1080/01431161.2013.879350

Harvey, J. (2002). Population estimation models based on individual TM pixels. *Photogrammetric Engineering and Remote Sensing*, *68*(11), 1181–1192. Retrieved from http://researchonline.federation.edu.au/vital/access/HandleResolver/1959.17/56693

Harvey, J. T. (2002). Estimating census district populations from satellite imagery: Some approaches and limitations. *International Journal of Remote Sensing*, *23*(10), 2071–2095. https://doi.org/10.1080/01431160110075901

Hashemian, M. S., Abakar, A. A., & Fatemi, S. B. (2004). Study of sampling methods for accuracy assessment of classified remotely sensed data. *20th International Society for Photogrammetry and Remote Sensing Congress*, 12–23.

Hay, G. J., & Castilla, G. (2006). Object-based image analysis: strengths, weaknesses, opportunities and threats (SWOT). *International Archives of Photogrammetry Remote Sensing and Spatial Information Sciences*, *36*, 4. https://doi.org/10.1007/978-3-540-77058-9_4

Hay, S. I., Noor, A. M., Nelson, A., & Tatem, A. J. (2005). The accuracy of human population maps for public health application. *Tropical Medicine and International Health*, *10*(10), 1073–1086. https://doi.org/10.1111/j.1365-3156.2005.01487.x

Hermosilla, T., Ruiz, L. A., Recio, J. A., & Estornell, J. (2011). Evaluation of automatic building detection approaches combining high resolution images and LiDAR data. *Remote Sensing*, *3*(6), 1188–1210. https://doi.org/10.3390/rs3061188

Herold, M., Gardner, M. E., & Roberts, D. a. (2003). Spectral resolution requirements for mapping urban areas. *IEEE Transactions on Geoscience and Remote Sensing*, *41*(9), 1907–1919. https://doi.org/10.1109/TGRS.2003.815238

Holloway, S. R., Schumacher, J., & Redmond, R. L. (1996). People and place: dasymetric mapping using Arc/Info. *Missoula: Wildlife Spatial Analysis Lab*, 1–11.

Holt, J. B., Lo, C. P., & Hodler, T. W. (2004). Dasymetric estimation of population density and areal interpolation of census data. *Cartography and Geographic Information Science*, *31*(2), 103–121. https://doi.org/10.1559/1523040041649407

Holt, J. B., & Lu, H. (2011). Dasymetric mapping for population and sociodemographic data redistribution. In X. Yang (Ed.), *Urban Remote Sensing: Monitoring, Synthesis andModeling in theUrban Environment* (pp. 195–210). Chichester. UK: John Wiley & Sons Ltd. https://doi.org/10.1002/9780470979563.ch14

Huang, X., & Zhang, L. (2012). Morphological building/shadow index for building extraction from high-resolution imagery over urban areas. *IEEE Journal of Selected Topics in Applied Earth Observations and Remote Sensing*, *5*(1), 161–172. https://doi.org/10.1109/JSTARS.2011.2168195

Huxley, J. S. (1932). *Problems of relative growth*. London, UK: Methuen And Company Limited.

Huyck, C. K., Adams, B. J., Cho, S., Chung, H.-C., & Eguchi, R. T. (2005). Towards rapid citywide damage mapping using neighborhood edge dissimilarities in very high-resolution optical satellite imagery—application to the 2003 Bam,Iran, earthquake. *Earthquake Spectra*, *21*(1), 255–266. https://doi.org/https://doi.org/10.1193/1.2101907

Iisaka, J., & Hegedus, E. (1982). Population estimation from Landsat imagery. *Remote Sensing of Environment*, *12*(4), 259–272. https://doi.org/10.1016/0034-4257(82)90039-6

Jia, P., & Gaughan, A. E. (2016). Dasymetric modeling: A hybrid approach using land cover and tax parcel data for mapping population in Alachua County, Florida. *Applied Geography*, *66*, 100–108. https://doi.org/10.1016/j.apgeog.2015.11.006

Jia, P., Qiu, Y., & Gaughan, A. E. (2014). A fine-scale spatial population distribution on the high-resolution gridded population surface and application in Alachua County, Florida. *Applied Geography*, *50*, 99–107. https://doi.org/10.1016/j.apgeog.2014.02.009

Johnson, B., Bragais, M., Endo, I., Magcale-Macandog, D., & Macandog, P. (2015). Image segmentation parameter optimization considering within- and between-segment heterogeneity at multiple scale levels: test case for mapping residential areas using landsat imagery. *ISPRS International Journal of Geo-Information*, *4*(4), 2292–2305. https://doi.org/10.3390/ijgi4042292

Joseph, M., Wang, L., & Wang, F. (2012a). Using Landsat Imagery and Census Data for Urban Population

Density Modeling in Port-au-Prince , Haiti Using Landsat Imagery and Census Data for Urban. *GIScience & Remote Sensing*, *49*(2), 228–250.
Joseph, M., Wang, L., & Wang, F. (2012b). Using landsat imagery and census data for urban population density modeling in Port-au-prince ,Haiti using landsat imagery and census data for urban. *GIScience & Remote Sensing*, *49*(2), 228–250.
Karume, K., Schmidt, C., Kundert, K., Bagula, M. E., & Safina, B. F. (2017). Use of remote sensing for population number determination. *The Open Access Journal of Science and Technology*, *5*, 1–9. https://doi.org/10.11131/2017/101227
Katartzis, A., & Sahli, H. (2008). A stochastic framework for the identification of building rooftops using a single remote sensing image. *IEEE Transactions on Geoscience and Remote Sensing*, *46*(1), 259–271. https://doi.org/10.1109/TGRS.2007.904953
Kim, T., & Muller, J.-P. (1999). Development of a graph-based approach for building detection. *Image and Vision Computing*, *17*(1), 3–14. https://doi.org/10.1016/S0262-8856(98)00092-4
Koc-San, D., & Turker, M. (2014). Support vector machines classification for finding building patches from IKONOS imagery: the effect of additional bands. *Journal of Applied Remote Sensing*, *8*(1), 83694. https://doi.org/10.1117/1.JRS.8.083694
Kraus, S., Senger, L., & Ryerson, J. (1974). Estimating population from photographically determined residential land use types. *Remote Sensing of Environment*, *42*(5), 35–42. Retrieved from http://www.sciencedirect.com/science/article/pii/0034425774900364
Lam, N. S.-N. (1983). Spatial interpolation methods: A review. *The American Cartographer*, *10*(2), 129–149. https://doi.org/10.1559/152304083783914958
Langford, M. (2006). Obtaining population estimates in non-census reporting zones: An evaluation of the 3-class dasymetric method. *Computers, Environment and Urban Systems*, *30*(2), 161–180. https://doi.org/10.1016/j.compenvurbsys.2004.07.001
Langford, M., Maguire, D. J., & Unwin, D. J. (1991). The areal interpolation problem: estimating population using remote sensing in a GIS framework. *Handling Geographical Information: Methodology and Potential Applications*, 55–77.
Langford, M., & Unwin, D. J. (1994). Generating and mapping population density surfaces within a geographical information system. *The Cartographic Journal*, *31*(1), 21–26. https://doi.org/10.1179/000870494787073718
Lein, J. K. (2012). Object-Based Analysis. In *Environmental sensing: analytical techniques for earth observation* (pp. 259–276). New York: Springer New York. https://doi.org/10.1007/978-1-4614-0143-8
Li, E., Femiani, J., Xu, S., Zhang, X., & Wonka, P. (2015). Robust rooftop extraction from visible band images using higher order CRF. *IEEE Transactions on Geoscience and Remote Sensing*, *53*(8), 4483–4495. https://doi.org/10.1109/TGRS.2015.2400462
Li, G., & Weng, Q. (2010). Fine-scale population estimation: How Landsat ETM+ imagery can improve population distribution mapping. *Canadian Journal of Remote Sensing*, *36*(3), 155–165. https://doi.org/10.5589/m10-035
Li, H., Jing, L., Tang, Y., Liu, Q., Ding, H., Sun, Z., & Chen, Y. (2015). Assessment of pan-sharpening methods applied to WorldView-2 image fusion. *International Geoscience and Remote Sensing Symposium (IGARSS)*, *2015–Novem*, 3302–3305. https://doi.org/10.1109/IGARSS.2015.7326524
Li, L., & Lu, D. (2016). Mapping population density distribution at multiple scales in Zhejiang Province using Landsat Thematic Mapper and census data. *International Journal of Remote Sensing*, *37*(18), 4243–4260. https://doi.org/10.1080/01431161.2016.1212422
Li, S., Tang, H., Huang, X., Mao, T., & Niu, X. (2017). Automated detection of buildings from heterogeneous vhr satellite images for rapid response to natural disasters. *Remote Sensing*, *9*(11), 1177. https://doi.org/10.3390/rs9111177
Linard, C., Alegana, V. A., Noor, A. M., Snow, R. W., & Tatem, A. J. (2010). A high resolution spatial population database of Somalia for disease risk mapping. *International Journal of Health Geographics*, *9*(1), 45. https://doi.org/10.1186/1476-072X-9-45
Linard, C., Gilbert, M., & Tatem, A. J. (2011). Assessing the use of global land cover data for guiding large area population distribution modelling. *GeoJournal*, *76*(5), 525–538. https://doi.org/10.1007/s10708-010-9364-8
Liu, X. (2003). *Estimation of the spatial distribution of urban population using high spatial resolution satellite imagery*. Ph.D thesis. University of California, Santa Barbara. 175 p.
Liu, X. H., Clarke, K. C., & Herold, M. (2006). Population density and image texture: a comparison study. *Photogrammetric Engineering and Remote Sensing*, *72*(2), 187–196. https://doi.org/0099-1112/06/7202–

0187
Liu, X., & Herold, M. (2006). Population estimation and interpolation using remote sensing. In Q. Weng & D. A. Quattrochi (Eds.), *Urban Remote Sensing* (1st ed., p. 450). Boca Raton: CRC Press.
Liu, Y., & Yamauchi, F. (2014). Population density, migration, and the returns to human capital and land: Insights from Indonesia. *Food Policy*, *48*, 182–193. https://doi.org/10.1016/j.foodpol.2014.05.003
Lloyd, C. T., Sorichetta, A., & Tatem, A. J. (2017). High resolution global gridded data for use in population studies. *Scientific Data*, *4*, 170001. https://doi.org/10.1038/sdata.2017.1
Lo, C. P. (1986). *Applied remote sensing*. New York: Longman.
Lo, C. P. (1995). Automated population and dwelling unit estimation from high-resolution satellite images: a GIS approach. *International Journal of Remote Sensing*, *16*(1), 17–34. https://doi.org/http://dx.doi.org/10.1080/01431169508954369
Lo, C. P. (2002). Urban indicators of china from radiance-calibrated digital dmsp-ols nighttime images. *Annals of the Association of American Geographers*, *92*(2), 225–240. https://doi.org/10.1111/1467-8306.00288
Lo, C. P. (2003). Zone-Based Estimation of Population and Housing Units from Satellite-Generated Land Use/Land Cover Maps. In V. Mesev (Ed.), *Remotely Sensed Cities* (pp. 157–180). London, UK/New York: Taylor & Francis.
Lu, D., Weng, Q., & Li, G. (2006). Residential population estimation using a remote sensing derived impervious surface approach. *International Journal of Remote Sensing*, *27*(16), 3553–3570. https://doi.org/10.1080/01431160600617202
Lung, T., Lübker, T., Ngochoch, J. K., & Schaab, G. (2013). Human population distribution modelling at regional level using very high resolution satellite imagery. *Applied Geography*, *41*, 36–45. https://doi.org/10.1016/j.apgeog.2013.03.002
Lwin, K. K., & Murayama, Y. (2011). Estimation of building population from LiDAR derived digital volume model. In Y. Murayama & R. B. Thapa (Eds.), *Spatial Analysis and Modeling in Geographical Transformation Process: GIS-based Applications* (p. 300). Springer Dordrecht Heidelberg London New York: Springer. https://doi.org/10.1007/978-94-007-0671-2
Ma, L., Li, M., Ma, X., Cheng, L., Du, P., & Liu, Y. (2017). A review of supervised object-based land-cover image classification. *ISPRS Journal of Photogrammetry and Remote Sensing*, *130*, 277–293. https://doi.org/10.1016/j.isprsjprs.2017.06.001
Maantay, J., & Maroko, A. (2017). Assessing population at risk: areal interpolation and dasymetric mapping. In R. Holifield, J. Chakraborty, & G. Walker (Eds.), *The Routledge Handbook of Environmental Justice* (1st ed., p. 670). New York: Routledge.
Martin, D. (1989). Mapping population data from zone centroid locations. *Transactions of the Institute of British Geographers*, *14*(1), 90–97. Retrieved from http://www.jstor.org/stable/622344 .
Martin, D. (2011). Directions in population GIS. *Geography Compass*, *5*(9), 655–665. https://doi.org/10.1111/j.1749-8198.2011.00440.x
McCleary, G. F. (1969). *The dasymetric method in thematic cartography*. University of Wisconsin.
Meng, Q., Liu, Z., & Borders, B. E. (2013). Assessment of regression kriging for spatial interpolation – comparisons of seven GIS interpolation methods. *Cartography and Geographic Information Science*, *40*(1), 28–39. https://doi.org/10.1080/15230406.2013.762138
Mennis, J. (2003). Generating surface models of population using dasymetric mapping. *The Professional Geographer*, *55*(1), 31–42. https://doi.org/http://dx.doi.org/10.1111/0033-0124.10042
Mennis, J. (2009). Dasymetric mapping for estimating population in small areas. *Geography Compass*, *3*(2), 727–745. https://doi.org/10.1111/j.1749-8198.2009.00220.x
Miura, H., Midorikawa, S., & Soh, H. (2012). Building damage detection of the 2010 haiti earthquake based on texture analysis of high-resolution satellite images. In *15th world conference on earthquake engineering*. lisbon, portugal.
Munoz, X., Freixenet, J., Cufí, X., & Martí, J. (2003). Strategies for image segmentation combining region and boundary information. *Pattern Recognition Letters*, *24*(1–3), 375–392. https://doi.org/10.1016/S0167-8655(02)00262-3
Nagle, N. N., Buttenfield, B. P., Leyk, S., & Speilman, S. (2014). Dasymetric modeling and uncertainty. *Ann Assoc Am Geogr.*, *104*(1), 80–95. https://doi.org/10.1080/00045608.2013.843439
Ok, A. O. (2013). Automated detection of buildings from single VHR multispectral images using shadow information and graph cuts. *ISPRS Journal of Photogrammetry and Remote Sensing*, *86*, 21–40. https://doi.org/10.1016/j.isprsjprs.2013.09.004
Pesaresi, M., & Benediktsson, J. A. (2001). A new approach for the morphological segmentation of high-

resolution satellite imagery. *IEEE Transactions on Geoscience and Remote Sensing*, *39*(2), 309–320. https://doi.org/10.1109/36.905239
Petersen, W. P., Callegari, S., Lake, G. R., Tkachenko, N., Weissmann, J. D., & Zollikofer, C. P. E. (2017). A stable finite-difference scheme for population growth and diffusion on a map. *PLoS ONE*, *12*(1), 1–19. https://doi.org/10.1371/journal.pone.0167514
Petrov, A. (2012). One hundred years of dasymetric mapping: back to the origin. *The Cartographic Journal*, *49*(3), 256–264. https://doi.org/10.1179/1743277412Y.0000000001
Prosperie, L., & Eyton, R. (2000). The relationship between brightness values from a nighttime satellite image and Texas county population. *The Southwestern Geographer*, *4*, 4–16.
Qiu, F., Sridharan, H., & Chun, Y. (2010). Spatial autoregressive model for population estimation at the census block level using lidar-derived building volume information. *Cartography and Geographic Information Science*, *37*(3), 239–257. https://doi.org/10.1017/CBO9781107415324.004
Rase, W.-D. (2001). Volume-preserving interpolation of a smooth surface from polygon-related data. *Journal of Geographical Systems*, *3*(2), 199–213. https://doi.org/10.1007/PL00011475
Reibel, M., & Bufalino, M. E. (2005). Street-weighted interpolation techniques for demographic count estimation in incompatible zone systems. *Environment and Planning A*, *37*(1), 127–139. https://doi.org/10.1068/a36202
Salah, M., Trinder, J., & Shaker, A. (2009). Evaluation of the self-organizing map classifier for building detection from lidar data and multispectral aerial images. *Journal of Spatial Science*, *54*(2), 15–34. https://doi.org/10.1080/14498596.2009.9635176
Sampson, R. J. (1978). *Surface II Graphics System* (Vol. 1). Kansas, USA: Kansas Geological Survey.
Shackelford, A. K., & Davis, C. H. (2003). A combined fuzzy pixel-based and object-based approach for classification of high-resolution multispectral data over urban areas. *IEEE Transactions on Geoscience and Remote Sensing*, *41*(10 PART I), 2354–2363. https://doi.org/10.1109/TGRS.2003.815972
Sirmacek, B., & Unsalan, C. (2009). Urban-area and building detection using SIFT keypoints and graph theory. *IEEE Transactions on Geoscience and Remote Sensing*, *47*(4), 1156–1167. https://doi.org/10.1109/TGRS.2008.2008440
Stein, M. L. (1999). *Interpolation of Spatial Data*. Springer New York. https://doi.org/10.1007/978-1-4612-1494-6
Sutton, P. C., Taylor, M. J., & Elvidge, C. D. (2010). Using DMSP OLS imagery to characterize urban populations in developed and developing countries. In T. Rashed & Jürgens (Eds.), *Remote Sensing of Urban and Suburban Areas* (pp. 329–348). Dordrecht, Heidelberg: Springer. https://doi.org/10.1017/CBO9781107415324.004
Tapp, A. F. (2010a). Areal interpolation and dasymetric mapping methods using local ancillary data. *Cartography and Geographic Information Science*, *37*(3), 215–228. https://doi.org/10.1559/152304010792194976
Tapp, A. F. (2010b). Areal interpolation and dasymetric mapping methods using local ancillary data. *Cartography and Geographic Information Science*, *37*(3), 215–228. https://doi.org/10.1559/152304010792194976
Tenerelli, P., Gallego, J. F., & Ehrlich, D. (2015). Population density modelling in support of disaster risk assessment. *International Journal of Disaster Risk Reduction*, *13*, 334–341. https://doi.org/10.1016/j.ijdrr.2015.07.015
Tian, J., & Chen, D. M. (2007). Optimization in multi-scale segmentation of high-resolution satellite images for artificial feature recognition. *International Journal of Remote Sensing*, *28*(20), 4625–4644. https://doi.org/10.1080/01431160701241746
Tobler, W., Deichmann, U., Gottsegen, J., & Maloy, K. (1997). World population in a grid of spherical quadrilaterals. *International Journal of Population Geography*, *3*(3), 203–225. https://doi.org/10.1002/(SICI)1099-1220(199709)3:3<203::AID-IJPG68>3.0.CO;2-C
Tobler, W. R. (1969). Satellite confirmation of settlement size coefficients. *The Royal Geographical Society*, *1*(3), 30–34. Retrieved from http://www.jstor.org/stable/20000359
Tobler, W. R. (1979). Smooth Pycnophylactic Interpolation for Geographical Regions. *Journal of the American Statistical Association*, *74*(367), 519–530.
Troya-Galvis, A., Gancarski, P., Passat, N., & Berti-Equille, L. (2015). Unsupervised quantification of under- and over-segmentation for object-based remote sensing image analysis. *IEEE Journal of Selected Topics in Applied Earth Observations and Remote Sensing*, *8*(5), 1936–1945. https://doi.org/10.1109/JSTARS.2015.2424457
Ural, S., Hussain, E., & Shan, J. (2011). Building population mapping with aerial imagery and GIS data.

International Journal of Applied Earth Observation and Geoinformation, *13*(6), 841–852. https://doi.org/10.1016/j.jag.2011.06.004
Varah, J. M. (1982). A spline least squares method for numerical parameter estimation in differential equations. *SIAM Journal on Scientific and Statistical Computing*, *3*(1), 28–46. https://doi.org/10.1137/0903003
Vijayaraj, V., Bright, E. a, & Bhaduri, B. L. (2008). High resolution urban feature extraction for global population mapping using high performance computing. *Ieee*, *1*(1), 278–281.
Wang, L., & Wu, C. (2010). Population estimation using remote sensing and GIS technologies. In *International Journal of Remote Sensing* (Vol. 31, pp. 5569–5570). https://doi.org/10.1080/01431161.2010.496809
Weber, C. (1994). Per-zone classification of urban land use cover for urban population estimation. In G. M. Foody & P. J. Curran (Eds.), *Environmental Remote Sensing from Regional to Global Scales* (pp. 142–148). Chichester, UK: New York: Wiley.
Webster, C. (1996). Population and dwelling unit estimates from space. *Third World Planning Review*, *18*(2), 155–176. https://doi.org/https://doi.org/10.3828/twpr.18.2.ul31w6q4447g120r
Wei, C., Taubenbock, H., & Blaschke, T. (2017). Measuring urban agglomeration using a city-scale dasymetric population map: A study in the Pearl River Delta, China. *Habitat International*, *59*, 32–43. https://doi.org/10.1016/j.habitatint.2016.11.007
Wei, Y., Zhao, Z., & Song, J. (2004). Urban building extraction from high-resolution satellite panchromatic image using clustering and edge detection. In *IEEE International Geoscience and Remote Sensing Symposium* (Vol. 7, pp. 2008–2010). Honolulu, HI, USA. https://doi.org/10.1109/IGARSS.2004.1370742
Wright, J. K. (1936). A method of mapping densities of population : with cape cod as an example. *Geographical Review*, *26*(1), 103–110. Retrieved from http://www.jstor.org/stable/209467
Wu, C., & Murray, A. T. (2007). Population estimation using landsat enhanced thematic mapper imagery. *Geographical Analysis*, *39*, 26–43.
Wu, S., Qiu, X., & Wang, L. (2005). Population estimation methods in gis and remote sensing: a review. *GIScience & Remote Sensing*, *42*(1), 80–96. https://doi.org/10.2747/1548-1603.42.1.80
Xie, Y., Weng, A., & Weng, Q. (2015). Population estimation of urban residential communities using remotely sensed morphologic data. *Geoscience and Remote Sensing Letters, IEEE*, *12*(5), 1111–1115. https://doi.org/10.1109/LGRS.2014.2385597
Yang, X., Jiang, G. M., Luo, X., & Zheng, Z. (2012). Preliminary mapping of high-resolution rural population distribution based on imagery from Google Earth: A case study in the Lake Tai basin, eastern China. *Applied Geography*, *32*(2), 221–227. https://doi.org/10.1016/j.apgeog.2011.05.008
Yao, Y., Liu, X., Li, X., Zhang, J., Liang, Z., Mai, K., & Zhang, Y. (2017). Mapping fine-scale population distributions at the building level by integrating multisource geospatial big data. *International Journal of Geographical Information Science*, *31*(6), 1–25. https://doi.org/10.1080/13658816.2017.1290252
Zaman, A. M. (2017, August 7). Dhaka and her rivers: A beautiful relationship gone sour | The Daily Star. Retrieved from http://www.thedailystar.net/opinion/environment/dhaka-and-her-rivers-1444537
Zandbergen, P. A. (2011). Dasymetric mapping using high resolution address point datasets. *Transactions in GIS*, *15*(SUPPL. 1), 5–27. https://doi.org/10.1111/j.1467-9671.2011.01270.x
Zha, Y., Gao, J., & Ni, S. (2003). Use of normalized difference built-up index in automatically mapping urban areas from TM imagery. *International Journal of Remote Sensing*, *24*(3), 583–594. https://doi.org/10.1080/01431160304987
Zhang, R., & Zhu, D. (2011). Study of land cover classification based on knowledge rules using high-resolution remote sensing images. *Expert Systems with Applications*, *38*(4), 3647–3652. https://doi.org/10.1016/j.eswa.2010.09.019
Zhao, W., Du, S., Wang, Q., & Emery, W. J. (2017). Contextually guided very-high-resolution imagery classification with semantic segments. *ISPRS Journal of Photogrammetry and Remote Sensing*, *132*, 48–60. https://doi.org/10.1016/j.isprsjprs.2017.08.011
Ziaei, Z., Pradhan, B., & Mansor, S. Bin. (2014). A rule-based parameter aided with object-based classification approach for extraction of building and roads from WorldView-2 images. *Geocarto International*, *29*(5), 554–569. https://doi.org/10.1080/10106049.2013.819039

APPENDICES

Appendix 1: Ward specific land use area (area in Acres) for different category of Dhaka City.

	Inhabitable								Non- Inhabitable							
Ward ID	**Administrative**	**Commercial**	**Educational**	**Manufacturing**	**Mixed Use**	**Residential**	**Restricted Area**	**Service Activity**	**Vacant Land**	**Water Body**	**Agriculture**	**Green Space & Recreational**	**Historical**	**playground**	**Roads**	**Total**
DNCC1		75.3	16.4			1103.3				37.1					167.1	1399.2
DNCC2			7.4			473.8	1.7	0.0		65.0		3.9			70.8	622.6
DNCC3	9.1		8.3		0.0	189.1		0.0		2.0					40.4	248.9
DNCC4	10.1		49.4		6.7	162.8		0.9		32.4					21.2	283.5
DNCC5			5.3		0.0	290.4		1.4		32.4					46.8	376.3
DNCC6		46.5	7.3		6.1	300.5	300.5			15.9		125.8			74.7	877.3
DNCC7	34.0	6.3	18.4		53.5	220.7				6.9		22.6			65.3	427.7
DNCC8		34.8	14.9		0.5	324.6	64.5			265.5		297.2			75.3	1077.3
DNCC9		0.0	2.4		6.1	210.9		13.0		115.7	212.1				43.0	603.2
DNCC10		29.8	6.9		29.8	287.2		1.3		36.8	33.3				48.7	473.8
DNCC11			12.4		13.5	218.5		0.1		16.6		0.5			36.7	298.3
DNCC12		40.5	5.6		22.6	142.0				10.3		0.3			34.5	255.8
DNCC13	21.0	6.7	7.4		4.0	505.8		0.2		14.2					64.0	623.3
DNCC14		74.2	4.6		4.1	287.8	4.7	0.1		8.4					56.9	440.8
DNCC15			4.6		0.5	1452.1	1.3	2.2		167.5		9.8			78.5	1716.5
DNCC16		1.2	6.9		23.6	299.2	616.1	0.1		9.4		0.7			114.7	1071.9
DNCC17						1854.7				28.9		0.5			106.1	1990.2
DNCC18		55.4				269.9				14.2					38.6	378.1
DNCC19	22.4	41.9			13.3	1058.9		0.1		146.3		2.1			108.9	1393.9
DNCC20	54.8	4.3			36.8	214.1		21.3		37.1		5.0			60.8	434.2
DNCC21		44.6				393.8				0.2					40.1	478.7
DNCC22		31.2				291.1	9.9	0.0		90.1					59.1	481.4
DNCC23		13.1				161.0				45.2					33.8	253.1
DNCC24	17.9		14.2	491.0	0.3	99.3		11.2		92.0					56.0	781.9
DNCC25		0.0	1.9	21.0	77.5	87.8	61.4	0.4		3.8					41.0	294.8
DNCC26	12.3	92.8	8.2	21.5	23.0	113.8	6.6			10.0		0.5			42.1	330.8
DNCC27	97.0	23.6	44.5		46.5	160.5	348.6	15.6		4.2		1.2			123.6	865.3
DNCC28	130.1		41.2		0.0	94.9	14.8			18.7					25.8	325.5
DNCC29		2.1	5.8		4.0	107.9				2.4					31.4	153.6
DNCC30			4.8		6.5	337.9				35.0	11.3	1.0			50.1	446.6
DNCC31			4.2		0.3	104.5		0.8							31.4	141.2
DNCC32			75.6		27.7	165.8		1.1		2.3					61.1	333.6
DNCC33		0.0	9.7		2.2	221.9				93.9		863.1			50.5	1241.3
DNCC34			12.4		0.6	231.6				36.7		1.1			22.3	304.7
DNCC35	2.3	18.4	2.1		5.9	177.9				31.5					32.9	271.0
DNCC36		5.5	1.1			128.6		0.1		19.8					24.1	179.2
DSCC1						162.2		0.1		23.2		0.3			52.8	238.6
DSCC2						159.9		0.0		14.8					33.5	208.2
DSCC3						485.1				0.5					52.9	538.5
DSCC4					0.1	186.5		0.5		18.4		1.5			41.4	248.4
DSCC5	3.8				9.3	210.1		0.2		22.9		0.1			37.4	283.8
DSCC6					18.3	83.7		1.1		2.6		0.0			20.4	126.1
DSCC7			1.8		15.9	59.1			1.0	1.8					11.2	90.8
DSCC8	134.5				0.9	55.3	0.1	0.0		2.1					24.4	217.3
DSCC9	57.2	27.6			6.0	60.7	0.1			2.2		51.3			47.0	252.1
DSCC10		4.0	7.4		3.3	77.4	0.9								19.9	112.9
DSCC11	1.0	22.1	1.5			124.7				3.2					34.7	187.2
DSCC12		10.8	2.1			90.3				3.9					24.9	132.0
DSCC13	54.5	41.8				129.8						41.7			59.3	327.1
DSCC14			20.3	63.3	45.0	527.5	27.7	0.0		179.1		1.9			48.4	913.2
DSCC15		11.4	35.5		20.7	354.2				35.5		0.9			98.3	556.5
DSCC16		25.3			0.0	113.2									25.5	164.0
DSCC17		36.1			0.2	134.8									36.1	207.2
DSCC18	0.9	64.9	30.2		12.2	147.7	72.8			5.9					30.4	365.0
DSCC19	49.5	51.4	22.3		28.6	119.9	0.0	5.7		1.0		121.9			66.0	466.3
DSCC20	154.1	38.0	160.8		0.2	23.5		10.0		11.1		200.4			83.6	681.7
DSCC21	12.2	4.2	122.9		0.1	87.5		9.2				6.3			41.6	284.0

	Inhabitable								Non- Inhabitable							
Ward ID	**Administrative**	**Commercial**	**Educational**	**Manufacturing**	**Mixed Use**	**Residential**	**Restricted Area**	**Service Activity**	**Vacant Land**	**Water Body**	**Agriculture**	**Green Space & Recreational**	**Historical**	**playground**	**Roads**	**Total**
DSCC22			2.3		13.4	337.3	49.6			3.6					31.5	437.7
DSCC23			0.6		0.7	63.3	12.5	2.7		5.9					11.4	97.1
DSCC24		2.0	0.9		11.4	81.3				3.0		0.7			12.8	112.1
DSCC25		6.0	1.6		13.4	34.0							13.5		14.5	83.0
DSCC26	2.4		52.9		4.5	109.5		19.7		5.7					36.6	231.3
DSCC27	5.4		40.6		68.3		3.4			1.3					20.9	139.9
DSCC28	0.3		0.6		36.6										7.5	45.0
DSCC29	4.7	12.7	0.6		47.2	12.0	2.6			1.5		2.6			15.1	99.0
DSCC30	6.5	40.3	0.0		21.8		1.8			6.1					14.0	90.5
DSCC31			3.1		66.8		28.1	0.3		1.0					19.6	118.9
DSCC32	1.2		1.5		53.2		1.7	0.2				0.2			13.8	71.8
DSCC33			1.4		87.3										17.8	106.5
DSCC34	6.2	16.6			46.3					0.3					16.6	86.0
DSCC35	0.6	6.4	0.0		11.0	27.3				1.0		0.5			14.6	61.4
DSCC36	6.0	0.0	2.0		33.3	3.8						0.0			9.6	54.7
DSCC37		20.6	11.9		38.0					0.1				2.0	12.4	85.0
DSCC38	1.1	11.3			78.1										22.4	112.9
DSCC39		5.7			32.4	66.1	0.4	1.3		3.3		0.7			22.2	132.1
DSCC40	7.4				29.7	49.1	0.7	10.0		0.8		1.4			16.5	115.6
DSCC41	1.2	2.1			34.1	26.3	1.0	2.0		0.3					12.6	79.6
DSCC42	8.1	14.3	2.1		38.8	17.5		0.1				1.4			13.7	96.0
DSCC43		9.4			76.7					0.6		0.3			11.2	98.2
DSCC44					25.5	15.7				3.2					8.5	52.9
DSCC45		8.1			130.1	7.4		0.4		3.2		8.0			26.6	183.8
DSCC46		8.1			34.1	54.5				0.3		0.2			10.8	108.0
DSCC47	3.5	31.4			37.8	71.4				3.4		0.2			24.7	172.4
DSCC48	7.7				2.8	212.3						0.4			22.2	245.4
DSCC49	17.8				2.6	86.4			85.3	3.4		0.3			19.0	214.8
DSCC50					22.7	117.3				14.0		1.0			30.8	185.8
DSCC51	6.9				5.9	152.2		0.5		18.3		0.8			30.0	214.6
DSCC52	4.0					58.1		0.0		1.5					5.3	68.9
DSCC53	2.2					140.3				1.7					14.5	158.7
DSCC54	2.3				15.8	124.6		1.4		4.4					19.6	168.1
DSCC55						415.5				43.7					22.7	481.9
DSCC56						320.0				147.1					17.1	484.2
Total	**974.2**	**1180.8**	**930.8**	**596.8**	**1696.7**	**18740.9**	**1633.5**	**135.3**	**86.3**	**2155.3**	**256.7**	**1780.3**	**13.5**	**2.0**	**3587.1**	**33770.2**

Appendix 2: Ward specific extracted buildings area (m²) for the Dhaka city.

DCC-ID	Admini-strative	Commer-cial	Educa-tional	Manufac-turing	Mixed	Residen-tial	Restric-ted	Service	Others	Total
DNCC1	0.00	216312.10	27662.84	0.00	0.00	2820313.33	0.00	0.00	2595757.41	**5660045.67**
DNCC2	0.00	0.00	8536.71	0.00	0.00	507228.05	391.84	35.30	2002134.04	**2518325.93**
DNCC3	0.00	0.00	12.39	0.00	0.00	323302.32	0.00	18.89	683319.42	**1006653.02**
DNCC4	0.00	0.00	1705.33	0.00	0.00	249427.67	0.00	950.93	894200.59	**1146284.51**
DNCC5	0.00	0.00	69.70	0.00	0.00	186084.56	0.00	775.06	1335509.31	**1522438.63**
DNCC6	0.00	0.00	12242.81	0.00	15599.83	469061.30	59990.09	0.00	2991635.39	**3548529.43**
DNCC7	27136.16	11348.33	22552.96	0.00	100901.93	0.00	0.00	0.00	1568105.51	**1730044.89**
DNCC8	0.00	44344.72	22161.05	0.00	175.58	295563.03	0.00	0.00	3995158.18	**4357402.57**
DNCC9	0.00	103.05	4812.72	0.00	373.15	0.00	0.00	7196.18	2427257.90	**2439742.99**
DNCC10	0.00	58266.03	6721.00	0.00	43103.25	13732.53	0.00	626.89	1794188.82	**1916638.52**
DNCC11	0.00	0.00	7772.44	0.00	10897.47	33554.73	0.00	0.00	1154151.34	**1206375.97**
DNCC12	0.00	81603.02	8276.20	0.00	49829.92	93402.68	0.00	0.00	801644.39	**1034756.22**
DNCC13	0.00	0.00	20508.83	0.00	0.00	705010.09	0.00	110.67	1795395.37	**2521024.96**
DNCC14	0.00	2595.65	38.75	0.00	0.00	138114.67	6120.40	53.97	1636259.81	**1783183.26**
DNCC15	0.00	0.00	5752.86	0.00	524.29	1045851.92	0.00	1071.59	5889971.98	**6943172.64**
DNCC16	0.00	0.00	8773.96	0.00	46133.83	515593.74	79579.21	49.70	3685947.61	**4336078.06**
DNCC17	0.00	0.00	0.00	0.00	0.00	1300021.37	0.00	0.00	6750191.06	**8050212.43**
DNCC18	0.00	109615.44	0.00	0.00	0.00	22132.86	0.00	0.00	1397534.26	**1529282.57**
DNCC19	27496.72	52326.81	0.00	0.00	25890.91	1236799.09	0.00	0.00	4296218.49	**5638732.01**
DNCC20	0.00	0.00	0.00	0.00	41598.93	215878.99	0.00	20118.15	1478751.88	**1756347.95**
DNCC21	0.00	68040.47	0.00	0.00	0.00	483311.74	0.00	0.00	1385235.71	**1936587.92**
DNCC22	0.00	878.40	0.00	0.00	0.00	295002.52	12718.41	78.54	1639028.82	**1947706.69**
DNCC23	0.00	0.00	0.00	0.00	0.00	266672.09	0.00	0.00	757578.61	**1024250.70**
DNCC24	0.00	0.00	22.93	366366.64	726.66	155258.39	0.00	14985.69	2625795.82	**3163156.12**
DNCC25	0.00	0.00	11.22	0.00	100362.18	128540.80	39618.15	266.89	923219.55	**1192018.79**
DNCC26	0.00	11596.43	45.54	23025.51	3806.88	19761.61	5970.56	0.00	1274192.04	**1338398.56**
DNCC27	0.00	0.00	33763.47	0.00	5372.30	0.00	108148.54	0.00	3352925.17	**3500209.47**
DNCC28	2963.75	0.00	453.98	0.00	34.39	0.00	0.00	0.00	1313660.84	**1317112.96**
DNCC29	0.00	0.00	9679.91	0.00	7102.31	228661.93	0.00	0.00	376408.35	**621852.50**
DNCC30	0.00	0.00	6275.40	0.00	0.00	506168.47	0.00	0.00	1293891.25	**1806335.12**
DNCC31	0.00	0.00	5373.41	0.00	953.15	225570.31	0.00	0.00	339354.82	**571251.69**
DNCC32	0.00	0.00	50277.47	0.00	67757.90	338661.98	0.00	0.00	892629.50	**1349326.85**
DNCC33	0.00	5.36	1334.55	0.00	5916.17	344083.55	0.00	0.00	4669718.89	**5021058.52**
DNCC34	0.00	0.00	14534.70	0.00	1562.10	375628.09	0.00	0.00	840486.03	**1232210.93**
DNCC35	0.00	0.00	2.12	0.00	10336.61	330482.94	0.00	0.00	755631.04	**1096452.71**
DNCC36	0.00	0.00	23.79	0.00	0.00	114313.30	0.00	42.12	610524.19	**724903.40**
DSCC1	0.00	0.00	0.00	0.00	0.00	325471.55	0.00	142.48	639682.63	**965296.67**
DSCC2	0.00	0.00	0.00	0.00	0.00	83593.80	0.00	53.24	758577.73	**842224.77**
DSCC3	0.00	0.00	0.00	0.00	0.00	139456.60	0.00	0.00	2038827.49	**2178284.09**
DSCC4	0.00	0.00	0.00	0.00	292.20	10576.90	0.00	73.62	994139.25	**1005081.97**
DSCC5	140.31	0.00	0.00	0.00	14602.22	282108.09	0.00	59.74	850796.52	**1147706.88**
DSCC6	0.00	0.00	0.00	0.00	38582.64	155897.43	0.00	440.42	315012.29	**509932.78**
DSCC7	0.00	0.00	2750.49	0.00	12214.28	0.00	0.00	0.00	351990.92	**366955.69**
DSCC8	120549.00	0.00	0.00	0.00	1867.62	104952.44	0.00	0.00	651504.27	**878873.33**
DSCC9	90870.94	44069.10	0.00	0.00	8400.07	103986.04	0.00	0.00	772192.07	**1019518.22**
DSCC10	0.00	3337.58	7992.50	0.00	6295.11	83483.59	1799.66	0.00	353967.26	**456875.70**
DSCC11	241.17	25203.96	1546.93	0.00	0.00	181795.93	0.00	0.00	548259.03	**757047.02**
DSCC12	0.00	0.00	0.00	0.00	0.00	187109.53	0.00	0.00	347046.21	**534155.75**
DSCC13	8776.95	77498.12	0.00	0.00	0.00	261416.57	0.00	0.00	975326.92	**1323018.55**
DSCC14	0.00	0.00	0.00	125593.50	75502.57	816104.68	10276.16	0.00	2666578.05	**3694054.96**
DSCC15	0.00	23.22	69971.91	0.00	39468.74	686990.61	0.00	0.00	1454850.02	**2251304.50**
DSCC16	0.00	31098.79	0.00	0.00	0.54	256421.56	0.00	0.00	376027.63	**663548.51**

DCC-ID	Admini-strative	Commer-cial	Educa-tional	Manufac-turing	Mixed	Residen-tial	Restric-ted	Service	Others	Total
DSCC17	0.00	0.00	0.00	0.00	13.82	258356.63	0.00	0.00	579995.70	**838366.15**
DSCC18	0.00	17054.79	16885.05	0.00	3190.57	113135.55	28408.42	0.00	1298093.21	**1476767.61**
DSCC19	0.00	0.00	0.00	0.00	54069.78	200315.02	0.00	3054.42	1628739.72	**1886178.94**
DSCC20	48185.62	46849.17	113458.33	0.00	99.68	44854.30	0.00	10639.30	2493424.55	**2757510.96**
DSCC21	0.00	0.00	51232.13	0.00	38.27	110177.44	0.00	14871.97	972473.05	**1148792.85**
DSCC22	0.00	0.00	0.00	0.00	0.00	0.00	10648.69	0.00	1759864.05	**1770512.75**
DSCC23	0.00	0.00	1103.14	0.00	0.00	0.00	4154.49	759.21	386485.51	**392502.36**
DSCC24	0.00	3376.02	1556.55	0.00	26190.54	166552.94	0.00	0.00	255561.82	**453237.87**
DSCC25	0.00	3139.65	2238.67	0.00	4685.79	66083.62	0.00	0.00	259489.83	**335637.56**
DSCC26	0.00	0.00	81.53	0.00	1388.33	43.90	0.00	980.64	932651.58	**935145.97**
DSCC27	0.00	0.00	23932.23	0.00	102581.31	0.00	4251.59	0.00	434796.79	**565561.92**
DSCC28	0.00	0.00	787.56	0.00	70135.18	0.00	0.00	0.00	111112.68	**182035.41**
DSCC29	5599.47	19887.01	1004.93	0.00	63400.05	25509.97	2406.70	0.00	282176.08	**399984.23**
DSCC30	0.00	75832.80	3.55	0.00	38778.66	0.00	3863.85	0.00	247129.99	**365608.86**
DSCC31	0.00	0.00	3063.34	0.00	108643.53	0.00	17195.36	0.00	351867.71	**480769.95**
DSCC32	0.00	0.00	2579.10	0.00	93264.44	0.00	2725.71	0.00	192035.85	**290605.11**
DSCC33	0.00	0.00	2230.01	0.00	141024.60	0.00	0.00	0.00	287445.25	**430699.86**
DSCC34	0.00	7614.64	0.00	0.00	91853.51	0.00	0.00	0.00	248289.05	**347757.19**
DSCC35	0.00	3372.50	0.02	0.00	21762.31	54301.82	0.00	0.00	168809.60	**248246.24**
DSCC36	2482.45	0	3554.42	0.00	61506.64	6580.44	0.00	0.00	147662.48	**221786.43**
DSCC37	0.00	37587.53	15541.64	0.00	51749.18	0.00	0.00	0.00	238892.55	**343770.91**
DSCC38	0.00	178.05	0.00	0.00	152619.08	0.00	0.00	0.00	304042.54	**456839.67**
DSCC39	0.00	7799.11	0.00	0.00	60235.39	120545.39	166.29	136.00	345113.71	**533995.89**
DSCC40	7738.62	0.00	0.00	0.00	51303.14	82501.25	1135.11	303.60	325293.23	**468274.96**
DSCC41	0.00	0.00	0.00	0.00	65444.56	52845.92	391.39	0.00	203374.86	**322056.72**
DSCC42	5055.57	27743.30	1899.96	0.00	70470.16	32190.28	0.00	0.00	251283.69	**388642.96**
DSCC43	0.00	16784.20	0.00	0.00	127199.85	0.00	0.00	0.00	252977.26	**396961.31**
DSCC44	0.00	0.00	0.00	0.00	48628.27	30316.75	0.00	0.00	135194.20	**214139.23**
DSCC45	0.00	12997.48	0.00	0.00	211426.34	11629.63	0.00	71.55	507720.30	**743845.31**
DSCC46	0.00	7355.07	0.00	0.00	37546.43	15547.98	0.00	0.00	376195.60	**436645.08**
DSCC47	0.00	16028.06	0.00	0.00	123.30	387.17	0.00	0.00	680301.81	**696840.33**
DSCC48	0.00	0.00	0.00	0.00	2172.27	126099.13	0.00	0.00	865026.59	**993297.98**
DSCC49	0.00	0.00	0.00	0.00	2659.26	679.38	0.00	0.00	865427.96	**868766.60**
DSCC50	0.00	0.00	0.00	0.00	2116.72	201231.58	0.00	0.00	548794.42	**752142.73**
DSCC51	3448.85	0.00	0.00	0.00	36.89	252239.95	0.00	315.53	611644.59	**867685.80**
DSCC52	90.96	0.00	0.00	0.00	0.00	100950.69	0.00	106.76	177655.60	**278804.01**
DSCC53	1149.09	0.00	0.00	0.00	0.00	227434.72	0.00	0.00	413510.42	**642094.23**
DSCC54	2391.37	0.00	0.00	0.00	296.16	185615.11	0.00	140.99	492096.03	**680539.65**
DSCC55	0.00	0.00	0.00	0.00	0.00	684635.70	0.00	0.00	1266885.00	**1951520.70**
DSCC56	0.00	0.00	0.00	0.00	0.00	347494.93	0.00	0.00	1611453.55	**1958948.48**
Total	**354316.99**	**1142015.23**	**602813.03**	**514985.64**	**2502690.49**	**21180813.14**	**399960.62**	**78530.06**	**109829380.07**	**136605505.27**

Appendix 3: Relative weight of population density for each building type within the ward generated from GWR model.

DCC_ID	Administrative	Commercial	Educational	Manufacturing	Mixed	Residential	Restricted	Service
DNCC1		43.59	48.48			7.93		
DNCC2			54.64			45.36		
DNCC3	35.23		34.10			30.67		
DNCC4	27.67		20.37		28.57	23.38		
DNCC5			53.13			46.87		
DNCC6		19.54	21.18		23.41	14.91	20.96	
DNCC7	20.10	21.39	18.13		25.45	14.93		
DNCC8		35.15	33.49			31.36		
DNCC9		23.22	22.17		23.59	15.06		15.95
DNCC10		23.86	26.74		29.57	19.83		
DNCC11			33.84		36.50	29.66		
DNCC12		22.88	25.77		28.52	22.83		
DNCC13	23.52	24.28	21.04		25.61	5.56		
DNCC14		14.29	22.43		24.50	14.82	23.96	
DNCC15			37.62			24.12	38.25	
DNCC16		24.32	22.28		26.38	11.89	15.12	
DNCC17						100.00		
DNCC18		49.69				50.31		
DNCC19	33.87	27.17			38.26	0.71		
DNCC20	18.21	21.54			24.06	16.47		19.72
DNCC21		52.44				47.56		
DNCC22		33.69				26.66	39.65	
DNCC23		53.25				46.75		
DNCC24	26.42		24.42	0.16		23.04		26.27
DNCC25			19.74	19.30	24.52	17.47	18.97	
DNCC26	1.76	72.78	2.17	3.00	5.32	11.31	3.66	
DNCC27	13.65	12.83	9.00		22.92	12.97	14.94	13.69
DNCC28	24.24		17.60			26.90	31.25	
DNCC29		26.46	24.81		27.12	21.60		
DNCC30			36.80		39.27	23.93		
DNCC31			52.20			47.80		
DNCC32			17.93		32.47	20.87		28.73
DNCC33		28.44	26.11		28.56	16.88		
DNCC34			53.20			46.80		
DNCC35	22.79	18.24	22.39		23.40	13.19		
DNCC36		34.40	35.33			30.27		
DSCC1						100.00		
DSCC2						100.00		
DSCC3						100.00		
DSCC4						100.00		
DSCC5					54.88	45.12		
DSCC6					51.77	48.23		
DSCC7			34.09		34.11	31.79		
DSCC8	43.99					56.01		
DSCC9	17.50	24.86			30.80	26.85		
DSCC10		25.83	24.70		26.13	23.34		
DSCC11		33.24	35.90			30.86		
DSCC12		33.78	35.61			30.61		
DSCC13	34.23	32.57				33.21		
DSCC14			22.84	22.81	29.22	1.83	26.96	

DCC_ID	Administrative	Commercial	Educational	Manufacturing	Mixed	Residential	Restricted	Service
DSCC15		33.19	17.89		37.61	11.31		
DSCC16		50.27				49.73		
DSCC17		49.36				50.64		
DSCC18		7.83	22.20		26.25	18.32	25.40	
DSCC19	14.28	8.26	16.03		23.14	15.42		22.87
DSCC20	13.01	23.33	8.15			27.29		28.23
DSCC21	23.08	22.96	10.71			20.37		22.89
DSCC22			29.15		30.20	11.22	29.43	
DSCC23			34.29			31.31	34.40	
DSCC24		26.02	26.24		26.24	21.50		
DSCC25		24.62	25.65		25.81	23.92		
DSCC26	27.26		21.86		27.58	23.30		
DSCC27	26.22		21.67		25.54		26.57	
DSCC28			50.29		49.71			
DSCC29	16.85	15.11	17.33		16.50	16.77	17.44	
DSCC30	21.27	13.21	22.06		21.43		22.02	
DSCC31			33.54		32.56		33.90	
DSCC32			33.52		32.59		33.89	
DSCC33			50.66		49.34			
DSCC34	34.09	31.98			33.93			
DSCC35		24.48	25.85		25.52	24.16		
DSCC36	19.76	20.50	19.95		19.48	20.31		
DSCC37		31.34	33.37		35.29			
DSCC38	34.75	32.89			32.35			
DSCC39		34.65			34.25	31.10		
DSCC40	34.04				33.74	32.22		
DSCC41		33.97			33.22	32.81		
DSCC42	20.26	18.00	21.34		19.96	20.45		
DSCC43		50.55			49.45			
DSCC44					49.96	50.04		
DSCC45		34.35			30.04	35.61		
DSCC46		34.09			34.02	31.89		
DSCC47	26.93	23.12			26.24	23.72		
DSCC48	37.87				38.87	23.26		
DSCC49	33.68				35.19	31.13		
DSCC50					53.17	46.83		
DSCC51	26.29	27.69			27.46	18.56		
DSCC52	51.28					48.72		
DSCC53	53.93					46.07		
DSCC54	35.34				35.11	29.55		
DSCC55						100.00		
DSCC56						100.00		

Appendix 4: Population density per cell for each building type in each ward. Here the missing value means that particular ward does not have this building type.

DCC_ID	Administrative	Commercial	Educational	Manufacturing	Mixed	Residential	Restricted	Service	Average
DNCC1	.	6.03	6.71	.	.	1.10	.	.	**4.61**
DNCC2	.	.	8.98	.	.	7.47	.	7.46	**7.97**
DNCC3	.	.	.	.	.	7.30	.	.	**7.30**
DNCC4	.	.	6.49	.	.	7.45	.	7.45	**7.13**
DNCC5	.	.	.	.	.	15.88	.	.	**15.88**
DNCC6	.	.	9.76	.	10.82	6.91	9.72	.	**9.30**
DNCC7	2.87	3.04	2.60	.	3.63	.	.	.	**3.03**
DNCC8	.	8.44	8.04	.	.	7.52	.	.	**8.00**
DNCC9	.	175.15	167.23	.	177.94	.	.	120.31	**160.16**
DNCC10	.	16.60	18.55	.	20.58	13.71	.	.	**17.36**
DNCC11	.	.	5.30	.	5.71	4.62	.	.	**5.21**
DNCC12	.	11.88	13.31	.	14.77	11.81	.	.	**12.94**
DNCC13	.	.	19.00	.	.	5.04	.	5.04	**9.69**
DNCC14	.	26.45	.	.	.	27.30	44.05	.	**32.60**
DNCC15	.	.	6.43	.	.	4.14	.	4.14	**4.90**
DNCC16	.	.	9.41	.	11.29	5.08	6.42	.	**8.05**
DNCC17	.	.	.	.	.	3.80	.	.	**3.80**
DNCC18	.	12.05	.	.	.	12.20	.	.	**12.12**
DNCC19	19.17	15.38	.	.	21.66	0.40	.	.	**14.15**
DNCC20	.	.	.	.	12.07	8.26	.	9.89	**10.07**
DNCC21	.	4.75	.	.	.	4.30	.	.	**4.53**
DNCC22	.	.	.	.	.	12.76	18.96	.	**15.86**
DNCC23	.	.	.	.	.	5.96	.	.	**5.96**
DNCC24	.	.	15.50	0.10	15.27	14.60	.	16.64	**12.42**
DNCC25	.	.	.	.	11.21	7.99	8.67	.	**9.29**
DNCC26	.	102.01	3.04	4.20	7.46	15.85	5.18	.	**22.96**
DNCC27	.	.	10.01	.	25.50	.	16.62	.	**17.38**
DNCC28	4.90	.	3.56	.	.	.	.	.	**4.23**
DNCC29	.	.	6.26	.	6.86	5.46	.	.	**6.20**
DNCC30	.	.	13.86	.	.	9.08	.	.	**11.47**
DNCC31	.	.	6.03	.	.	5.52	.	.	**5.77**
DNCC32	.	.	3.23	.	5.85	3.76	.	.	**4.28**
DNCC33	.	.	12.31	.	13.57	8.03	.	.	**11.30**
DNCC34	.	.	7.77	.	.	6.81	.	.	**7.29**
DNCC35	.	.	.	.	9.40	5.30	.	.	**7.35**
DNCC36	.	.	.	.	.	15.63	.	.	**15.63**
DSCC1	.	.	.	.	.	5.28	.	.	**5.28**
DSCC2	.	.	.	.	.	33.88	.	.	**33.88**
DSCC3	.	.	.	.	.	15.53	.	.	**15.53**
DSCC4	.	.	.	.	4.98	5.02	.	.	**5.00**
DSCC5	.	.	.	.	6.17	5.08	.	.	**5.62**
DSCC6	.	.	.	.	10.84	10.09	.	10.10	**10.34**
DSCC7	.	.	96.16	.	96.34	.	.	.	**96.25**
DSCC8	3.46	.	.	.	3.45	4.41	.	.	**3.77**
DSCC9	3.23	4.58	.	.	5.68	4.95	.	.	**4.61**
DSCC10	.	6.01	5.75	.	6.08	5.43	.	.	**5.82**
DSCC11	.	7.59	8.20	.	.	7.05	.	.	**7.62**
DSCC12	.	.	.	.	.	6.85	.	.	**6.85**
DSCC13	4.48	4.26	.	.	.	4.34	.	.	**4.36**
DSCC14	.	.	.	10.73	13.75	0.87	12.68	.	**9.51**
DSCC15	.	5.71	3.06	.	6.49	1.95	.	.	**4.30**
DSCC16	.	7.00	.	.	.	6.92	.	.	**6.96**
DSCC17	.	.	.	.	.	5.69	.	.	**5.69**
DSCC18	.	2.94	8.16	.	9.51	6.76	9.33	.	**7.34**
DSCC19	.	.	.	.	7.38	4.92	.	7.29	**6.53**
DSCC20	2.97	5.32	1.86	.	.	6.23	.	6.44	**4.57**
DSCC21	.	.	2.87	.	.	5.45	.	6.12	**4.81**
DSCC22	.	.	.	.	.	3.36	8.80	.	**6.08**

DCC_ID	Administrative	Commercial	Educational	Manufacturing	Mixed	Residential	Restricted	Service	Average
DSCC23	.	.	8.82	.	.	8.05	8.88	.	**8.59**
DSCC24	.	9.88	9.96	.	9.96	8.15	.	.	**9.49**
DSCC25	.	9.78	10.16	.	10.25	9.49	.	.	**9.92**
DSCC26	.	.	4.68	.	5.57	4.69	.	.	**4.98**
DSCC27	.	.	4.80	.	5.64	.	5.88	.	**5.44**
DSCC28	.	.	8.87	.	8.77	.	.	.	**8.82**
DSCC29	12.80	11.45	13.13	.	12.53	12.74	13.25	.	**12.65**
DSCC30	.	5.71	.	.	9.26	.	9.51	.	**8.16**
DSCC31	.	.	7.05	.	6.86	.	7.13	.	**7.01**
DSCC32	.	.	9.16	.	8.92	.	9.28	.	**9.12**
DSCC33	.	.	11.54	.	11.24	.	.	.	**11.39**
DSCC34	.	12.03	.	.	12.73	.	.	.	**12.38**
DSCC35	.	8.86	.	.	9.24	8.75	.	.	**8.95**
DSCC36	8.99	9.33	9.08	.	8.85	9.24	.	.	**9.10**
DSCC37	.	4.01	4.27	.	4.54	.	.	.	**4.28**
DSCC38	.	7.64	.	.	7.51	.	.	.	**7.57**
DSCC39	.	5.44	.	.	5.37	4.88	.	.	**5.23**
DSCC40	8.50	.	.	.	8.43	8.04	.	.	**8.32**
DSCC41	.	.	.	.	8.70	8.61	.	.	**8.65**
DSCC42	5.14	4.57	5.42	.	5.06	5.20	.	.	**5.08**
DSCC43	.	7.16	.	.	7.01	.	.	.	**7.08**
DSCC44	.	.	.	.	8.46	8.48	.	.	**8.47**
DSCC45	.	5.98	.	.	5.24	6.21	.	.	**5.81**
DSCC46	.	16.85	.	.	16.81	15.77	.	.	**16.48**
DSCC47	.	70.93	.	.	80.50	60.10	.	.	**70.51**
DSCC48	.	.	.	.	17.34	11.12	.	.	**14.23**
DSCC49	.	.	.	.	9.44	6.92	.	.	**8.18**
DSCC50	.	.	.	.	7.97	7.07	.	.	**7.52**
DSCC51	9.56	.	.	.	9.99	6.76	.	.	**8.77**
DSCC52	16.09	.	.	.	.	10.78	.	.	**13.44**
DSCC53	8.63	.	.	.	.	7.22	.	.	**7.93**
DSCC54	11.09	.	.	.	11.02	9.39	.	.	**10.50**
DSCC55	.	.	.	.	.	3.44	.	.	**3.44**
DSCC56	.	.	.	.	.	5.89	.	.	**5.89**
Average	**8.12**	**18.08**	**13.87**	**5.01**	**15.39**	**8.68**	**12.15**	**18.26**	**12.29**
Dhaka North Average	**8.98**	**34.71**	**15.80**	**2.15**	**21.98**	**8.47**	**15.66**	**24.42**	**14.34**
Dhaka South Average	**7.91**	**10.13**	**11.65**	**10.73**	**12.60**	**8.82**	**9.41**	**7.49**	**10.97**

Appendix 5: Ward specific actual population and estimated population from different model to calculate the RMSE.

DCC_ID	Actua Pop	**Building based GWR**	**Building based OLS**	**Land use based GWR**	**Land use based OLS**	**Dasymetric Model**
DNCC1	183298	202457	250599	164224	171833	183326
DNCC2	151868	123647	110467	115074	101631	151867
DNCC3	94664	97190	80813	93941	73216	94713
DNCC4	75246	84421	73377	79248	66575	75264
DNCC5	118110	109208	93068	101572	83830	117975
DNCC6	163770	120410	110218	135907	128209	163930
DNCC7	113750	101892	79180	93744	66158	113785
DNCC8	111251	95301	80421	111431	99444	111470
DNCC9	71260	83216	82563	80658	72670	70430
DNCC10	87879	96962	77094	100795	82905	88150
DNCC11	97033	87877	76636	93184	74708	96810
DNCC12	116544	89333	68163	92038	71686	116315
DNCC13	157206	140162	124973	115933	102999	157754
DNCC14	163797	109775	91606	103325	93752	163580
DNCC15	173842	136905	129547	177232	195215	173807
DNCC16	142413	149268	162998	146813	158260	142385
DNCC17	196479	188819	203488	200838	234075	196479
DNCC18	63616	92649	84988	92452	89789	63701
DNCC19	96291	152460	153632	139313	159076	96347
DNCC20	98618	84159	69759	87771	61955	98431
DNCC21	96111	95390	96259	92214	100335	96116
DNCC22	160316	91419	95273	83321	90361	160473
DNCC23	63763	71492	75148	68823	73666	63865
DNCC24	103274	104781	106770	104674	107022	103177
DNCC25	99727	83383	69439	86616	62998	99604
DNCC26	67876	63075	58112	63175	77450	67944
DNCC27	90224	88305	84838	91910	96213	90226
DNCC28	65984	59019	55503	69718	52232	65968
DNCC29	54739	70027	67868	76453	66087	54731
DNCC30	186639	121274	102578	105157	87640	186514
DNCC31	51384	67561	68302	70434	65949	51237
DNCC32	72973	71506	72564	65258	62971	72979
DNCC33	114756	94973	86176	88644	76858	114892
DNCC34	106548	78637	78973	85945	77761	106328
DNCC35	74069	70401	73864	68889	74775	74174
DNCC36	70984	63646	67945	65935	69446	70981
DSCC1	68931	68981	75853	66237	72037	68906
DSCC2	113273	67841	74919	65717	71813	113273
DSCC3	86931	101920	114007	93284	102647	86931
DSCC4	82701	69539	77059	65709	72687	82701
DSCC5	60788	65266	72570	69369	74938	60883
DSCC6	79305	53923	61706	53911	61542	79301
DSCC7	58316	47682	58363	49589	59577	58632
DSCC8	34867	45347	50790	44841	48707	34880
DSCC9	42105	47246	50070	48978	59532	42238
DSCC10	21968	44444	57325	52355	63568	21968
DSCC11	59999	56771	64315	61390	71156	60175
DSCC12	51067	57070	64801	57584	66390	51075
DSCC13	59639	63357	63191	59747	69287	59647
DSCC14	128921	143928	119114	142791	108765	129975
DSCC15	72449	96076	97296	98746	86619	72505
DSCC16	79983	64139	68925	59517	70670	79985

DCC_ID	Actua Pop	**Building based GWR**	**Building based OLS**	**Land use based GWR**	**Land use based OLS**	**Dasymetric Model**
DSCC17	58863	66652	68328	66313	74186	58863
DSCC18	49523	55934	68877	63889	84641	49694
DSCC19	55920	57633	54994	58742	62793	55947
DSCC20	38201	24724	39057	26296	35919	38260
DSCC21	33513	41742	58386	37281	53982	33518
DSCC22	84519	95483	94395	100260	93205	84588
DSCC23	48875	45245	61571	47643	63119	48992
DSCC24	66470	52380	62788	50166	62790	66465
DSCC25	29832	40562	55282	42124	58419	29881
DSCC26	44540	38569	59941	49225	57996	44534
DSCC27	28525	34478	47363	36662	43469	28555
DSCC28	24656	37286	49055	38206	50834	24549
DSCC29	58233	43075	49713	41666	52095	58240
DSCC30	33613	37456	48147	38320	58135	33649
DSCC31	35656	42832	51467	42521	49761	35649
DSCC32	36147	39863	49021	40020	48551	36132
DSCC33	65289	43867	45466	42316	43343	65217
DSCC34	50624	40945	46104	40498	51160	50619
DSCC35	28074	40960	54662	42306	58117	28077
DSCC36	26199	37631	49175	39371	51145	26207
DSCC37	18170	33531	47901	38134	52670	18171
DSCC38	46140	44404	44593	42016	46176	46134
DSCC39	38322	50992	58005	50616	58519	38328
DSCC40	46434	46473	55226	49472	53788	46440
DSCC41	40587	44053	52977	44343	53708	40587
DSCC42	27882	42256	49408	42385	53259	27993
DSCC43	40043	42887	45822	41671	46174	39973
DSCC44	26939	40562	52153	41608	54022	26939
DSCC45	50419	48747	43437	45081	38828	50339
DSCC46	40267	45816	56756	47977	57654	40257
DSCC47	48026	47847	56241	51242	61399	48280
DSCC48	58741	72520	78654	70386	75654	58787
DSCC49	60966	50724	61045	52778	62538	60956
DSCC50	56766	57478	65202	57377	64280	56767
DSCC51	69399	60976	69238	61889	69505	70086
DSCC52	43954	45723	59060	47864	61596	43948
DSCC53	58954	58105	68345	57513	68139	58961
DSCC54	66637	55090	64265	57161	65093	66725
DSCC55	94573	110205	102201	107716	96489	94460
DSCC56	82069	93156	92273	89812	87270	82006
RMSE		**19106**	**25676**	**20160**	**26259**	**194**